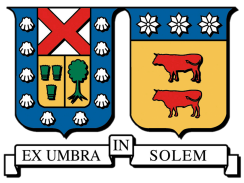

UNIVERSIDAD TÉCNICA FEDERICO SANTA MARÍA
DEPARTAMENTO DE FÍSICA

Non-Relativistic QCD Estimates for B_c Meson Production at LHCb

Franco Eduardo Barattini Osorio

Thesis submited to the Physics Department of Universidad Técnica Federico Santa María for the academic degree of Master of Science, mention Physics

May 2025
Valparaíso, Chile

Thesis Advisor: Dr. Claudio Dib
Co-Advisor: Dr. Benjamin Guiot
Co-Advisor: Dr. Boris Kopeliovich

Internal Examiner: Dr. Marat Siddikov
External Examiner: Dr. York Schröder **(UBB)**

CONSTANCIA DE VALIDACIÓN Y CONFIDENCIALIDAD DE MONOGRAFÍA A REPOSITORIO ACADÉMICO

1.- IDENTIFICACIÓN DEL TRABAJO ACADÉMICO

Tipo de monografía (marcar una opción): ☐ Memoria o trabajo de título; ☒ Tesis de Postgrado;

Título del trabajo: Non-Relativistic QCD Estimates for Bc Meson Production at LHCb

Nombre del candidato(a): Franco Eduardo Barattini Osorio

Carrera / Grado: Magister en Ciencias, Mención Física

Campus: Casa Central Valparaiso**;** **Departamento**: Física

2.- VALIDACIÓN DEL PROFESOR GUÍA/DIRECTOR DE TESIS

Yo, Claudio Dib V., en mi calidad de profesor(a) guía/director(a) del trabajo académico mencionado anteriormente **DEJO CONSTANCIA** que:

- He revisado esta versión del documento y corresponde a la versión final aprobada del trabajo.
- El trabajo cumple con los requisitos académicos y de formato establecidos por la institución

3.- EVALUACIÓN DE CONFIDENCIALIDAD POR PROPIEDAD INDUSTRIAL

☒ El trabajo **NO contiene información que amerite confidencialidad** y puede ser publicado de inmediato en repositorio con acceso abierto.

☐ El trabajo **CONTIENE** información con potenciales implicancias de propiedad industrial o intelectual y requiere un periodo de confidencialidad (embargo) por:

☐ 6 meses; ☐ 12 meses; ☐ 2 años; ☐ 3 años; ☐ 5 años; ☐ 10 años

Fundamentación de la necesidad de confidencialidad (obligatorio si se solicita embargo):

4.- FIRMAS

Profesor(a) guía o director(a) de memoria o tesis:

Fecha: 24/06/2025 ; **Firma:** 

Estudiante o Candidato(a):

Fecha: 24/06/2025 ; **Firma:** 

Este formulario debe ser insertado como página 2 de la memoria o tesis, completado y firmado por estudiante y profesor(a) antes de la entrega en portal PRISMA de Biblioteca USM.

"*The core of how things are created in the universe is through collision, so you got to be prepared to collide if you want to create something.*"

Will Smith on what it takes to chase your dreams

Abstract

Among the family of B mesons, the B_c meson is unique for being composed of two distinct heavy flavors: bottom and charm. This distinctive structure makes its production and detection significantly more challenging than that of other bottom-flavored mesons or heavy quarkonia, resulting in large uncertainties in its dynamic properties. Due to these experimental difficulties, the absolute differential production cross section of B_c mesons has not yet been fully determined.

To improve our theoretical understanding of B_c meson production, we employ the framework of Non-Relativistic Quantum Chromodynamics (NRQCD). This effective field theory allows for a systematic perturbative expansion in the relative velocity of the constituent heavy quarks, making it particularly suited for describing bound states of heavy quarks. Within this framework, we focus on a widely used method known as the *Fragmentation Approach*.

We compute the leading-order color-singlet fragmentation functions, used to predict the transverse momentum (p_T) dependence of the B_c production cross section in high-energy proton-proton collisions. Comparing against the last measurements of the LHCb collaboration, we find that the predictions show an underestimation in all the kinematic range measured, which becomes more significant in the low-p_T region. This discrepancy suggests the potential relevance of next-to-leading power contributions, different from the fragmentation mechanisms, at the current energies of the LHCb reports.

Agradecimientos

Quisiera empezar dando mi profundo agradecimiento al Prof. Claudio Dib, quien ha sido mi tutor desde la licenciatura, por haberme guiado con respeto, paciencia y generosidad, y por todo el conocimiento que me ha transmitido a lo largo de estos años.

También agradezco sinceramente al Dr. Benjamin Guiot, quien asumió el rol de co-tutor de forma repentina y, sin embargo, me acompañó con mucha paciencia y dedicación en la realización de esta tesis, siendo el principal impulsor de mi trabajo.

Deseo expresar mi más sincero agradecimiento a los profesores del comité de examen por su comprensión y, en particular, por su generosa disposición a leer y evaluar este trabajo en un plazo tan breve, a pesar de los retrasos.

Me gustaría también expresar mi profunda gratitud a mi madre, por su amor incondicional y su apoyo constante a lo largo de mi vida, y a mi hermana, cuya fe inquebrantable en mi persona ha sido una fuente de fortaleza inagotable y una línea de vida en los momentos más duros.

Por último, pero no por ello menos importante, agradezco a todas las personas del programa de magíster y doctorado con quienes compartí este último año. Su presencia hizo de mi paso por el magíster una experiencia muy agradable y de la cual guardaré buenos recuerdos.

Contents

Introduction

Quantum Chromo-Dynamics (QCD) is the fundamental theory that describes the strong interactions among elementary particles. Formulated as a non-Abelian gauge theory based on the SU(3) color symmetry group, it governs the behavior of quarks and gluons, the fundamental constituents of hadronic matter. A special feature of QCD is that, unlike the photon in Quantum Electrodynamics (QED), gluons themselves carry color charge, leading to rich and complex self-interactions. This characteristic gives rise to important phenomena such as *Asymptotic Freedom* (discovered independently by 't Hooft [1], Gross and Wilczek [2] and Politzer [3]), where the strength of the interaction decreases as the energy scale increases, and the still not completely understood phenomenon of *Colour Confinement*, which prevents the isolation of individual quarks or gluons. Despite the challenges raised by the theory becoming strongly coupled (non-perturbative) at low energies, QCD has provided many important insights and accurate predictions for a wide variety of phenomena, from the structure of hadrons to the behavior of matter under extreme conditions. Thanks to its success in explaining experimental results, QCD is now considered a central part of the Standard Model of particle physics, and it continues to inspire the development of new theoretical tools in the search to deepen our understanding of the strong force.

One of the most widely used and powerful predictive tools within QCD is *Perturbative Quantum Chromo-Dynamics* (pQCD), which relies on perturbative expansions in the strong coupling constant. This approach is justified by the phenomenon of asymptotic freedom, which allows us to use perturbative techniques to study the interactions between quarks and gluons with considerable success in processes involving energies much higher than the scale Λ_{QCD}, where perturbation theory predicts its own break down (the strong coupling becomes divergent). At lower energies, the strong coupling grows large and non-perturbative methods must be employed. When this two types of dynamics are bound together in a same proces, the factorization theorems provide a systematic framework that separates short-distance dynamics from the long-distance effects, and encapsulate the laters in universal, process-independent functions such as parton distribution and fragmentation functions. When both perturbative and non-perturbative dynamics are involved in the same process, the *Factorization Theorems* offer a systematic framework to separating them, enconding the latters in universal, process-independent functions which are fitted to data.

Within QCD, quarks are classified according to their masses compared to the characteristic scale of strong interactions, Λ_{QCD}. Heavy quarks are those whose masses are much larger than Λ_{QCD} ($m_Q \gg \Lambda_{\mathrm{QCD}}$). According to this criterion, the charm, bottom, and top quarks (c, b, t) are considered heavy flavors, while the up, down, and strange quarks (u, d, s) are refered to as light flavours. The large intrinsic mass scale associated with heavy quarks suppresses the strong coupling at the relevant energies ($\alpha_s(m_Q) \ll 1$), making it possible to calculate processes involving heavy quarks using perturbative QCD methods. Consequently, systems containing heavy quarks provide an especially valuable environment to probe QCD, offering insights into both its perturbative and non-perturbative regimes.

An important class of such systems is formed by mesons containing one or more heavy quarks. The large masses of their constituent heavy flavours allows the application of per-

turbative techniques to describe their production and decay at short distances. Meanwhile, the binding of heavy quarks into mesons brings in non-perturbative effects related to hadronization and bound-state formation. These aspects can be addressed systematically using effective field theories such as Heavy Quark Effective Theory (HQET) [4] [5] for heavy-light systems and Non-Relativistic QCD (NRQCD) [6] [7] for heavy-heavy systems (which we would refer to as Heavy Mesons). In particular, the last offers an especially clean environment where perturbative and non-perturbative dynamics can be clearly separated. Since the heavy quarks move with relatively small velocities within the meson, non-relativistic approximations can be used along with factorization theorems to connect theoretical calculations with experimental observables. In this way, these systems serve as important laboratories for testing QCD and extracting fundamental parameters such as heavy-quark masses and CKM matrix elements.

Within this category, the B_c meson has a particularly special place, being the only known meson made of two different heavy flavors, a bottom quark and a charm antiquark, or vice-versa. This special composition leads to many remarkable properties, one of which is that it has explicit flavor quantum numbers. This means that, unlike heavy quarkonia like charmonium ($c\bar{c}$) and bottomonium ($b\bar{b}$), the B_c meson cannot decay through strong or electromagnetic interactions, but only through weak interactions. The first excited states, like the vector B_c^*, mainly decay electromagnetically into the ground state B_c, while higher excitations below the BD threshold go through hadronic and electromagnetic transitions before reaching the ground state. (It is worth mentioning that in literature the term "B_c" refers both to the ground-state pseudoscalar meson and, more generally, to the whole family of bound states formed by a bottom quark and a charm antiquark.)

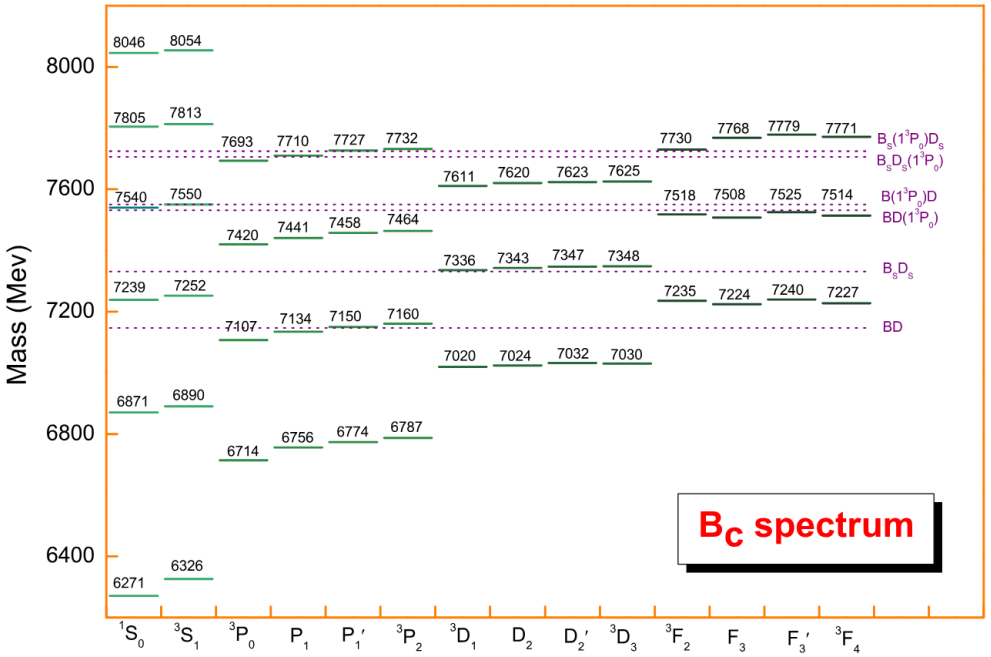

Figure 1: Estimates for the spectrum of B_c bound states [8].

Despite the interesting properties properties of B_c mesons, their production and detection is a considerable experimental challenge, as their production cross sections are significantly smaller than those of quarkonia. This suppression arises from the fact that, in a single hard collision, it is necessary to produce both a $b\bar{b}$ and a $c\bar{c}$ pair (since stable nucleons contain neither bottom nor charm quarks) in order to create a single B_c state.

As a consequence, it not only requires more energy to create, but also the leading-order production mechanisms are of higher order in the strong coupling than in the case of quarkonia.

The small production rates made the first searches for B_c mesons at e^+e^- and ep colliders particularly difficult. Although theoretical estimates suggested that B_c production at the Z^0 resonance could be marginally observable, dedicated searches at LEP during the mid-90s by the ALEPH, DELPHI, and OPAL experiments found not enough evidence for B_c production [9], [10], [11].

It was not until 1998 that the CDF Collaboration at the Tevatron achieved the first clear signal of the B_c through its weak decay channels [12], [13], a result confirmed a decade later by the D$\emptyset$ Collaboration [14]. Since then, the higher energies and luminosities of the LHC have allowed LHCb, CMS and ATLAS to not only reaffirm the discovery but also to study production rates, lifetimes, and excited states, with improved precision [15], [16], [17].

The work presented in this thesis aims to reproduce the observations published a few years ago by LHCb [18] regarding the production ratio between B_c mesons and $B_u + B_d$ mesons (where this notation collectively refers to the B mesons and their corresponding antiparticles, grouped according to their lighter flavour companions). This study employs tools from both perturbative QCD and NRQCD, and explores the various theoretical components required to compute the production rates, such as parton distribution functions, fragmentation functions, and the different factorization frameworks used to study heavy mesons. With this foundation, the main goal of this thesis is to contribute to a better understanding of the dynamics of heavy-quark systems and to explore the relevance of the fundamental procesess that contribute to the formation of heavy mesons in the context of Quantum Chromodynamics.

The thesis is organized as follows. In Chapter 1, we review the main concepts and techniques used in the application of perturbative QCD to processes involving initial- and final-state hadrons, emphasizing key aspects relevant for the following chapters, such as the DGLAP evolution equations and the definition of fragmentation functions. Chapter 2 introduces the methods used to study the formation of heavy mesons within the NRQCD factorization framework, including a brief overview of power counting rules and the matching procedure with full QCD. In Chapter 3, we present the framework that combines NRQCD with fragmentation functions, which we then use to obtain our results for the B_c meson production cross section, and compare them with LHCb data. Finally, in Chapter 4, we present our conclusions and discuss possible directions for future work.

1 Perturbative Quantum Chromo-Dynamics

Understanding high energy processes in particle physics often begins with the use of perturbation theory, which is a powerful tool to calculate observables in quantum field theories. In the case of Quantum Chromodynamics, this method works well for particles that carry colour charge (like quarks and gluons) as long as the interactions happen at very short distances or at very high energies. In this regime, the strong coupling becomes weak enough that quarks and gluons behave almost like free particles.

However, in nature, we do not observe free quarks or gluons. Instead, all detectable particles are colour neutral bound states, such as mesons and baryons, collectively known as hadrons. These hadrons are formed through a nonperturbative mechanism called *Confinement*, which hides the colour charge and binds quarks and gluons into observable composite states. This phenomenon raises the challenge of studying a theory defined in terms of fundamental particles whose connection to experimentally observed particles is not yet fully understood.

In this chapter, we will explore how the *Parton Model*, and later the *Factorization Theorems*, allow the effective application of perturbative QCD in high-energy processes involving hadrons in both the initial and final states. We will discuss how applying these concepts allows us to make predictions of physical observables, which can then be compared to experimental data. Additionally, we will examine the challenges and limitations of this approach, as well as its implications for understanding the structure of hadrons and strong interactions.

1.1 The Structure of Hadrons at High Energies

Towards the end of the 60's there was no established fundamental theory of strong interactions. However, at that time experiments on high-energy proton-proton collisions (above 10 GeV center-of-mass energy) had already shown that the large spectrum of pions produced in the collision was primarily concentrated in a region of phase space that was almost collinear with the collision axis. The probability of producing a pion with relatively large transverse momentum was exponentially suppressed as the transverse momentum increased. This observation led to a picture of the hadron as a loosely bound state of many parts, where the constituents inside a hadron would have momenta nearly collinear with the initial hadron's momentum.

At first sight, this idea seemed paradoxical. How could the strong interaction, known to be extremely powerful, allow a weak coupling behavior? he resolution to this puzzle emerged in 1973 with the theoretical discovery of asymptotic freedom, which explained why the strong force becomes weaker at high energies, allowing the constituents of a hadron to behave as if they were almost free. However, before this breakthrough, the behavior of the strong interaction at high energies remained a complete mystery.

To explore this mystery and test the loosely picture of hadronic structure, Deep Inelastic Scattering (DIS) experiments were run at SLAC and MIT. These experiments

involved an electron beam (with energy up to 21 GeV) scattering off a fixed hydrogen target. A DIS event occurred when the proton was shattered by the electron, producing a large number of hadrons in the final state. Since the detectors were sensitive only to the scattered electrons, the cross section was measured in terms of the 4-momentum transferred from the electron to the proton in the target, through an electromagnetic interaction. At large scattering angles, i.e. large 4-momentum transfer, the results of these measurements were consistent with what would have been expected if the proton were a point-like elementary particle with fractional electric charge.

Parton Distribution Functions

The *Parton Model*, proposed by Feynman [19] and later developed by Bjorken and Paschos [20], provided a framework that combined these experimental results. In this model, the hadrons were described as loosely bounds states of a small number of constituents, referred to as *Partons*. Today, we understand that partons include quarks, gluons, and even antiquarks (strictly speaking, any particle in the Standard Model), but at the time they were introduced, their nature was unknown. The only requirement for these partons was that at least some of them must be electrically charged so that photons could interact with them as point-like particles from QED.

The word "loosely" means that the binding of hadrons happens by continuous exchanges of gluons and quark–antiquark pairs with energies and momenta around Λ_{QCD}, where the strong coupling $\alpha_s \gtrsim 1$ makes these exchanges very likely to happen.Therefore, these binding interactions take place in a time of order

$$\tau_{\text{bind}} \sim 1/\Lambda_{\text{QCD}} \tag{1.1}$$

On the other hand, a high-energy probe with momentum transfer Q interacts in a time

$$\tau_{\text{coll}} \sim 1/Q \tag{1.2}$$

When $Q \gg \Lambda_{\text{QCD}}$ (so that $\tau_{\text{coll}} \ll \tau_{\text{bind}}$), the probe can disturb the binding and see inside the hadron.

In such a scenario, a struck parton escapes from the strong field inside the hadron, interacting with the rest of the system only through soft exchanges that do not significantly alter its momentum shortly before or after the collision. As a result, the remnants of the hadron remain nearly unaffected. This approximated separation of the hadron's internal dynamics from the high-energy interaction (commonly referred to as *Hard Scattering*) allows us to treat them as two incoherent processes. This key theoretical principle is what is addressed as to *Factorization*.

Although partons move in all directions inside a hadron, in its rest frame, their momenta are bounded by the hadron mass. Therefore, when the hadron is boosted along a given direction by a large factor, the longitudinal components of the parton momenta spreads while the transverse components remain essentially unchanged. Consequently, in a reference frame where the hadron carries a very large momentum, the parton momenta become approximately collinear with that of the hadron.

Applying this collinear picture along with the incoherent separation of dynamics, a relativistic flux of composite particles in QCD can be treated as an equivalent collinear flux

of their free constituents, with each constituent carrying a fraction ξ of the total momentum. Such fluxes will be ξ-distributed according to the non-perturbative interactions among the constituents, which will require experimental measurement to determinate them. But as they only depend on the internal dynamics of the hadron, they must be process-independent. These distributions receive the name of *Parton Distribution Functions* (PDFs) also refered to as *Parton Densities*.

The total hadronic cross section is related to the partonic cross section of a perturbatively calculable subprocess, known as the *Hard Scattering*, through the Parton Distribution Functions. Since PDFs describe the distribution of collinear momenta among partons inside the hadron, in a way that resembles a number density (although, we will see they are not), the initial momentum of the parton entering the hard scattering is not fixed but given by a fraction ξ of the hadron's momentum P. Consequently, integration over the different values of ξ is required. Considering that the weight for each ξ value is given by $f_{j/h}(\xi)$, the PDF for a parton j inside a hadron h, the general formula for the total hadronic cross section is given by

$$d\sigma = \sum_j \int_0^1 d\xi f_{j/h}(\xi) d\hat{\sigma}_j(\xi P) \tag{1.3}$$

where $d\hat{\sigma}$ represents the partonic cross section of the hard scattering subprocess involving an initial parton j, and the sum runs over all relevant initial partons in the process. Naturally, both cross sections should be chosen to be differential in the same kinematic variables.

Since the primary goal of the Parton Model was to study the structure of hadrons rather than the interactions that bind partons together, most of its applications were limited to the lowest order in QCD. This restriction spared the Parton Model from the complications that arise when incorporating higher-order QCD corrections, that we will treat in the next sections. Despite this, some important results were obtained from this simple model, the most importants being the Bjorken Scaling and the Callan-Cross relation, that where a demonstration that that proton contains spin 1/2 partons. Those achievements are presented in almost any book on the fundamentals of quantum field theory or quantum chromo-dynamics [21] [22] [23] [24].

Fragmentation Functions

When studying the production of specific final-state hadrons, a new class of non-perturbative functions is required to relate these distributions to the spectra of partons produced in the hard scattering. These are the *Fragmentation Functions* (FFs), previously known as *Decay Functions*. Roughly speaking, a FF $D_{h/j}(z)$ represents the number density of hadrons of a given kind h within a jet initiated by a specific parton j, where the hadron carries a fraction z of the parton's longitudinal momentum.

Fragmentation functions are often considered the counterparts of parton distribution functions, but they encode a fundamentally different phenomena. While PDFs describe the momentum distribution of partons inside a hadron, FFs govern the formation of colorless bound states from colored partons, making them intrinsically linked to colour confinement (one of the most profound and unresolved aspects of QCD). Understanding FFs is therefore crucial for unraveling the mechanism that ensures quarks and gluons are

never observed in isolation. Given their significance, the concept of FFs emerged shortly after the introduction of the Parton Model and PDFs [25][26]. Although their study has been historically less prominent than that of PDFs, several research groups continue to refine our knowledge of FFs, particularly through fits to collider data.

Similar reasoning to that used for PDFs justifies the separation of non-perturbative dynamics in the application of FFs. Specifically, when both the parton and the hadron are highly boosted in the lab frame, they are expected to move in nearly the same direction. Moreover, in this regime, the parton's virtuality (again constrained by the hadron's mass) is negligible compared to its boosted momentum component, allowing it to be approximated as an on-shell particle. The factorized expression for the hadronic cross section has the form

$$E_p \frac{d\sigma_h}{d^3p} = \sum_j \int_0^1 \frac{dz}{z^2} E_k \frac{d\hat{\sigma}_j}{d^3k} D_{h/j}(z) \tag{1.4}$$

where we used $d\hat{\sigma}_j$ to denote the perturbatively calculable parton production cross section (which can be convoluted with PDFs), which considers the inclusive production of an on-shell parton of type j and momentum k.

A small caveat to avoid confusion is that the Particle Data Group (PDG) uses the term "fragmentation function" to refer to both the partonic fragmentation function, and the following normalized cross section:

$$F^h(x, Q) = \frac{1}{\sigma_{\text{tot}}} \frac{d\sigma}{dx}(e^+e^- \to hX)$$

which, in general, differs from the fragmentation function that encapsulates the non-perturbative dynamics of the final state.

The Naïve Parton Model

The first implementation of the Parton Model was merely a heuristic argument based on the kinematics of hadronic processes, as we have just presented. Of course, this is far from a rigorous proof. For this reason, we will refer to this realization of the Parton Model as the *Naïve Parton Model*, since it neither accounts for quantum and radiative corrections nor provides a justification for the factorization of the low-energy dynamics in hadronic processes. Moreover, it does not quantify the order of corrections required for a complete description of QCD processes.

1.2 Improving the Model

As we have just mentioned, the Naïve Parton Model relies on hard processes with simple matrix elements and massless quarks. If we were to naïvely introduce more complex matrix elements or apply corrections to the ones previously discussed, we would encounter infrared divergences in nearly every amplitude. For sufficiently inclusive observables, these divergences cancel in the sum of real and virtual diagrams, as guaranteed by the Kinoshita-Lee-Nauenberg (KLN) theorem. Unfortunately, the usefulness of this theorem diminishes when addressing infrared divergences related to the initial state, as it cannot be treated inclusively, and becomes even less relevant if we aim to analyse specific final states.

This situation might seem problematic, but in reality, it is not. Since PDFs are defined to encapsulate the non-perturbative dynamics of the collision, any collinear or soft radiation is expected to be already accounted for within these distributions, at least up to the scale of non-perturvative interactions Λ_{QCD}. As a result, including these contributions in the hard part of the process would lead to a double counting. Infrared divergences are then not physical, as they are related to this redundancy.

Despite this observation, collinear emissions above the threshold of the non-perturbative effects still pose challenges in calculations, as they give rise to large logarithms that contribute significantly at all orders in perturbation theory. Resuming these terms into the PDFs translates effectively into a redistribution of parton densities at higher scales. The corresponding renormalization group equations that explicitly express this evolution are the famous *Dokshitzer–Gribov–Lipatov–Altarelli–Parisi Equations* (DGLAP).

Before presenting a rigorous derivation of how the renormalization of PDFs and FFs emerges, we will first guide the discussion towards the approach used in [22] which emphasizes conceptual clarity and physical intuition, and is inspired on the method used by Altarelli and Parisi in their foundational work [27]. This will provide a foundation for understanding how the effects we have just mentioned arise naturally in the calculations.

Collinear Gluon Emission

The type of corrections that we are interested in studying are the collinear initial state emissions in the hard scattering subprocess. A straightforward example to study is the case where an initial quark radiates a final state on-shell gluon, as depicted in Fig. 1.1. The hard part of these diagrams is related to an amplitude with the following structure:

$$i\mathcal{M}(q\mathcal{X} \to g\mathcal{Z}) = (...)_j \frac{i\not{k}}{k^2} igT^a_{ji}\gamma^\mu u_i(p)\varepsilon^{a*}_\mu(q) \tag{1.5}$$

In this expression, we show only the part of the amplitude related to the gluon emission. The term $(...)_j$ is a spinor that stands for the rest of the diagram and carries colour index j. The factor $i\not{k}/k^2$ comes from the virtual quark propagator, while the vertex $igT^a_{ji}\gamma^\mu$ describes the gluon emission. The spinor $u_i(p)1$ represents the incoming quark with color i, and $\varepsilon^{a*}_\mu(q)$ is the polarization vector of the outgoing gluon.

The omitted part in (1.5) involves the interaction of the virtual quark with a general target in the state $\mathcal{X}$, which produces the final state $\mathcal{Z}$. In this expression, k is the four-momentum of the quark after emitting a gluon with four-momentum q. As visible from this expression, the amplitude increases rapidly when the intermediate quark approaches the on-shell condition ($k^2 = -2q^0p^0(1-\cos\theta) \to 0$) i.e. when the emitted gluon is soft or collinear to the initial quark.

A key insight in analysing the contribution of these emissions lies in recognizing that the associated amplitude can be factorized into two components: the amplitude of the process without emissions ($q'\mathcal{X} \to \mathcal{Z}$) and the matrix element describing the splitting of a quark into a quark and a gluon ($q \to q'g$). This separation becomes valid in the collinear limit, where the intermediate quark approaches the on-shell condition. In this regime, the numerator of the intermediate propagator can be expressed in terms of

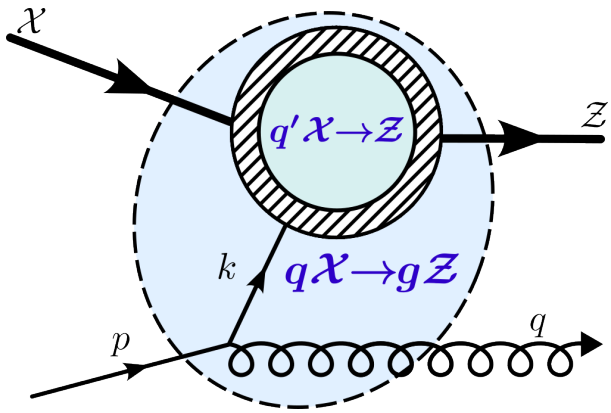

Figure 1.1: Diagram for a hard subprocess involving a quark and a single collinear gluon emission. The dashed lines enclose the entire subprocess while the hatched circle represents the part free from collinear emissions.

polarization-dependent spinors for massless quarks.

$$\not{k} = \sum_{pols} u(k)\overline{u}(k) \tag{1.6}$$

As a result, the gluon emission vertex and the remainder of the amplitude can be separated by contracting each part with on-shell spinors for a massless quark. The amplitude for the full process can be then rewritten as

$$i\mathcal{M}(q\mathcal{X} \to g\mathcal{Z}) = \sum_n \frac{i}{k^2}\mathcal{M}(q \to q'_n g) \cdot \mathcal{M}(q'_n\mathcal{X} \to \mathcal{Z}) \tag{1.7}$$

$$\mathcal{M}(q \to q'_n g) = ig\overline{u}_j(k)T^a_{ij}\gamma^\mu u_i(p)\epsilon^{a*}_\mu(q) \tag{1.8}$$

where the subscript n denotes the polarization and colour state of the intermediate quark, which must be the same for both parts of the diagram.

It is natural to ask whether the separation of amplitudes in (1.7) still holds after squaring the total amplitude. Due to helicity and color charge conservation at the quark-gluon vertex, the polarization and color of the intermediate quark are fully determined by those of the external quark and gluon. This implies that there is no interference between different intermediate states in (1.7), because only one of them is different from zero. Therefore, for an unpolarized process, the spin and colour averaged squared amplitude of the full process can be written as

$$\left|\overline{\mathcal{M}}(q\mathcal{X} \to g\mathcal{Z})\right|^2 = \frac{1}{2N_c}\frac{1}{N_\mathcal{X}}\sum|\mathcal{M}(q\mathcal{X} \to g\mathcal{Z})|^2 \tag{1.9}$$

$$= \frac{1}{2N_c}\frac{1}{N_\mathcal{X}}\sum|\mathcal{M}(q \to q_n g)|^2\frac{1}{k^4}|\mathcal{M}(q_n\mathcal{X} \to \mathcal{Z})|^2 \tag{1.10}$$

where the sum runs over the polarization and colour state of the initial quark, the final gluon, and the states $\mathcal{X}$ and $\mathcal{Z}$. The value of $N_\mathcal{X}$ is the number of colour-helicity configurations that the $\mathcal{X}$ state can have. In general, there are multiple ways to obtain the same value of n from the external particles.

The colour and parity symmetries of QCD ensure that the squared amplitudes are invariant under global rotations of all colour states and simultaneous flips of all helicities.

Because of this, when we sum over the squared amplitudes for all external quark and gluon helicities and colors, such that the total only depends on the configuration of the intermediate quark, these symmetries guarantee that the result is the same for any choice of intermediate quark color and helicity. As a result, we can relate the sum over squared splitting amplitudes for each fixed intermediate configuration m to the fully averaged squared amplitude, as if the intermediate quark were a final-state particle:

$$\sum_{\ell k} |\mathcal{M}(q_\ell \to q_n g_k)|^2 \delta_{nm} = \frac{1}{2N_c} \sum_{m\ell k} |\mathcal{M}(q_\ell \to q_n g_k)|^2 \delta_{nm} = \left|\overline{\mathcal{M}}(q \to q' g)\right|^2 \tag{1.11}$$

The importance of this observation is that it allows us to rewrite the expression (1.10) in a way that completely decouples the splitting squared amplitudes from those of the remaining part of the entire process.

$$\begin{aligned}
\left|\overline{\mathcal{M}}(q\mathcal{X} \to g\mathcal{Z})\right|^2 =& \frac{1}{2N_c}\frac{1}{N_\mathcal{X}} \sum_{\mathcal{X}\mathcal{Z}} \left[\sum_{\ell k} |\mathcal{M}(q_\ell \to q_n g_k)|^2\right] \frac{1}{k^4} |\mathcal{M}(q'_n \mathcal{X} \to \mathcal{Z})|^2 && (1.12)\\
=& \frac{1}{2N_c}\frac{1}{N_\mathcal{X}} \sum_{\mathcal{X}\mathcal{Z}} \sum_m \left[\sum_{\ell k} |\mathcal{M}(q_\ell \to q_n g_k)|^2 \delta_{nm}\right] \frac{1}{k^4} |\mathcal{M}(q'_m \mathcal{X} \to \mathcal{Z})|^2 && (1.13)\\
=& \frac{1}{2N_c}\frac{1}{N_\mathcal{X}} \sum_{\mathcal{X}\mathcal{Z}} \sum_m \left|\overline{\mathcal{M}}(q \to q' g)\right|^2 \frac{1}{k^4} |\mathcal{M}(q'_m \mathcal{X} \to \mathcal{Z})|^2 && (1.14)\\
=& \left|\overline{\mathcal{M}}(q \to q' g)\right|^2 \frac{1}{k^4} \left[\sum_{\mathcal{X}\mathcal{Z}} \sum_m \frac{1}{2N_c}\frac{1}{N_\mathcal{X}} |\mathcal{M}(q'_m \mathcal{X} \to \mathcal{Z})|^2\right] && (1.15)\\
=& \left|\overline{\mathcal{M}}(q \to q' g)\right|^2 \frac{1}{k^4} \left|\overline{\mathcal{M}}(q'\mathcal{X} \to \mathcal{Z})\right|^2 && (1.16)
\end{aligned}$$

Using this result, we will be able to analyze the nature of collinear emissions in general, regardless of the process in which they are involved.

Splitting Amplitudes

To explicitly evaluate the amplitudes related to the gluon emission, let us consider that the initial quark moves along the third direction. The on-shell gluon and the intermediate quark momenta will slightly deviate from this axis, by carrying a small transverse momentum k_t, for instance, in the second direction. As their momenta remain primarily aligned with the initial quark's motion, we can define z as the fraction of longitudinal momentum that the quark retains after the emission. Consequently, up to terms $\mathcal{O}(k_t^2)$, the momenta of the particles involved can be expressed as

$$p^\mu = (p, 0, 0, p) \qquad p^2 = 0 \tag{1.17}$$

$$q^\mu = ((1-z)p, 0, -k_t, (1-z)p) - \frac{k_t^2}{2(1-z)p}\hat{\boldsymbol{e}}_3 \qquad q^2 = 0 \tag{1.18}$$

$$k^\mu = (zp, 0, k_t, zp) + \frac{k_t^2}{2(1-z)p}\hat{\boldsymbol{e}}_3 \qquad k^2 = -\frac{k_t^2}{1-z} \tag{1.19}$$

where $\hat{\boldsymbol{e}}_3 = (0, 0, 0, 1)$ is the unit vector along the third direction. Notice that $\mathcal{O}(k_t^2)$ terms have been explicitly separated in these definitions, as they will only appear in the denominator of the quark propagator, which gets no contribution from lower orders. In

contrast, the splitting amplitudes will start already at order $\mathcal{O}(k_t)$, so in the rest of the calculation we can keep in mind just the first part of these definitions.

Regarding the polarization of external particles, by the quark helicity conservation property of the quark-gluon vertex, we have 4 non-zero amplitudes

$$\mathcal{M}_1(q_L \to q_L g_L) \qquad \mathcal{M}_2(q_L \to q_L g_R) \qquad \mathcal{M}_3(q_R \to q_R g_R) \qquad \mathcal{M}_4(q_R \to q_R g_L) \tag{1.20}$$

but the parity symmetry of QCD allows us to directly tell that $\mathcal{M}_1 = \mathcal{M}_3$ and $\mathcal{M}_2 = \mathcal{M}_4$, so we can calculate just those where the quarks are left-handed.

Working in the chiral representation, the corresponding expression for the left-handed spinor for the initial quark is given by

$$u_L(p) = \sqrt{2p}\begin{pmatrix}\xi(p)\\0\end{pmatrix} \qquad\qquad \xi(p) = \begin{pmatrix}0\\1\end{pmatrix} \tag{1.21}$$

Since the intermediate quark is slightly deflected from the third axis, in which lies the initial quark's momentum direction, its corresponding spinor will have a similar expression but rotated by the same small angle $\theta_q = k_t/zp$ as its momentum.

$$u_L(k) = \sqrt{2zp}\begin{pmatrix}\xi(k)\\0\end{pmatrix} \qquad\qquad \xi(k) = (1 + i\sigma_2\theta_q/2)\begin{pmatrix}0\\1\end{pmatrix} = \begin{pmatrix}\dfrac{k_t}{2zp}\\1\end{pmatrix} \tag{1.22}$$

Similarly, to get the emitted gluon polarization vectors, the common definition of the polarization vectors in the third direction

$$\varepsilon_R^*(q) = \frac{1}{\sqrt{2}}(0, i, 1, 0) \qquad\qquad \varepsilon_L^*(q) = \frac{1}{\sqrt{2}}(0, -i, 1, 0) \tag{1.23}$$

needs to be rotated by an angle $\theta_g = -k_t/(1-z)p$ in the direction of the gluon's deflection.

$$\varepsilon_R^*(q) = \frac{1}{\sqrt{2}}\left(0, i, 1, \frac{-k_t}{(1-z)p}\right) \qquad \varepsilon_L^*(q) = \frac{1}{\sqrt{2}}\left(0, -i, 1, \frac{-k_t}{(1-z)p}\right) \tag{1.24}$$

Inserting these definitions inside the equation (1.8), we get the following expressions for the needed left-handed quark splitting amplitudes

$$i\mathcal{M}(q_L \to q_L g_L) = ig\frac{\sqrt{2z}}{1-z}k_t T^a_{ji} \qquad i\mathcal{M}(q_L \to q_L g_R) = ig\frac{\sqrt{2z}}{z(1-z)}k_t T^a_{ji} \tag{1.25}$$

where the indices i, a, and j, are related to the colour of the initial quark, the final gluon, and the intermediate quark, respectively. Using these results, the averaged squared splitting amplitude is

$$\begin{aligned}\left|\overline{\mathcal{M}}(q \to q'g)\right|^2 &= \left[\frac{1}{N_c}\sum_{aij} T^a_{ji}T^a_{ij}\right] 2g^2\left(\frac{k_t^2}{z(1-z)}\right)\left(\frac{1+z^2}{1-z}\right) \\ &= 2g^2 C_F\left(\frac{k_t^2}{z(1-z)}\right)\left(\frac{1+z^2}{1-z}\right)\end{aligned} \tag{1.26}$$

where $C_F = (N_c^2 - 1)/2N_c = 4/3$ in QCD.

Splitting Function

Having computed all the pieces needed to get the contribution of the collinear emissions shown in Fig. 1.1, we now show that the complete partonic cross section

$$d\hat{\sigma}(q\mathcal{X} \to g\mathcal{Z}) = \frac{1}{(1+v_{\mathcal{X}})2p2E_X}\left|\overline{\mathcal{M}}(q\mathcal{X} \to g\mathcal{Z})\right|^2 \frac{d^3q}{2q^0(2\pi)^2} d\Pi_{\mathcal{Z}} \tag{1.27}$$

where $v_{\mathcal{X}}$ is the velocity of $\mathcal{X}$ and $d\Pi_{\mathcal{Z}}$ is the phase space of $\mathcal{Z}$, can be understood as the product of a splitting probability and the partonic cross section of the remaining part of the process. To prove this statement, let us replace the squared amplitude of the entire process with our recent finding in the equation (1.16).

$$d\hat{\sigma}(q\mathcal{X} \to g\mathcal{Z}) = \frac{1}{(1+v_{\mathcal{X}})2p2E_X}\left|\overline{\mathcal{M}}(q \to q'g)\right|^2 \frac{1}{k^4}\left|\overline{\mathcal{M}}(q'\mathcal{X} \to \mathcal{Z})\right|^2 \frac{d^3q}{2q^0(2\pi)^2} d\Pi_{\mathcal{Z}} \tag{1.28}$$

Then, we change the variables related to the integral measure over the q^μ phase space, to the variables z and k_t^2 from (1.18) that we already used to calculate the splitting amplitudes:

$$\frac{d^3q}{2q^0(2\pi)^3} = \frac{dq_3 d^2q_t}{2q^0(2\pi)^3} = \frac{1}{16\pi^3}\frac{dz d^2k_t}{1-z} \Rightarrow \frac{1}{16\pi^2}\frac{dz dk_t^2}{1-z} \tag{1.29}$$

By doing so, we can construct the expression of the corresponding partonic cross section without emissions inside the complete expression (1.28), obtaining the following:

$$d\hat{\sigma}(q\mathcal{X} \to g\mathcal{Z}) = \frac{1}{16\pi^2}\frac{dz dk_t^2}{1-z}\left|\overline{\mathcal{M}}(q \to q'g)\right|^2 \frac{z}{k^4}\left[\frac{1}{(1+v_X)2zp2E_X}\left|\overline{\mathcal{M}}(q'\mathcal{X} \to \mathcal{Z})\right|^2 d\Pi_Z\right] \tag{1.30}$$

$$= \frac{dk_t^2}{k_t^4}\frac{dz}{16\pi^2} z(1-z)\left|\overline{\mathcal{M}}(q \to q'g)\right|^2 d\hat{\sigma}(q'X \to \mathcal{Z}) \tag{1.31}$$

where we aditionally replaced $k^4 = k_t^4/(1-z)$, according to the (1.19) definitions.

To derive the corresponding expression of the emission probability, we substitute the unpolarized, colour-averaged, squared splitting amplitude from (1.26) into the differential cross-section.

$$d\hat{\sigma}(q\mathcal{X} \to g\mathcal{Z}) = dz\frac{dk_t^2}{k_t^2}\frac{\alpha_s}{2\pi}C_F\left[\frac{1+z^2}{1-z}\right] d\hat{\sigma}(q'X \to \mathcal{Z}) \tag{1.32}$$

Finally, we integrate over the squared transverse momentum k_t^2. To do so, recall that the virtuality of the intermediate quark (1.19) is proportional to k_t^2. Since particles with large virtualities exist only for short times, the transverse momentum of the intermediate quark can be related to the scale of the hard process. Consequently, the upper limit of the k_t^2 integration should be Q, while the lower limit is set to Q_0, whose significance will be explored later.

$$d\hat{\sigma}(q\mathcal{X} \to g\mathcal{Z}) = \ln\left(\frac{Q^2}{Q_0^2}\right)\frac{\alpha_s}{2\pi} dz C_F\left[\frac{1+z^2}{1-z}\right] d\hat{\sigma}(q'\mathcal{X} \to \mathcal{Z}) \tag{1.33}$$

From the previous result, we can naïvely identify the *quark-to-quark Splitting Function*, which describes the first correction to the quark distribution as a function of the momentum fraction z retained by the quark after gluon emission:

$$\widetilde{P}_{qq}(z) = C_F\left[\frac{1+z^2}{1-z}\right] \tag{1.34}$$

The tilde on $\widetilde{P}_{qq}(z)$ indicates that this expression is not complete. In particular, it contains an infrared divergence in the limit $z \to 1$, corresponding to the emitted gluon becoming soft.

However, such soft divergences cancel when both real emissions and virtual corrections are included. This implies that the corresponding virtual corrections to the partonic cross section $d\hat{\sigma}_{q\mathcal{X}\to\mathcal{Z}}(p)$, which we have not computed here, must contain a soft singularity that cancels the divergence from the real emission.

The total finite contribution is obtained by combining the real corrections, where the quark emits a gluon and retains a momentum fraction z of its initial momentum (integrated over all z), with the virtual correction and the leading term, which correspond to the case with no gluon emission ($z = 1$):

$$\int_0^1 dz\left[\ln\left(\frac{Q^2}{Q_0^2}\right)\frac{\alpha_s}{2\pi}\widetilde{P}_{qq}(z) + \delta(1-z)\left(1+\ln\left(\frac{Q^2}{Q_0^2}\right)\frac{\alpha_s}{2\pi}A\right)\right]d\hat{\sigma}_{q\mathcal{X}\to\mathcal{Z}}(zp) \tag{1.35}$$

Here, A denotes the soft-divergent term of order α_s that arises from the virtual corrections.

We can determine the value of A by interpreting the bracketed expression in eq. (1.35) as a distribution describing the momentum fraction carried by the quark after gluon emission. Since we are only considering gluon radiation, the total number of quarks must be conserved. Therefore, the integral over the entire distribution must give unity:

$$\int_0^1 dz\left[\ln\left(\frac{Q^2}{Q_0^2}\right)\frac{\alpha_s}{2\pi}\widetilde{P}_{qq}(z) + \delta(1-z)\left(1+\ln\left(\frac{Q^2}{Q_0^2}\right)\frac{\alpha_s}{2\pi}A\right)\right] = 1 \tag{1.36}$$

As we mentioned before, the integral over $\widetilde{P}_{qq}(z)$ is divergent. To handle this, we introduce a soft cut-off λ to regularize the expression. In this way, we can solve the normalization condition, and the divergent part from the virtual correction becomes

$$A = -\lim_{\lambda\to 0}\int_0^{1-\lambda} dz C_F\frac{1+z^2}{1-z} = \lim_{\lambda\to 0} C_F\left(\frac{3}{2}+2\ln\lambda\right). \tag{1.37}$$

With this result, the complete and finite quark-to-quark splitting function can be regularized and written as

$$P_{qq}(x) = \lim_{\lambda\to 0}\left\{\widetilde{P}_{qq}(x)\theta(1-\lambda-x) + A(\lambda)\delta(1-x)\right\} \tag{1.38}$$

$$= C_F\lim_{\lambda\to 0}\left\{\frac{1+x^2}{1-x}\theta(1-\lambda-x) + \left(\frac{3}{2}+2\ln\lambda\right)\delta(1-x)\right\}. \tag{1.39}$$

The previous expression can be written in a more elegant way by realizing that $\delta(1-x)$ and hence $P_{qq}(x)$ is a distribution. Therefore, to regularize the splitting function we use the *Plus Prescription*, defined by its action on a function $g(x)$ (which is regular at $x = 1$):

$$\frac{1}{(1-x)} \Rightarrow \frac{1}{(1-x)_+} \qquad \int dx\frac{g(x)}{(1-x)_+} = \int dx\,\frac{g(x)-g(1)}{(1-x)} \tag{1.40}$$

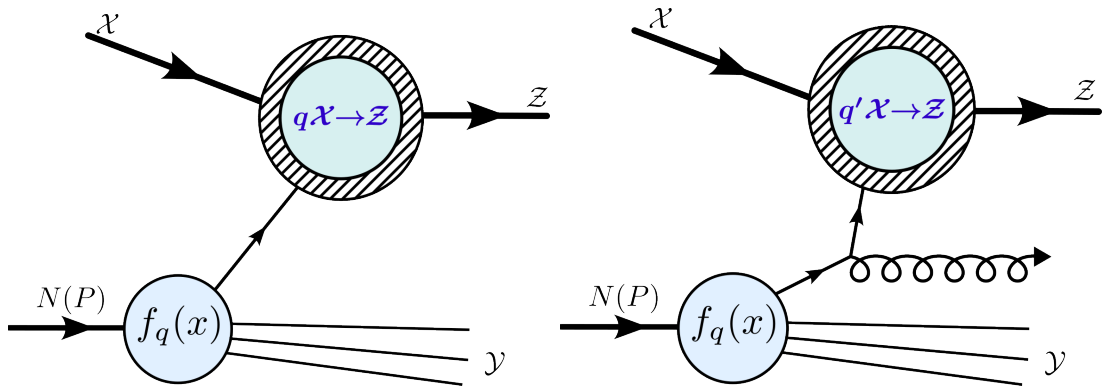

Figure 1.2: Representative diagrams for a hard scattering process involving quarks. The left diagram shows the lowest-order contribution, while the right diagram includes the first radiative correction from collinear gluon emission in the initial state. In inclusive processes, both configurations contribute to the observed parton distributions.

This distribution eliminates the need to introduce the soft cut-off λ and take the limit of the difference between two diverging quantities, enabling us to write

$$P_{qq}(x) = C_F\left(\frac{1+x^2}{(1-x)_+} + \frac{3}{2}\delta(1-x)\right). \tag{1.41}$$

Evolution of Parton Densities

As discussed earlier in this section, the parton distribution functions (or parton densities) encapsulate all the initial non-perturbative effects of the collision i.e. radiation occurring below the characteristic scale of non-perturbative interactions Λ_{QCD}. However, in practice, the situation is more nuanced. From a phenomenological perspective, since we generally do not compute the hard process to all orders in the strong coupling, the distributions observed in experiments can also include collinear radiation extending up to the hard scale of the process (Q). As this scale increases, it is natural to expect a corresponding variation in these distributions.

The use of PDFs inherently assumes that the process under study is, to some extent, inclusive. This means we cannot differentiate between scenarios where partons lose energy due to collinear emissions and those where no such emissions occur, as long as the parton that participates in the hard scattering carries the same momentum (Otherwise, the kinematics would differ). Therefore, we should always consider that inclusive processes account for both cases illustrated in Fig. 1.2.

To explore the impact of collinear contributions on PDFs, consider a general scenario where a nucleon N undergoes an inelastic scattering with a state $\mathcal{X}$, such that only a single quark flavour inside N participates in the hard subprocess, interacting with $\mathcal{X}$ and producing a final state $\mathcal{Z}$ (as shown in Fig. 1.1). Additionaly, suppose the PDF of a quark inside N has been determined at a reference scale Q_0. The objective is to examine how collinear emissions between Q_0 and a slightly higher scale Q are resummed into the PDF, and how this addition makes it evolve. To study this effect, let us roughly use the PDF measured at Q_0 to compute the total hadronic cross section of the process occurring at the scale Q, so the factorized expression is

$$d\sigma_{N\mathcal{X}} = \int dx f_{q/N}(x, Q_0) d\hat{\sigma}_{q\mathcal{X}}(x, Q, Q_0) \tag{1.42}$$

where x is the hadron's momentum fraction that the initial quark carries.

The partonic cross section $d\hat{\sigma}_{q\mathcal{X}}$ in equation (1.42) is not just the cross section for the subprocess $q\mathcal{X} \to \mathcal{Z}$ it also contains terms corresponding to the subprocess $q\mathcal{X} \to g\mathcal{Z}$ which includes the emission of a collinear gluon between the scales Q_0 and Q (or many more if these scales are not so close), as they are not present in $f_q(x, Q_0)$.

$$d\hat{\sigma}_{q\mathcal{X}}(x, Q, Q_0) = d\hat{\sigma}_{q\mathcal{X}\to\mathcal{Z}}(x, Q) + d\hat{\sigma}_{q\mathcal{X}\to g\mathcal{Z}}(x, Q, Q_0) \tag{1.43}$$

$$= d\hat{\sigma}_{q\mathcal{X}\to\mathcal{Z}}(x, Q) + \ln\left(\frac{Q^2}{Q_0^2}\right)\frac{\alpha_s}{2\pi}\int dz P_{qq}(z) d\hat{\sigma}_{q\mathcal{X}\to\mathcal{Z}}(zx, Q) \tag{1.44}$$

$$= \int dz\left[\delta(1-z) + \ln\left(\frac{Q^2}{Q_0^2}\right)\frac{\alpha_s}{2\pi}P_{qq}(z)\right] d\hat{\sigma}_{q\mathcal{X}\to\mathcal{Z}}(zx, Q) \tag{1.45}$$

The first term represents the scenario with no gluon emission, while the second term accounts for the case where the emitted gluon carries a momentum fraction $1 - z$ of the quark's initial momentum, leaving the quark with a reduced momentum fraction zx from the hadron's momentum.

As you can see from expression (1.45) the momentum fraction of the quark involved in the hard scattering is not x nor z, but its product $\xi = xz$. To express the complete hadronic cross section in terms of a convolution over ξ, let us change variables from $(x.z)$ to (ξ, z) (notice that the integrals over x and z run from 0 to 1).

$$d\sigma_{N\mathcal{X}} = \iint dx dz f_{q/N}(x, Q_0)[...](z) d\hat{\sigma}_{q\mathcal{X}\to\mathcal{Z}}(zx, Q)\int d\xi\,\delta(\xi - zx) \tag{1.46}$$

$$= \iint \frac{d\xi dz}{z}\int dx\,\delta\left(x - \frac{\xi}{z}\right) f_{q/N}(x, Q_0)[...](z) d\hat{\sigma}_{q\mathcal{X}\to\mathcal{Z}}(zx, Q) \tag{1.47}$$

$$= \int d\xi\left(\int_\xi^1 \frac{dz}{z} f_{q/N}\left(\frac{\xi}{z}, Q_0\right)[...](z)\right) d\hat{\sigma}_{q\mathcal{X}\to\mathcal{Z}}(\xi, Q) \tag{1.48}$$

where the omited term $[...](z)$ is the bracketed term from (1.45). This last expression bears a clear resemblance to the standard (naïve) parton model formula, as the partonic cross section now contains only the hard scattering subprocess, without emissions. This becomes more evident if we define

$$f_{q/N}(z, Q) = f_{q/N}(z, Q_0) + \ln\left(\frac{Q^2}{Q_0^2}\right)\frac{\alpha_s}{2\pi}\int_z^1 \frac{dy}{y} P_{qq}(y) f_{q/N}\left(\frac{z}{y}, Q_0\right) \tag{1.49}$$

as the PDF of a quark inside N evaluated at $Q > Q_0$. In this way, the hadronic cross section can be rewritten as

$$d\sigma_{N\mathcal{X}} = \int d\xi\, f_{q/N}(\xi, Q)\, d\sigma_{qX\to\mathcal{Z}}(\xi, Q), \tag{1.50}$$

where the resemblance to the parton model is now explicit.

For an infinitesimal increment in the process scale, we can rearrange the redefinition of the quark PDF as an integro-differential equation that resembles those of the renormalization group.

$$\frac{df_{q/N}(\xi, Q)}{d\ln Q^2} = \frac{\alpha_s}{2\pi}\int_\xi^1 \frac{dz}{z} P_{qq}(z) f_q(\xi/z, Q) \tag{1.51}$$

DGLAP Equations

What we have presented in equation (1.51) is just one component of a system of $2N_f + 1$ coupled differential equations (where N_f is the number of active quark flavors), known as the *Dokshitzer–Gribov–Lipatov–Altarelli–Parisi* (DGLAP) equations. Denoting the PDFs with the letter of its respective parton, the DGLAP equations can be expressed as

$$\frac{d}{d\ln Q^2}\begin{pmatrix} q_k(\xi,\mu) \\ g(\xi,\mu) \\ \bar{q}_k(\xi,\mu) \end{pmatrix} = \sum_\ell \frac{\alpha_s}{2\pi}\int_\xi^1 \frac{dz}{z}\begin{pmatrix} P_{qq}(z,Q) & P_{qg}(z,Q) & P_{q\bar{q}}(z,Q) \\ P_{gq}(z,Q) & P_{gg}(z,Q) & P_{g\bar{q}}(z,Q) \\ P_{\bar{q}q}(z,Q) & P_{\bar{q}g}(z,Q) & P_{\bar{q}\bar{q}}(z,Q) \end{pmatrix}\begin{pmatrix} q_\ell(\xi/z,\mu) \\ g(\xi/z,\mu) \\ \bar{q}_\ell(\xi/z,\mu) \end{pmatrix} \tag{1.52}$$

These equations describe the Q^2 evolution of parton densities within a given hadron. They were independently derived by Dokshitzer in 1977 [28], by Altarelli and Parisi [27] in the same year, an by Gribov and Lipatov in 1972 [29].

The splitting functions act as the kernels of this evolution and can be computed analytically by expanding them perturbatively in the strong coupling constant:

$$P_{ab}(z,\alpha_s) = P_{ab}^{[0]}(z) + \frac{\alpha_s}{2\pi}P_{ab}^{[1]}(z) + \dots \tag{1.53}$$

Only the first term of this expansion can be computed using techniques similar to those we employed in the derivation of $P_{qq}(z)$. For higher-order terms, it is more convenient to work within formal theoretical frameworks, which we will introduce in the following sections.

As evident from equation (1.52), the full DGLAP evolution incorporates additional splitting processes, such as gluon splitting ($g \to q\bar{q}$ and $g \to gg$) and quark radiation ($q \to qg$). At leading order (LO), the nonzero splitting functions are given by:

$$P_{qq'}^{[0]}(z) = \delta_{qq'}C_F\left[\frac{1+z^2}{(1-z)_+} + \frac{3}{2}\delta(1-z)\right] \tag{1.54}$$

$$P_{qg}^{[0]}(z) = T_F\left[z^2 + (1-z)^2\right] \tag{1.55}$$

$$P_{gq}^{[0]}(z) = C_F\left[\frac{1+(1-z)^2}{z}\right] \tag{1.56}$$

$$P_{gg}^{[0]}(z) = 2C_A\left[\frac{1-z}{z} + \frac{z}{(1-z)_+} + z(1-z)\right] + \frac{\beta_0}{2}\delta(1-z) \tag{1.57}$$

where $T_F = 1/2$, $C_A = N_c = 3$, $C_F = (N_c^2 - 1)/2N_c = 4/3$, and $\beta_0 = (11C_A - 4N_fT_F)/3$, in QCD. The Kronecker delta enforces flavor conservation. By charge parity conservation, the splitting functions involving antiquarks have the same values as those for quarks.

A similar equation describes the coupled Q^2 evolution of the fragmentation functions associated with final-state hadrons. These two evolution equations are usually distinguished by the sign of the parton virtuality; PDFs correspond to space-like partons, while FFs correspond to time-like partons. The only practical difference between these two equations lies in the values of the corresponding splitting functions. At LO, the splitting functions for FFs are identical to their space-like counterparts; however, differences arise at next-to-leading order and beyond. Since the analytical expressions at higher orders are too lengthy to be displayed here, we refer the reader to [30] and [31] for the NLO expressions of space-like and time-like evolutions, respectively. The NNLO expressions can be found in [32] and [33].

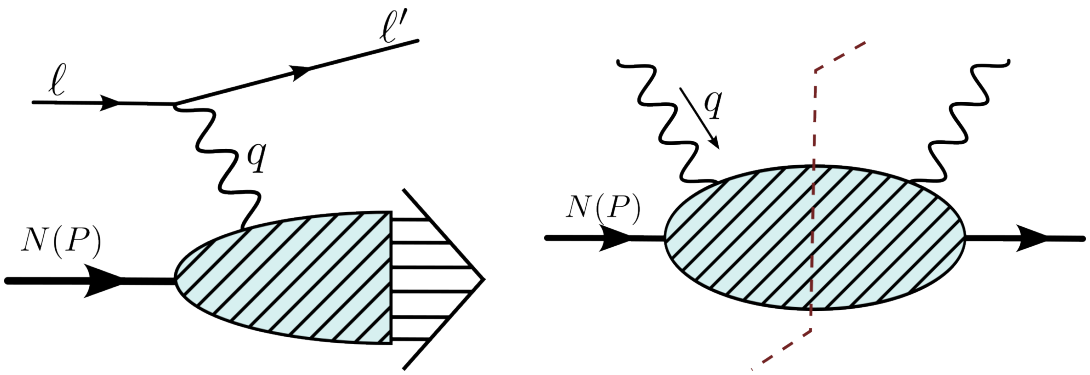

Figure 1.3: On the left, a diagram of the DIS process is shown, where an electron scatters off a proton N with initial momentum P via the exchange of a virtual photon with momentum q. On the right, the cut diagram illustrates the definition of the hadronic tensor.

1.3 Collinear Factorization

While the parton model has provided an intuitive picture to understand high-energy hadronic processes, it does not come from a formal derivation within QCD. To go beyond this limitation, a more systematic framework was developed by J. Collins and collaborators, who established a theoretical proof of the factorization theorems. Each of these theorems states that it is possible to separate the effects coming from different dynamical scales in a given process. In this approach, PDFs and FFs are defined through lightcone projections of proton matrix elements [34], giving a precise field operator definition that is consistent with QCD. This formalism not only improves the conceptual understanding of factorization but also makes clear the assumptions and conditions under which it holds. A comprehensive review can be read in [35]. Thus, a brief overview of the fundamental caracteristics of this perspective will be of great help to understand how to correctly apply factorization to QCD.

A crucial subtlety about the naïve parton model is that it does not hold literally for most quantum field theories. As discussed in [36], its validity requires super-renormalizable theories that are not based on gauge invariance principles (both integral aspects of QCD). This is not a surprise: we have already seen that DGLAP equations modify the values of PDFs and FFs in QCD. However, the foundational ideas of the parton model are so general that it is reasonable to view it as an approximation to QCD. Therefore, to understand how the naïve parton model must be modified to accommodate the complexities of QCD, it is instructive to start examining the scenario where the naïve parton model is valid, i.e. correct to the leading power of the hard scale.

A rigorous derivation of the results we will present require introducing several advanced tools and extensive formalism, as done by J. C. Collins in his famous book [36]. Of course, this lies far beyond the scope of this thesis. Instead, we will take these results as given, providing only a few remarks of the approximations that have been done. This way, we will have freedom to focus on the key conclusions that will be relevant for our later discussions, while also having a general idea of where this framework comes from.

Factorization of Simple Theories

Basic ideas about the space-time structure of Deep Inelastic Scattering (DIS) inspired the development of the naïve parton model. Due to this close connection, DIS is the most natural and straightforward process in which factorization can be rigorously established. We will therefore focus our discussion on the DIS case, as it provides a clear and controlled setting to illustrate the key assumptions and general features of the Collinear Factorization framework.

In this process, depicted in Fig. 1.3, a high-energy lepton scatters off a proton via the exchange of a virtual photon. When the momentum transfer $Q^2 = -q^2$ is sufficiently large, the virtual photon probes short distances and effectively resolves the quark content inside the hadron. As a result, the nucleon breaks apart, producing a multitude of hadrons.

Neglecting the lepton and proton masses, the DIS cross section can be expressed (without assumptions) using the optical theorem as

$$E' \frac{d\sigma_{\ell N \to \ell X}}{d^3 l'} = \frac{2\alpha^2}{SQ^4} L_{\mu\nu} W^{\mu\nu}(P, q) \tag{1.58}$$

where S is the squared center-of-mass energy, α is the electromagnetic coupling, and $L_{\mu\nu}$ is the leptonic tensor, which contains the contribution from the QED vertex of the scattered lepton. The non-perturbative QCD dynamic describing the hadron's response to the virtual photon is encoded in the hadronic tensor $W^{\mu\nu}(P, q)$, which is defined in [36] as

$$W^{\mu\nu}(P, q) = \frac{1}{4\pi} \int d^4 z \, e^{iq\cdot z} \langle N(P) | [J^\mu(z), J^\nu(0)] | N(P) \rangle \tag{1.59}$$

where J^μ denotes the electromagnetic current of quarks.

To formulate the parton model within the framework of Quantum Field Theory, we must prove that the dominant contributions to the DIS process stem from cut diagrams resembling the *Handbag Diagram* in Fig. 1.4, while higher corrections remain suppressed (those involving interactions with the remnants). Such a demonstration is not an easy task, but let us consider this idealized scenario where the naïve parton model is valid. For that case, the subgraphs enclosed by regions L and U correspond to lines collinear to the target and the struck quark, respectively, and the related hadronic tensor has the following general structure

$$W^{\mu\nu} = \frac{e_q^2}{4\pi} \int \frac{d^4 k}{(2\pi)^4} \mathrm{Tr}[\gamma^\mu U(k+q) \gamma^\nu L(k, P)] \tag{1.60}$$

where the trace runs over colour and Dirac indices. The functions U and L are general matrices in the spinor space, encoding the contributions from their respective subdiagrams (or bubbles).

A particulart convenient frame to analyze the kinematics of a DIS process is the so called *Breit Frame*, a reference frame in which the four-momentum transfer q^μ carried by the virtual photon is purely spatial. By orienting the photon along the $-\hat{e}_3$ direction and assuming that the proton's momentum in the $\hat{e}_3$ direction is large enough to neglect its mass, their momenta are expressed as

$$q_\mu = (0, \mathbf{0}_\mathrm{T}, -Q) \qquad\qquad P_\mu = (P, \mathbf{0}_\mathrm{T}, P) \tag{1.61}$$

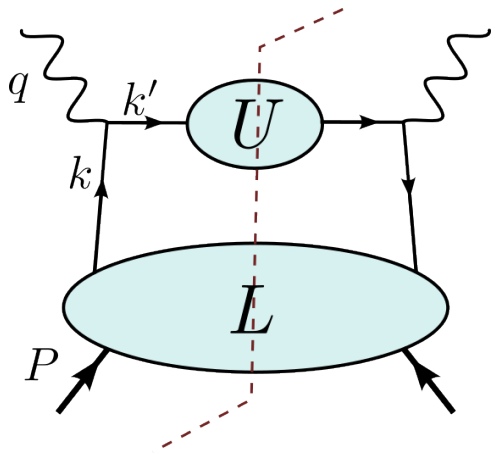

Figure 1.4: Schematic diagram representing the leading contribution to a DIS process within the Collinear Factorization framework. A quark inside the nucleon is struck by the virtual photon and exits the hadron without interacting with the remnants.

In this frame, quarks (and electrons) retain their initial energy, scattering elastically as if rebounding off a rigid surface. This defining feature is what gives this frame the alternative name of *Brick Wall Frame*.

However, while choosing a convenient reference frame simplifies the kinematics, obtaining a factorized expression for DIS requires more than that. It also demands a careful separation of contributions related to the parton kinematics from the rest of the diagram. This involves making controlled approximations (collectively referred to as the *Parton Approximator*) about the behavior of the upper (U) and lower (L) subdiagrams as functions of momenta, hoping they allow us to undo the convolution between both bubbles.

A powerful tool to carry out this separation is given by *Light-Cone Coordinates*, a coordinate system in which any four-vector V^μ is written as $(V^+, V^-, \boldsymbol{V}_\mathrm{T})$, where $V^\pm = (V^0 \pm V^3)/\sqrt{2}$. In this basis, boosts along the third axis act in a very simple way, changing the plus and minus components by a multiplicative factor, $V^+ \to e^\eta V^+$ and $V^- \to e^{-\eta} V^-$, where η is the rapidity of the boost. Because of this, the light-cone coordinates are useful to identify how different momentum components behave as Q becomes large. Writing the relevant momenta in this form gives:

$$q_\mu = (-x_B P^+, Q/\sqrt{2}, \mathbf{0}_\mathrm{T}) \qquad P_\mu = (P^+, 0, \mathbf{0}_\mathrm{T}) \tag{1.62}$$

$$k^\mu = \left(\xi P^+, k^-, \boldsymbol{k}_\mathrm{T}\right) \qquad k'^\mu = \left((\xi - x_B)P^+, Q + k^-, \boldsymbol{k}_\mathrm{T}\right) \tag{1.63}$$

where $x_B = Q^2/(2P \cdot q) = Q/\sqrt{2}P^+$ in the Breit frame. Here, the plus-momentum of the incoming quark is given by a fraction ξ of the hadron's momentum, which can differ from the Bjorken variable x_B. Unlike in the simple approximation to DIS that the naïve parton model gave us, we now allow partons to carry nonzero transverse momentum, a crucial feature to address the full complexity of QCD and moving beyond a purely collinear picture.

A first step towards the intended factorization is to decouple the integration of the subdiagrams U an L. While not immediately obvious, it can be shown that the upper part U is approximately insensitive to the small momentum components transferred from L. Since the initial quark is highly boosted from its rest frame, its plus component k^+ must be the largest component. Therefore, for the relevant contributions, we can neglect

the values of $\boldsymbol{k}_T$ and k^- inside U. Applying these approximations, the corresponding expression of the hadronic tensor becomes

$$W^{\mu\nu} \approx \frac{e_q^2}{4\pi} \int d\xi \; P^+ \mathrm{Tr}\left[\gamma^\mu U\Big((\xi - x_B)P^+, q^-, \mathbf{0}_\mathrm{T}\Big)\gamma^\nu \left(\int \frac{dk^- d^2k_\mathrm{T}}{(2\pi)^4} L\Big((\xi P^+, k^-, \boldsymbol{k}_\mathrm{T}), P\Big)\right)\right] \tag{1.64}$$

where the convolution of the upper and lower bubbles was decoupled by restricting the integration over k^- and $\boldsymbol{k}_\mathrm{T}$ to L only, while the integration over k_+, i.e. over ξ, is general.

While the trace over colour indices is trivial, we still have both factors (U and L) coupled by a trace in the Dirac spinor space. To project out the leading part of the Dirac trace, we apply the fact that a general matrix in the spinor space can be decomposed as

$$L = \mathcal{S} + \gamma_5 \mathcal{P} + \gamma_\mu \mathcal{V}^\mu + \gamma_5 \gamma_\mu \mathcal{A}^\mu + \frac{1}{2}\sigma_{\mu\nu}\mathcal{T}^{\mu\nu} \tag{1.65}$$

where $\mathcal{S}$, $\mathcal{P}$, $\mathcal{V}^\mu$, $\mathcal{A}^\mu$, and $\mathcal{T}^{\mu\nu}$, are coefficients transforming under Lorentz transformations as scalars, pseudo-scalars, vectors, axial-vectors, and second-rank antisymmetric tensors, respectively.

Boosting from the rest frame to the Breit frame significantly enhances plus components while suppressing minus components. Consequently, in the lower bubble, only the terms $\mathcal{V}^+$, $\mathcal{A}^+$, and $\mathcal{T}^{+i}$, contribute to the hadronic tensor, appearing multiplied by a γ^- factor. This structure allow us to extract these terms from the full expression of L by using the standard trace identities of the Dirac matrices:

$$\mathcal{V}^+ = \frac{1}{4}\mathrm{Tr}\Big[\gamma^+ L\Big] \qquad \mathcal{A}^+ = \frac{1}{4}\mathrm{Tr}\Big[\gamma^5\gamma^+ L\Big] \qquad \mathcal{T}^{+i} = \frac{1}{4}\mathrm{Tr}\Big[\sigma^{+i} L\Big] \tag{1.66}$$

In the unpolarized case, the dominant contribution arises from the component of L that transforms as a vector. We can fully decouple this term from the upper bubble by expressing L in the hadronic tensor as $L \approx \gamma^- \mathcal{V}^+$. The result is that we can now define the parton distribution functions as

$$f_{j/h}(\xi) = \mathrm{Tr}\frac{\gamma^+}{2}\int \frac{dk^- d^2k_\mathrm{T}}{(2\pi)^4} L(k,P) = \mathrm{Tr}\frac{\gamma^+}{2}\int \frac{dk^- d^2k_\mathrm{T}}{(2\pi)^4} \tag{1.67}$$

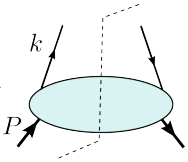

where the traces run over both colour and Dirac indices. With this definition, the hadronic tensor takes the following form

$$W^{\mu\nu} \approx \frac{e_q^2}{4\pi}\int \frac{d\xi}{\xi} f_{q/h}(\xi)\mathrm{Tr}\left[\gamma^\mu U\Big((\xi - x_B)P^+, q^-, \mathbf{0}_\mathrm{T}\Big)\gamma^\nu \frac{\hat{\not{k}}}{2}\right], \tag{1.68}$$

where $\hat{k} = (\xi P^+, 0, \mathbf{0}_\mathrm{T})$ is the massless collinear approximation of the initial quark's momentum.

Operator Definition of Parton Densities

The quark parton density, as defined in (1.67), is obtained by integrating over the lower bubble in Fig. 1.4, tracing over its Dirac indices, and projecting onto the light-cone

plus direction using a γ^+ matrix. In general, the lower bubble represents the sum of all possible cut diagrams of a specific topology. In the context of parton densities, the relevant contributions come from cut diagrams that generate an off-shell quark with plus momentum ξP^+, where P^+ is the plus momentum of the target's initial state.

Since the factorized fermionic lines do not cross the final-state cut, the corresponding amplitude must include field operators at the ends of each line. On the left side of the diagram, the upper end represents the annihilation of a quark by the field, while on the right side, it corresponds to the creation of a quark. Therefore, we would expect that the quark density has an expression in terms of the matrix element of a bilocal field operator. Such a representation can be derived within the framework of lightcone pertubation theory, where the corresponding expression is

$$f_{j/h}(\xi) = \int \frac{dw^-}{2\pi} e^{-i\xi P^+ w^-} \langle P|\overline{\psi}_j(0, w^-, \mathbf{0}_\mathrm{T}) \frac{\gamma^+}{2} \psi_j(0)|P\rangle_c \tag{1.69}$$

The subscript c stands for "connected", meaning that the only contributions included are those where the quark fields are connected to the target's initial state.

To define a quark density gauge invariantly, we need to add a *Wilson Line* (also known as *Gauge Link*) along the light-like line joining the quark and antiquark fields. Then the Wilson line will depend only on the A^+ component of the gauge field, as shown in (1.71). Thus, the gauge-invariant definition reduces to the basic definition (1.69) in the light-cone gauge ($A+ = 0$), as the Wilson line becomes unity. Consequently, when working in this gauge, we can directly apply the same operator definition introduced in the previous paragraph. Despite this fact, a gauge-invariant definition is still useful and is given by the following expression

$$f_{(0)j/h}(\xi) = \int \frac{dw^-}{2\pi} e^{-i\xi P^+ w^-} \langle P|\overline{\psi}_{(0)j}(0, w^-, \mathbf{0}_\mathrm{T}) W(w^-, 0) \frac{\gamma^+}{2} \psi_{(0)j}(0)|P\rangle_c \tag{1.70}$$

where $W(w^-, 0)$ is the Wilson Line given by

$$W(w^-, 0) = \mathcal{P}\left\{ \exp\left(-ig_0 \int_0^{w^-} dy^- A^{\alpha+}_{(0)}(0, y^-, \mathbf{0}_\mathrm{T}) T_\alpha \right) \right\} \tag{1.71}$$

As we will show later, Wilson lines outside the light cone gauge contribute to the amplitudes of cut diagrams, necessitating the definition of their own Feynman rules.

In a renormalizable theory parton densities exhibit ultraviolet (UV) divergences not only due to the fields renormalization but also from the integration over the full transverse momentum $\boldsymbol{k}_\mathrm{T}$ and minus component k^-. Consequently, the subscript (0) in equation (1.70) means that the definition is for bare parton densities. Following the method of BPHZ (Bogoliubov-Parasiuk-Hepp-Zimmermann), we can obtain finite renormalized parton densities by multiplying the bare parton densities with a regulator dependent renormalization factor.

$$f_{j/h}(x) = \sum_k \int_x^1 \frac{d\xi}{\xi} Z_{jk}(\xi, g, \varepsilon) f_{(0)k/h}(x/\xi, \varepsilon) \tag{1.72}$$

In this context, the multiplication corresponds to a convolution over the longitudinal momentum fraction and a summation over flavor indices, over the bare parton density $f_{(0)k/h}$ and the renormalization factor $Z_{jk}(\xi, g, \varepsilon)$.

Bare gauge invariant antiquark densities are obtained by swapping the roles of the quark ψ and antiquark fields $\bar{\psi}$, and taking the Hermitian conjugate of the Wilson line factor, in equation (1.70).

$$f_{(0)j/h}(\xi) = \int \frac{dw^-}{2\pi} e^{-i\xi P^+ w^-} \mathrm{Tr} \frac{\gamma^+}{2} \langle P|\psi_{(0)j}(0, w^-, \mathbf{0}_\mathrm{T}) W^\dagger(w^-, 0) \overline{\psi}_{(0)j}(0)|P\rangle_c \tag{1.73}$$

Operator Definition of Fragmentation Functions

The factorization proof for fragmentation functions is more intricate than for PDFs, primarily because the fragmenting parton does not have a fixed momentum. Nevertheless, after careful analysis, the results obtained rely on approximations that closely resemble those used in the factorization of parton densities. Consequently, the factorization theorem for fragmentation functions in single-inclusive e^+e^- annihilation (the simplest process in which the theorem has been proven) can be extended to semi-inclusive DIS, multi-hadron production in e^+e^- annihilation, and high-transverse-momentum hadron production in hadron-hadron collisions, with a few extra steps [37].

For instance, in the case of semi-inclusive DIS, the separation of kinematic regions follows a structure similar to Fig. 1.4, except that a final-state hadron emerges from the upper bubble. This upper bubble can be treated analogously to how the lower one was treated in fully inclusive DIS, leading to the definition of the fragmentation function as the sum over all cut diagrams that produce a hadron carrying a fraction z of the initial off-shell parton's plus momentum, i.e. $P^+ = zk^+$, where k^+ is the plus component of the fragmenting parton's momentum.

A result of the similarity of the approximations used for the FFs to those employed for PDFs, is that the corresponding definition of the bare fragmentation function for an unpolarized Dirac quark has a strong resemblance to equation (1.70).

$$\begin{aligned} d_{(0)h/j}(z) =& z^{n-3} \sum_X \int d\Pi_X \int \frac{dx^-}{2\pi} e^{ik^+x^-} \frac{\mathrm{Tr}_\mathrm{Dirac}}{4} \frac{\mathrm{Tr}_\mathrm{Colour}}{N} \gamma^+ \\ & \times \langle 0|\psi_{(0)}(0)\overline{\mathcal{P}} \exp\Big(ig_0 \int_{w^-}^{\infty} dy^- A^{\alpha+}_{(0)}(0, y^-, \mathbf{0}_\mathrm{T}) T_\alpha\Big)|P, X, \mathrm{Out}\rangle \\ & \times \langle P, X, \mathrm{Out}|\overline{\psi}_{(0)}(x^-)\mathcal{P} \exp\Big(-ig_0 \int_{w^-}^{\infty} dy^- A^{\alpha+}_{(0)}(0, y^-, \mathbf{0}_\mathrm{T}) T_\alpha\Big)|0\rangle \end{aligned} \tag{1.74}$$

The key difference compared to the PDF definition is that the field operators now act between an initial vacuum state $|0\rangle$ and a final inclusive state $|P, X, Out\rangle$, rather than on an exclusive hadronic state. This distinction arises because, unlike PDFs, which describe an incoming parton extracted from a hadron, fragmentation functions characterize an outgoing off-shell parton that produces a final-state hadron plus many other particles.

In the same way as for parton densities, the fragmentation function of an antiquark can be obtained by just interchanging the role of the quark field ψ, and its Dirac conjugate $\overline{\psi}$, in the definition of quarks fragmentation function.

$$\begin{aligned} d_{(0)h/j}(z) =& \frac{z^{n-3}}{4N} \sum_X \int d\Pi_X \int \frac{dx^-}{2\pi} e^{ik^+x^-} \\ & \times \langle 0|\overline{\psi}_{(0)}(0)\overline{\mathcal{P}} \exp\Big(-ig_0 \int_{w^-}^{\infty} dy^- A^{\alpha+}_{(0)}(0, y^-, \mathbf{0}_\mathrm{T}) T_\alpha\Big)|P, X, \mathrm{Out}\rangle \gamma^+ \\ & \times \langle P, X, \mathrm{Out}|\psi_{(0)}(x^-)\mathcal{P} \exp\Big(ig_0 \int_{w^-}^{\infty} dy^- A^{\alpha+}_{(0)}(0, y^-, \mathbf{0}_\mathrm{T}) T_\alpha\Big)|0\rangle \end{aligned} \tag{1.75}$$

Feynman Rules for PDFs and FFs in Gauge Theories

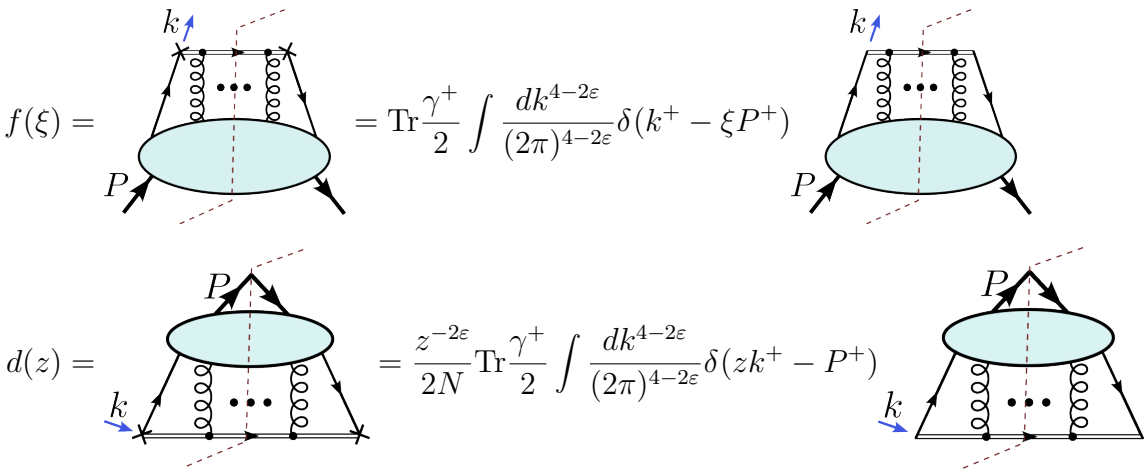

Figure 1.5: Feynman rules for the integrals and traces over gamma matrix factors of the quark PDFs and FFs, in gauge theories. The blue arrow represents the external momenta that enters or escapes from the hard scattering.

The Feynman rules that indicate on which part of a cut diagram the action of the operator definition needs to be applied, in order to obtain the actual PDF or FF, can be conveniently depicted drawing a crossed vertex. The primary role of these crossed vertices is to create or annihilate the quark that enters or escapes from the hard scattering process, as they are neither part of the initial state nor the final state. Additionally, if we consider an integrated unpolarized quark density, this vertex also denotes the integration over the off-shell quark's virtual momentum, the trace with $\gamma^+/2$, and the constraint that fixes the plus component of the quark's momentum to $k^+ = \xi P^+$ for PDFs or $k^+ = P^+/z$ for FFs.

To represent gauge-invariant parton densities in Feynman diagrams, the Wilson line is depicted as a double line connecting the fields at its endpoints, as illustrated in Fig. 1.5. This line interacts with the rest of the diagram through an arbitrary number of gluon exchanges, ranging from zero to infinitely many. Notably, the trace over Dirac indices in a quark density remains unaffected by the presence of the Wilson line.

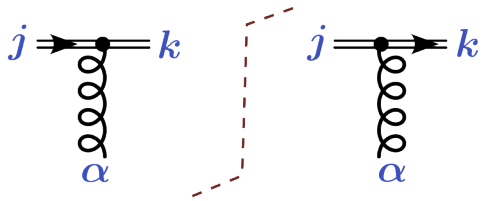

Bare Fields:	$-ig_0 n^\mu (T_\alpha)_{kj}$	$ig_0 n^\mu (T_\alpha)_{kj}$
Renorm. Fields:	$-ig_0 Z_3^{1/2} n^\mu (T_\alpha)_{kj}$	$ig_0 Z_3^{1/2} n^\mu (T_\alpha)_{kj}$

Figure 1.6: Feynman rules for the gluon-WilsonLine vertex in quark PDFs or FFs (for antiquarks a negative sign must be added on each side).

To derive the Feynman rules for the interaction vertex between a Wilson line and a gluon in a quark PDF or FF, we expand the Wilson line exponential in powers of the strong coupling (part of its argument). Each term in this expansion provides a target matrix

element involving multiple gluon fields and the endpoint fields of the Wilson line, integrated over specific positions. The interaction terms, given by $-ig_0 A^+_{(0)\alpha} T_\alpha = -ig_0 n^\mu T_\alpha A^\mu_{(0)\alpha}$ (where $n = (0, 1, \mathbf{0}_\mathrm{T})$), lead to the vertex rules shown in Fig. (1.6).

The Wilson-line propagator can be derived by expanding each path-ordered exponential as a power series and rewriting the path-ordered product of integrals as an integral over ordered variables. To evaluate these integrals, we express the remaining parts of the bi-local definition of PDFs or FFs (the shaded bubble from Fig. 1.5) in the momentum space. This way the integration over the coordinates of the gluons attached to the Wilson line has the form of the Fourier transform of a theta function.

Those integrals will give a value for each double line segment on the left side of a cut diagram that follows the following pattern:

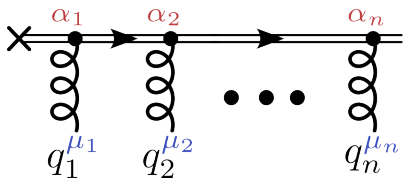

$$= (-ig_s T_{\alpha_n} n^{\mu_n}) \frac{i}{q_n^+ + i0} \times \cdots \times$$
$$(-ig_s T_{\alpha_2} n^{\mu_2}) \frac{i}{q_2^+ + i0} (-ig_s T_{\alpha_1} n^{\mu_1}) \frac{i}{q_1^+ + i0}$$

Therefore, the double lines between each pair of Wilson Line vertices behave like normal propagators in a Feynman diagram, but carrying only plus momenta. As the Wilson-line propagator is independent of the minus and transversal momentum components, the integral over d^2k_T and dk^- is unaffected by its presence in the definition, and the Cutkosky rule for the Wilson Line crossing the final state cut corresponds to a delta function of the projection of its momentum along the n direction.

Thus, the double lines connecting Wilson-line vertices behave like standard propagators in a Feynman diagram, except that they carry only plus-momentum components. Since the Wilson-line propagator is independent of the minus and transverse components of momentum, the integration over d^2k_T and dk^- remains unaffected in the parton density definition. Consequently, according to the Cutkosky rules, when the Wilson line crosses the final-state cut, it contributes with a delta function that cancels any plus momentum at the final state.

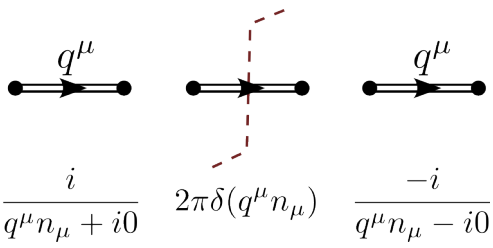

Figure 1.7: Feynman rules for the propagators of a Wilson line.

1.4 Heavy Flavour Hadro-production

Hadro-production processes (the production of particles in hadronic collisions) constitute an important and fruitful area of both theoretical and experimental research. In particular, single inclusive hadro-production processes provide a wide range of observables that can be compared with current experimental data, allowing us to test the reliability of perturbative

quantum chromodynamics and probing the non-perturbative internal structure of hadrons at different energy scales.

A systematic treatment of hadro-production can be carried out within the collinear factorization framework, which expresses the differential cross-section as

$$d\sigma_{N_1N_2\to QX} = \sum_{AB} \int dx_1 dx_2 \, f_{A/N_1}(x_1,\mu_i) f_{B/N_2}(x_2,\mu_i) d\hat{\sigma}_{AB\to CX}(x_1,x_2;\mu_R,\mu_i,\mu_f) \quad (1.76)$$

being x_1 and x_2 the momentum fractions carried by the partons A and B from the initial hadrons (nucleons) N_1 and N_2, respectively. The final partonic state consists of a parton C plus an unobserved remnant X. The sum runs over all the possible initial partons A and B that contribute to the production of C. The three different scales μ_R, μ_i, mu_f, represent the renormalization scale, the inital factorization scale, and the final factorization scale, respectively. The last two describe the evolution of the PDFs and the FFs acording with DGLAP equations.

In hadronic collisions, final-state particles are typically characterized by their *transverse momentum* P_T and their *rapidity* Y a long the collision axis. If the collsion occurs long the z axis, rapidity is defined as

$$Y = \frac{1}{2}\ln\left(\frac{E+P_z}{E-P_z}\right) \quad (1.77)$$

where E is the energy and p_z the longitudinal momentum. At sufficiently high transverse momentum, the parton C fragments into a jet containing final-state hadrons. When an inclusive final state involves a single identified hadron H, the corresponding hadronic differential cross-section includes a convolution with the fragmentation function $D_{H/C}(z,\mu_R)$, which describes the non-perturbative transition of parton C into hadron H:

$$\frac{d\sigma_{N_1N_2\to HX}}{dY\,dP_T^2}(Y,P_T) = \sum_C \int \frac{dz}{z^2} D_{H/C}(z,\mu_f) \frac{d\sigma_{N_1N_2\to CX}}{dy\,dp_T^2}(y,p_T/z,\mu_f) \quad (1.78)$$

Here, z is the momentum fraction carried by hadron H from parton C, and the sum runs over all partons contributing to H's production.

These two expressions, while fundamental for the application of factorization, are not sufficient on their own to accurately describe the hadroproduction of heavy flavours, whether quarks or hadrons. A consistent treatment of heavy flavours in perturbative QCD requires theoretical considerations beyond the massless parton picture that was built in the previous sections.

While light partons require a large kinematic scale, typically proportional to the transverse momentum, to ensure the applicability of perturbative methods and the factorization of non-perturbative dynamics, the heavy-quark mass acts as a cutoff for initial and final state collinear singularities and establishes a minimum scale that is significantly larger than $\Lambda_{\rm QCD}$. This allows perturbative methods to remain valid even at zero transverse momentum of the observed particle. Consequently, heavy quarks introduce an additional large scale, leading to distinct kinematic regions, each with its own theoretical challenges that require specialized treatment.

At low energies ($Q \sim m_Q$), heavy quarks behave as on-shell massive particles and should not be considered as partons within the proton's initial state. This observation leads

to the so called *Fixed Flavour Number Scheme* (FFNS), which is applicable when the heavy quark mass m_Q is of the same order as the hard scale Q of the process under consideration, and both are much larger than the typical scale of strong interactions $m_Q \sim Q \gg \Lambda_{QCD}$. This scheme keeps the number of active flavours N_f fixed, treating active quarks as massless regardless of the actual value of their masses (some "less" heavy quarks can still be included). However, heavy quarks with masses larger than the active ones are not considered part of the proton and not receiving their corresponding parton densities. Instead, they appear only as final state particles produced in the hard interaction, leaving all their contributions within the hard-scattering matrix elements, where their masses m_Q are explicitly taken into account regardless of the value of transverse momentum p_t. While the heavy quark mass acts as a natural cutoff for collinear singularities, terms proportional to $\alpha_s \ln\left(p_t^2/m_Q^2\right)$ arising from collinear emissions, can become large for $p_t \gg m_Q$, potentially spoiling the convergence of the perturbative expansion.

In contrast, at high energy scales ($Q \gg m_Q$), heavy quarks can be treated as massless partons. This leads to the so-called zero-mass variable-flavour-number (ZM-VFN) scheme, which is valid when the characteristic scale of the process is much larger than both the heavy quark mass and the characteristic scale of strong interactions $Q \gg m_Q \gg \Lambda_{QCD}$. In this approach, the number of active flavours increases with the typical energy scale (hence the term "variable" in its name). Above a certain threshold, the heavy quark is also considered an incoming massless parton originating from the initial hadrons, possessing its own parton density. The presence of heavy quark PDFs introduces additional contributions to the hard scattering processes, in addition to those initiated by light quarks and gluons, where the quark mass is completely neglected. Consequently, large logarithmic terms of the form $\alpha_s \ln\left(p_t^2/m_Q^2\right)$ related to collinear emissions in the hard subprocess are resumed by DGLAP equations into the heavy quark PDFs, allowing a better perturbative convergence at large transverse momentum.

These two schemes were developed long ago, following the conventional proof of the factorization theorem, which relies on the zero-mass limit of partons. However, neither provides a complete description of all relevant kinematic regions within a unique framework. To address this limitation, new schemes were developed over time, initially guided by heuristic arguments [38]. It was not until 1998 that J. Collins provided a general proof of the factorization theorem (at all orders in perturbation theory) valid for massive quarks [39]. His work demonstrated that heavy-quark contributions can be consistently and systematically incorporated by combining the key aspects of the two previously discussed schemes. The resulting framework is known as the *General-Mass Variable Flavour Number Scheme* (GM-VFNS), also referred to as the Aivazis-Collins-Olness-Tung (ACOT) scheme [40] [41]. This approach smoothly interpolates between the regimes $m_Q \sim Q$ and $m_Q \ll Q$, effectively transitioning between multiple FFNS with different number of active quarks, or using massive hard matrix elements in the ZM-VFNS. By applying this procedure, we overcome the limitations of both purely massless and purely massive schemes, enabling reliable predictions across a broad range of scales.

It is important to note that in our discussion about the ZM-VFNS and GM-VFNS, we have assumed that heavy quark flavors are generated exclusively through perturbative QCD evolution, arising from gluons and lighter quarks at scales above $\mu = m_Q$. This approach is commonly known as the radiatively generated heavy flavour scenario, which should not be confused with the intrinsic heavy flavour scenario. A brief discussion on

the implications of an intrinsic charm and how it arises in the framework of GM-VFNS can be found in [42].

1.5 Parametrizations of Heavy Quark Fragmentation Functions

As Quantum Chromodynamics does not allow us to compute parton distribution functions or fragmentation functions with perturbative methods, these functions must be obtained from experimental data. Despite this, we still can try to provide a parametrization from theoretical considerations, such as kinematic constraints, power counting, or phenomenological models. The purpose of this procedure is to reduce the parameter freedom of PDFs and FFs while enabling us to test how well these distributions align with our theoretical expectations.

A particularly intuitive case is the fragmentation of heavy quarks into heavy-light systems, such as D mesons. The key observation here is that the fragmenting heavy quark needs to create a light quark pair in order to create a heavy-light system, so the momentum lost by the heavy quark is proportional to Λ_{QCD}. Since the heavy quark mass is much larger than the hadronic scale Λ_{QCD}, the heavy quark retains almost all of its original momentum throughout the hadronization process. Consequently, the probability of heavy quarks fragmenting into a heavy-light hadron peaks at a large fraction of its momentum ($z \sim 1$).

To capture this behaviour, various phenomenological models propose functional forms for the fragmentation function $D_{Q\to H}(x)$, introducing free parameters that control its shape. Among them, the most well-known parametrizations are those proposed by Peterson et al. [43], Collins and Spiller [44], and Kartvelishvili et al. [45]. Their corresponding expressions are given by

$$\text{Peterson } \textit{et al.} : \quad D_{H_Q/Q}(z) = f_{Q\to H_Q} N(\varepsilon_p) z \left(1 - \frac{1}{z} - \frac{\varepsilon_p}{(1-z)}\right)^{-2} \tag{1.79}$$

$$\text{Collins and Spiller} : \quad D_{H_Q/Q}(z) = f_{Q\to H_Q} N(\varepsilon_c)(1+z^2) \frac{\left(\frac{1-z}{z} + \frac{2-z}{1-z}\varepsilon_c\right)}{\left(1 - \frac{1}{z} - \frac{\varepsilon_c}{(1-z)}\right)^2} \tag{1.80}$$

$$\text{Kartvelishvili } \textit{et al.} : \quad D_{H_Q/Q}(z) = f_{Q\to H_Q} N(\alpha) z^{\alpha}(z-1) \tag{1.81}$$

where N is just a normalization factor. Each of these models presents slightly different arguments on the dynamics of heavy-quark hadronization, but all of them rely on the idea mentioned in the previous paragraph.

The values of the parameters in equations (1.79) (1.80) (1.81) are not directly predicted by the models but need to be fitted to experimental data. The first extractions of these parameters were performed by the ALEPH [46], OPAL [47], and SLD [48], and (a few years later) DELPHI [49] collaborations as part of their studies on b-quark fragmentation using parton shower simulations. Over time, more sophisticated fits have been developed, most notably in the work of Kniehl et al. [50], where they fit these expressions to calculations done in perturbative QCD with collinear factorization, using the General-Mass Variable flavour Number Scheme.

2 Heavy Meson Production in Non-Relativistic QCD

The study of bound states of heavy quark–antiquark pairs $Q\overline{Q}$ (here referred to as *Heavy Mesons*) became a major research topic after the discovery of the first charmonium states in 1974 [51] [52] and the observation of bottomonium states in 1977 [53]. As these composite particles were expected to be the first systems where perturbative QCD could be applied, at least approximately, their discoveries quickly established them as valuable probes for testing the validity of this theory across a wide range of kinematics and different processes. Being such an important object, several models and effective field theories have been developed over the decades in an attempt to accurately reproduce experimental observations and provide a theoretical framework for describing the production, spectroscopy, and decay of these interesting particles.

The defining feature that makes heavy mesons special in QCD, is that the masses of their heavy constituents is much larger than the QCD scale ($m_Q \gg \Lambda_{\text{QCD}}$). In this situation, the heavy quark and antiquark are naturally expected to move non-relativistically within the bound system, meaning they have a small velocity in the center-of-mass frame ($v \ll 1$). As a result, multiple energy scales govern the internal dynamics of these bound states. These characteristic scales are the heavy quark mass m_Q, its typical momentum $m_Q v$, and its kinetic energy $m_Q v^2$. The mass m_Q sets the fundamental energy threshold for both the creation and annihilation of the bound state. The inverse momentum scale, $1/(m_Q v)$, defines the spatial extent of the meson's wave function, effectively determining its characteristic size. Finally, the kinetic energy $m_Q v^2$ dictates the fine structure of the spectrum, setting the scale for energy splittings between radial and orbital excitations.

Since these energy scales are separated by powers of v, a sufficiently small velocity parameter ensures a clear separation between them. In particular, the three scales mentioned above establish a well-separated hierarchy where different types of interactions dominate the dynamics:

$$m_Q \quad \gg \quad m_Q v \quad \gg \quad m_Q v^2 \tag{2.1}$$

This natural hierarchy of scales provides strong motivation for the formulation of a factorization hypothesis, which enables a systematic decoupling of short and long distance dynamics. This way, high-energy effects (such as those associated with quark production and annihilation) could be treated independently from the lower-energy interactions governing bound state formation and evolution.

Among the earliest attempts to apply perturbative QCD along with a non-relativistic factorization procedure to the production of heavy mesons, we can find the approach that is usually referred to as Colour-Singlet Model (CSM) [54] [55]. In this model, heavy quarks are produced on-shell, and only a $Q\overline{Q}$ pair in a color-singlet state can hadronize into a heavy meson state with identical quantum numbers (spin and angular momentum). The total production rate is factorized into a perturbative component that is process-dependent and governs the creation or annihilation of the heavy quarks, and an universal component that describes the non-perturbative transition from the quark pair to the physical heavy meson.

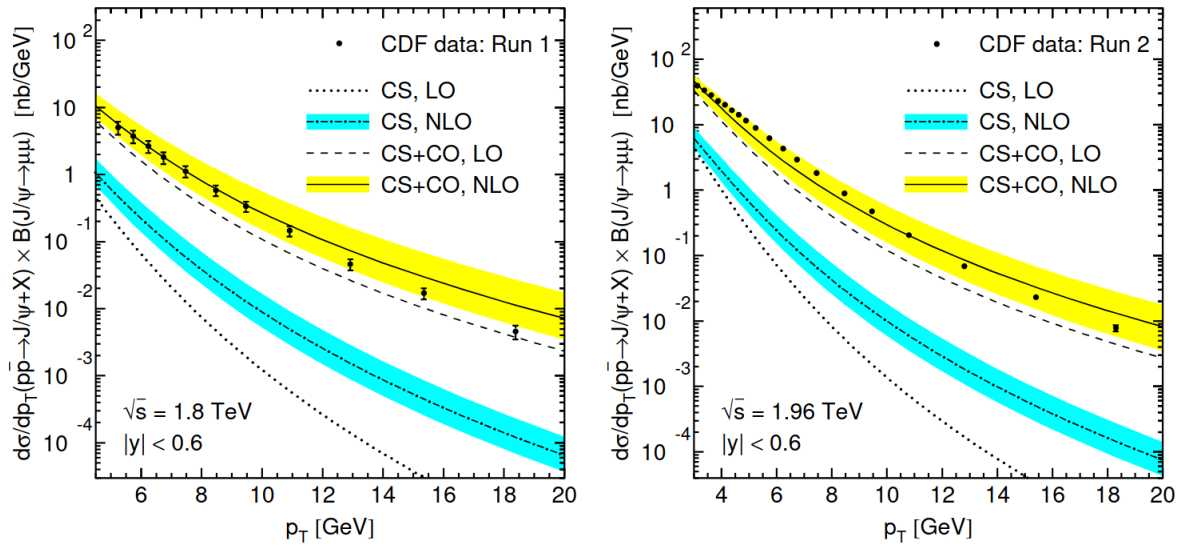

Figure 2.1: Comparisons between the contributions of colour singlet (CS) and colour octet (CO) channels to the observed charmonium decay $J/\psi \to \mu\mu$ by the CDF collaboration at Tevatron. Many more examples on the importance of colour octet contributions are displayed in [58].

Despite its physical transparency, the CMS not only suffers from significant theoretical limitations, but also presented an striking discrepancy which was observed by the CDF [56] and D$\emptyset$ [57] experiments at Tevatron. They reported large-p_T production rates of J/ψ and ψ' states exceeding theoretical predictions by more than an order of magnitude. This compelling evidence indicated that the CSM was missing essential physics.

As an attempt to establish a more rigorous factorization framework, the Colour-Singlet Model was replaced by the factorization approach proposed by Bodwin, Braaten, and Lepage in 1994 [7], based on the rigorously derived effective field theory known as *Non-Relativistic QCD* (NRQCD) [6]. This approach provides a well-founded method for analysing heavy meson production and decay, as it is constructed from a perturbative expansion around the non-relativistic limit ($v \to 0$). Similar to the CSM, this framework also takes advantage of the natural hierarchical separation of energy scales in heavy quark systems, decoupling the physics occurring at scales above the heavy quark mass m_Q from the phenomena taking place at the characteristic bound-state momentum scale $m_Q v$ or lower.

This separation allows NRQCD to incorporate transitions in which a perturbatively produced heavy-quark pair evolves into a physical heavy meson state through intermediate quantum states. Such transitions, which naturally arise within the v expansion, introduce the concept of colour-octet contributions. As shown in fig. 2.1, these contributions played an essential role in resolving the discrepancies between theoretical predictions and experimental measurements that were observed under the CSM.

In this chapter, we introduce the NRQCD factorization framework, detailing its fundamental assumptions and theoretical foundations. We present how this effetive theory is applied to processes involving heavy mesons, which includes the charmonium, bottonium, and B_c, families. Particular attention is given to the production mechanisms relevant to collider experiments, highlighting the essential steps required to construct reliable

theoretical predictions. Following the discussions presented in many good articles and reviews [7] [59] [60] [60] [61] [62], this chapter lays the necessary foundation for the study of heavy meson phenomenology in high-energy interactions, serving as a corner stone for the calculations of the following chapter.

2.1 The NRQCD Lagragian

The NRQCD Lagrangian is derived from the full QCD Lagrangian by introducing an ultraviolet cut-off Λ, chosen to be of the same order as the heavy quark mass m_Q. This cut-off effectively integrates out the relativistic degrees of freedom associated with heavy quarks, as well as gluons and light quarks carrying momenta above Λ. Since the dominant non-perturbative dynamics for heavy mesons involves momenta of order $m_Q v$ or lower, NRQCD provides a suitable framework for analysing such systems.

In this effective theory, the complex fields describing the heavy quarks and antiquarks are decoupled and replaced by two-component Pauli spinors fields, ψ and χ, corresponding to the heavy quark and the a heavy antiquark fields, respectively. The momentum-space representations of these fields are then

$$\psi(\boldsymbol{r}) = \int \frac{d^3k}{2E_k} a(k)\xi(k)e^{i\boldsymbol{r}\cdot\boldsymbol{k}} \qquad \chi(\boldsymbol{r}) = \int \frac{d^3k}{2E_k} b^\dagger(k)\eta(k)e^{-i\boldsymbol{r}\cdot\boldsymbol{k}} \tag{2.2}$$

where $a(k)$ the heavy quark annihilation operator and $b(k)$ the heavy antiquark creation operator (We have omitted the spin and colour indices in these expressions).

In the Dirac representation of the gamma matrices, the Pauli spinors ξ and η correspond to the upper and lower components of the original Dirac spinors in the rest frame of the particle. In any other frame, these components cannot be identified so easily, making the Dirac spinor field an entangled combination of the fields ψ and χ.

$$u(\boldsymbol{p}) = \sqrt{\frac{E+m}{2m}}\begin{pmatrix} \xi(p) \\ \frac{\boldsymbol{p}\cdot\boldsymbol{\sigma}}{E+m_Q}\xi(p) \end{pmatrix} \qquad v(\boldsymbol{p}) = \sqrt{\frac{E+m}{2m}}\begin{pmatrix} \frac{\boldsymbol{p}\cdot\boldsymbol{\sigma}}{E+m_Q}\eta(p) \\ \eta(p) \end{pmatrix} \tag{2.3}$$

Therefore, the decomposition into ψ and χ reflects the standard behaviour of non-relativistic systems, which can be performed by expanding the QCD Lagrangian as a power series. In [63], this expansion is carried out in powers of the light speed $(1/c)$, since it is not immediately clear how each operator in the Lagrangian scales with the characteristic velocity v.

As a result, the NRQCD Lagrangian is primarily built from separate Pauli spinor fields for the heavy quark and antiquark. The full Lagrangian can be organized as

$$\mathcal{L}_{\text{NRQCD}} = \mathcal{L}_{\text{light}} + \mathcal{L}_{\text{heavy}} + \delta\mathcal{L}, \tag{2.4}$$

where the lagrangian $\mathcal{L}_{\text{light}} + \mathcal{L}_{\text{heavy}}$ describes ordinary QCD coupled to a Schrödinger field theory for the heavy quarks and antiquarks. In particular, $\mathcal{L}_{\text{light}}$ includes the low-energy dynamics of gluons and light quarks, while $\mathcal{L}_{\text{heavy}}$ describes the low-momentum behaviour of the heavy quark fields.

$$\mathcal{L}_{\text{heavy}} = \psi^\dagger\left(iD_t + \frac{\boldsymbol{D}^2}{2m_Q}\right)\psi + \chi^\dagger\left(iD_t - \frac{\boldsymbol{D}^2}{2m_Q}\right)\chi, \tag{2.5}$$

$$\mathcal{L}_{\text{light}} = -\frac{1}{2}\text{Tr}(G_{\mu\nu}G^{\mu\nu}) + \sum_q \bar{q}\, i\not{D} q, \tag{2.6}$$

In these expressions, D_t and $\boldsymbol{D}$ denote the temporal and spatial components of the gauge covariant derivative D_μ.

The term $\delta\mathcal{L}$ inside the complete NRQCD lagrangian (2.4), includes all possible operators consistent with the symmetries of QCD and reproduces the relativistic effects of the full theory, reproducing their effects up to a certain power of v. The leading correction terms in the NRQCD effective lagrangian are bilinear in the quark field or the antiquark field,

$$\begin{aligned}\delta\mathcal{L}_{bilinear} = &\frac{c_1}{8m_Q^2}\Big(\psi^\dagger \boldsymbol{D}^4\psi - \chi^\dagger \boldsymbol{D}^4\chi\Big) \\ &+ \frac{c_2}{8m_Q^2}\Big(\psi^\dagger(\boldsymbol{D}\cdot g\boldsymbol{E} - g\boldsymbol{E}\cdot\boldsymbol{D})\psi - \chi^\dagger(\boldsymbol{D}\cdot g\boldsymbol{E} - g\boldsymbol{E}\cdot\boldsymbol{D})\chi\Big) \\ &+ \frac{c_3}{8m_Q^2}\Big(\psi^\dagger(i\boldsymbol{D}\times g\boldsymbol{E} - g\boldsymbol{E}\times i\boldsymbol{D})\cdot\boldsymbol{\sigma}\psi - \chi^\dagger(i\boldsymbol{D}\times g\boldsymbol{E} - g\boldsymbol{E}\times i\boldsymbol{D})\cdot\boldsymbol{\sigma}\chi\Big) \\ &+ \frac{c_4}{2m_Q}\Big(\psi(g\boldsymbol{B}\cdot\boldsymbol{\sigma})\psi - \chi^\dagger(g\boldsymbol{B}\cdot\boldsymbol{\sigma})\chi\Big)\end{aligned} \tag{2.7}$$

where $E_i = G_{0i}$ and $B_i = \frac{1}{2}\varepsilon_{ijk}G^{jk}$ are the electric-like and magnetic-like components of the gluon field strength tensor $G^{\mu\nu}$. If we keep including operators of increasing dimension, the matrix elements derived from the NRQCD Lagrangian will approximate those computed in full QCD to the desired order in the characteristic heavy-quark velocity v. As a result, observables associated with heavy mesons can be reproduced with arbitrary precision after carefully matching the corresponding Wilson coefficients c_i to full QCD.

It is worth noting that bilinears involving mixed fields ψ and χ are not included in NRQCD, as they would correspond to the creation or annihilation of a single heavy quark-antiquark pair. To conserve energy and momentum, such processes would require a gluon with energy greater than the ultraviolet cut-off $\Lambda \sim m_Q$, which is forbidden by definition in NRQCD. Therefore, the NRQCD Lagrangian conserves the quark and antiquark numbers.

To describe the annihilation process of a heavy quark-antiquark pair $Q\overline{Q}$ within a heavy meson, it is necessary to introduce four-fermion effective operators into the NRQCD Lagrangian. These operators account for local interactions in which a heavy quark and antiquark are annihilated and re-created at the same spacetime point. As such, they can be used through the optical theorem to study the inclusive annihilation of heavy mesons. Naturally, the form of these operators is constrained by the symmetries of full QCD, order by order in the characteristic heavy quark velocity v. Specifically, they must respect gauge invariance, rotational symmetry, and the global phase symmetries associated with the heavy quark and antiquark fields.

The general form of the four-fermion operators can be expressed as

$$\delta\mathcal{L}_4 = \sum_{nm} C_{nm}\mathcal{O}_{nm}, \qquad \mathcal{O}_{nm} = (\psi^\dagger\mathcal{K}_n\chi)(\chi^\dagger\mathcal{K}_m\psi) \tag{2.8}$$

where the factors $\mathcal{K}_n$ and $\mathcal{K}_m$ are composed of spin matrices $\boldsymbol{\sigma}$, color matrices T^a_{ij}, or polynomials of the spatial derivative $\boldsymbol{D}$. Following the idea of local interactions, each of these operators acts by annihilating a $Q\overline{Q}$ pair with quantum numbers specified by $\mathcal{K}_m$ and creating a new $Q\overline{Q}$ pair in a state given by $\mathcal{K}_m$. The Wilson coefficients C_{nm} encapsulate the short-distance physics at scales above $\Lambda \sim m_Q$. As with the 2-fermion

operators, these coefficients have to be determined by matching scattering amplitudes computed in NRQCD with those calculated in full QCD.

The lowest energy dimension four-fermion operators relevant for quarkonium physics begin at dimension six. For the case of a single heavy quark flavour, there are only four such operators

$$\mathcal{O}(^1S_0^{[1]}) = \psi^\dagger\chi\chi^\dagger\psi \qquad \mathcal{O}(^3S_1^{[1]}) = \psi^\dagger\vec{\sigma}\chi\cdot\chi^\dagger\vec{\sigma}\psi \tag{2.9}$$

$$\mathcal{O}(^1S_0^{[8]}) = \psi^\dagger T^a\chi\chi^\dagger T^a\psi \qquad \mathcal{O}(^3S_1^{[8]}) = \psi^\dagger\vec{\sigma}T^a\chi\cdot\chi^\dagger\vec{\sigma}T^a\psi \tag{2.10}$$

where the labels [1] and [8] denote the color-singlet and color-octet configurations of the $Q\overline{Q}$ pair, and the spectroscopic notation $^{2S+1}L_J$ is used to specify their spin and angular momentum quantum numbers. As you can see, these operators only describe the annihilation and creation of $Q\overline{Q}$ pairs in S-wave states.

To account for orbital and radial excitations, operators of higher energy dimension must be included. At dimension eight, for example, the following operators describe transitions involving P-wave states

$$\mathcal{O}(^1P_1^{[1]}) = \psi^\dagger\Big(-\frac{i}{2}\overleftrightarrow{\boldsymbol{D}}\Big)\chi\cdot\chi^\dagger\Big(-\frac{i}{2}\overleftrightarrow{\boldsymbol{D}}\Big)\psi \tag{2.11}$$

$$\mathcal{O}(^3P_0^{[1]}) = \frac{1}{3}\psi^\dagger\Big(-\frac{i}{2}\overleftrightarrow{\boldsymbol{D}}\cdot\boldsymbol{\sigma}\Big)\chi\,\chi^\dagger\Big(-\frac{i}{2}\overleftrightarrow{\boldsymbol{D}}\cdot\boldsymbol{\sigma}\Big)\psi \tag{2.12}$$

$$\mathcal{O}(^3P_1^{[1]}) = \frac{1}{2}\psi^\dagger\Big(-\frac{i}{2}\overleftrightarrow{\boldsymbol{D}}\times\boldsymbol{\sigma}\Big)\chi\cdot\chi^\dagger\Big(-\frac{i}{2}\overleftrightarrow{\boldsymbol{D}}\times\boldsymbol{\sigma}\Big)\psi \tag{2.13}$$

$$\mathcal{O}(^3P_2^{[1]}) = \psi^\dagger\Big(-\frac{i}{2}\overleftrightarrow{D}^{(j}\sigma^{k)}\Big)\chi\cdot\chi^\dagger\Big(-\frac{i}{2}\overleftrightarrow{D}^{(j}\sigma^{k)}\Big)\psi \tag{2.14}$$

along with similar operators that include insertions of the colour matrix T^a, representing colour octet contributions. In the above expressions, we have used the following notations

$$\chi^\dagger\overleftrightarrow{\boldsymbol{D}}\psi = \chi^\dagger\boldsymbol{D}\psi - (\boldsymbol{D}\chi)^\dagger\psi \qquad T^{(ij)} = \frac{1}{2}(T^{ij}+T^{ji}) - \frac{1}{3}T^{kk}\delta_{ij} \tag{2.15}$$

to shorten the expressions needed to construct operators with definite angular momentum and spin quantum numbers.

The production of a heavy meson H can also be described using four-fermion operators. The key difference between the operators describing annihilation and those describing production is that the latter include a projection operator to ensure the appearance of the heavy meson in the final state. The general form of the production operator is

$$\mathcal{O}^H_{nm} = (\psi^\dagger\mathcal{K}_n\chi)\,\mathcal{P}_H(\chi^\dagger\mathcal{K}_m\psi) \qquad \mathcal{P}_H = \sum_X |H+X\rangle\langle H+X| \tag{2.16}$$

where $\mathcal{P}_H$ is known as the *State Projector*. The sum runs over all additional soft particles X that are sufficiently low in energy to be described within NRQCD. To distinguish them from annihilation operators, production operators are often labelled by the specific heavy meson state they project onto.

The heavy meson states $|H\rangle$ that appear in the definition of the state projector $\mathcal{P}_H$ can be decomposed as a superposition of Fock states involving a heavy quark, a heavy

antiquark, an arbitrary number of dynamical gluons, and even light quark pairs. In particular, for a heavy meson H in a ${}^1S_0$ state, we can represent $|H\rangle$ as

$$\left|H({}^1S_0)\right\rangle = c_0\left|Q\overline{Q}({}^1S_0^{[1]})\right\rangle + c_g\left|Q\overline{Q}({}^3S_1^{[8]})g\right\rangle + c_{gg}\left|Q\overline{Q}({}^1S_0^{[1]})gg\right\rangle \ldots \tag{2.17}$$

where we used the same notation adopted for the four-fermion operators to label the quantum numbers of the $Q\overline{Q}$ pair state. The gluonic components reflect the nontrivial QCD dynamics within the bound state and play a central role in the NRQCD framework. They allow the $Q\overline{Q}$ pair to be treated as an intermediate state whose quantum numbers may differ from those of the final physical quarkonium being produced or decaying.

2.2 NRQCD Production Factorization

Due to the large separation between the energy scale at which a heavy quark-antiquark pair is produced and the softer scale associated with its hadronization into a heavy meson, the NRQCD factorization framework assumes that these two processes are sensible only to interactions occuring at their respective scales. As a result, the production rate can be expressed in terms of perturbative Wilson coefficients and vacuum expectation values of local four-fermion operators in the NRQCD Lagrangian, impliying that the short-distance production and long-distance hadronization proceed in two distinct stages.

Taking as a reference [59] the differential cross section for the inclusive production of a heavy meson H can be expressed as a sum where each term is factorized into a short-distance coefficient and a long-distance matrix element.

$$d\sigma(H(\lambda)+X) = \frac{1}{4E_1E_2v_{12}}\frac{d^3P}{(2\pi)^3 2E_P}\sum_{nm} C_{nm}(k_1,k_2,P)\langle\mathcal{O}_{nm}^{H(\lambda)}\rangle \tag{2.18}$$

$$\langle\mathcal{O}_{nm}^{H(\lambda)}\rangle = \sum_X \langle 0|\chi^\dagger\mathcal{K}_n\psi|H(\lambda)+X\rangle\langle H(\lambda)+X|\psi^\dagger\mathcal{K}_m\chi|0\rangle \tag{2.19}$$

The coefficient C_{nm} is a function of the relevant momenta (the meson momentum P, and the initial momenta denoted by the subscripts 1 and 2), and it describes the short-distance production of a $Q\overline{Q}$ pair in the colour, spin, and angular momentum state specified by n and m. On the other hand, $\langle\mathcal{O}_{nm}^{H(\lambda)}\rangle$ is the vacuum expectation value of an effective four-fermion production operator from NRQCD, usually referred to as *Long Distance Matrix Elements* (LDME). They encode the non-perturbative transition of the $Q\overline{Q}$ pair into the observable heavy meson H. For different values of n and m, these matrix element account for the interference between different intermediate $Q\overline{Q}$ states that can contribute to the formation of the same final meson. It is also worth noting that the fields ψ, χ, and their adjoints, are evaluated at the same spacetime point (often suppressed in notation but typically taken as $x = 0$).

This factorization formula involves a double expansion in the QCD coupling constant α_s and the in the characteristic heavy quark velocity v. The short-distance coefficients are computed perturbatively, order by order in α_s, and are therefore depend on the process studied. In contrast, the long-distance matrix elements are universal and can be ordered by their scaling behaviour as powers of v, determining the relative importance of each of this matrix elements.

The procedure used to determine the short-distance coefficients in (2.18) is known as *Matching*. Since the production of a physical heavy meson is a non-perturbative process

and cannot be computed directly in perturbative QCD, the matching is instead performed at the level of perturbative quark pair production. Specifically, one requires that the production rate of a heavy $Q\overline{Q}$ pair, calculated in NRQCD, reproduces the corresponding perturbative result obtained in full QCD. This leads to the following matching condition

$$\sum_X (2\pi)^4 \delta^4(k_1 + k_2 - P - k_X) \left(\mathcal{M}^*_{12\to Q\overline{Q}[a]+X}\right)\left(\mathcal{M}_{12\to Q\overline{Q}[b]+X}\right)\Big|_{\text{pQCD}} \tag{2.20}$$

$$= \sum_{nm} C_{nm}(k_1, k_2, P)\, \langle \mathcal{O}^{Q\overline{Q}}_{nm} \rangle \Big|_{\text{NRQCD}} \tag{2.21}$$

where the NRQCD matrix element describes the creation of a perturbative $Q\overline{Q}$ pair instead of a heavy meson. Its expression is given by

$$\langle \mathcal{O}^{Q\overline{Q}}_{nm} \rangle = \sum_X \langle 0|\chi^\dagger \mathcal{K}_n \psi \Big| Q\overline{Q}[a]+X \Big\rangle \Big\langle Q\overline{Q}[b]+X \Big| \psi^\dagger \mathcal{K}_m \chi |0\rangle \tag{2.22}$$

where the subscripts a and b label the quantum numbers of the intermediate $Q\overline{Q}$ states.

To ensure consistency, the normalization of the fields and states in NRQCD must match that used in the perturbative QCD (pQCD) matrix elements. However, it is common in the NRQCD literature to encounter mixed normalization conventions, with correction factors introduced only at later stages of the calculation.

In this work, we adopt the standard relativistic normalization throughout, in order to maintain clarity and avoid misunderstandings arising from mixed conventions. Accordingly, our normalization conditions are

$$\langle H(\boldsymbol{P}', \lambda') \,|\, H(\boldsymbol{P}, \lambda) \rangle = 2E_P (2\pi)^3 \delta^3(\boldsymbol{P} - \boldsymbol{P}') \delta_{\lambda\lambda'} \tag{2.23}$$

$$\Big\langle Q\overline{Q}[a] \Big| Q\overline{Q}[b] \Big\rangle = 2E_1 2E_2 (2\pi)^3 \delta^3(\boldsymbol{q}_1' - \boldsymbol{q}_1) \delta^3(\boldsymbol{q}_2' - \boldsymbol{q}_2) \delta_{ab} \tag{2.24}$$

$$u^\dagger(p) u(p) = \xi^\dagger(p) \xi(p) = 2E_p \tag{2.25}$$

$$v^\dagger(p) v(p) = \eta^\dagger(p) \eta(p) = 2E_p \tag{2.26}$$

2.3 Power counting

As the NRQCD factorization formula (2.18) includes an infinite series of terms, its practical applicability relies on our ability to estimate their relative importance. This is achieved through NRQCD power counting, which organizes contributions based on their scaling with the heavy-quark velocity v. Each matrix element $\langle \mathcal{O}_H(n) \rangle$ is associated with a specific power of v, establishing a hierarchy that allows for a systematic truncation of the expansion. Consequently, at any fixed order in v, only a finite number of terms contribute meaningfully to the production cross section. In the Coulomb gauge and at tree level, simple power counting rules were developed in [64] assuming that one can do perturbation theory in the characteristic heavy quark velocity v, we summarize them in Fig. 2.2. This perturbation theory relies on the asumption that soft gluons have a weak coupling to heavy quarks, not because the coupling constant α_S is small, but because the interaction is proportional to v.

These power counting rules show that the terms in $\delta\mathcal{L}_{\text{bilinear}}$, as given in eq. (2.7), contribute corrections suppressed by v^2 relative to those from the leading-order Lagrangian

Operator	Estimate
ψ	$(m_Q v)^{3/2}$
χ	$(m_Q v)^{3/2}$
D_0 (acting on ψ or χ)	$m_Q v^2$
$\mathbf{D}$	$m_Q v$
$g\mathbf{E}$	$m_Q^2 v^3$
$g\mathbf{B}$	$m_Q^2 v^4$
gA_0 (in Coulomb gauge)	$m_Q v^2$
$g\mathbf{A}$ (in Coulomb gauge)	$m_Q v^3$

Figure 2.2: Approximate contributions from the NRQCD operators to the magnitudes of the matrix elements in heavy quark-antiquark systems. The scaling with the heavy quark mass m_Q follows simply from dimensional analysis.

$\mathcal{L}_{\text{heavy}}$. Consequently, these terms can be included to compute NRQCD matrix elements between heavy quarkonium states with an accuracy up to corrections of order v^4.

Furthermore, since the covariant derivative $\boldsymbol{D} = \boldsymbol{\nabla} + ig\boldsymbol{A}$ scales as v, while the gluon field term $g\boldsymbol{A}$ scales as v^3, contributions from Fock states containing dynamical gluons such as $\left|Q\overline{Q}g\right\rangle$ are generally subleading. However, notable exceptions exist, for example, the decay rates of P-wave quarkonia [65], [66] where the effects of these Fock states enter at leading order in the v expansion.

2.4 Matching and Covariant Projectors

As discussed in the previous sections, the short-distance coefficients for a given process are determined by matching the cross-section calculations for the production of a perturbative heavy-quark pair in both theories, QCD and NRQCD. In principle, there is not a single way of getting the matching coefficients. In the standard NRQCD matching procedure, one begins by computing the corresponding on-shell amplitude in full QCD. This amplitude is then expanded in powers of the heavy quark momentum q in the center of mass frame, so that each term has a definite scaling in the velocity expansion. The short-distance coefficients are extracted by identifying the relevant NRQCD matrix elements within this expansion. However, performing the matching by directly decomposing the four-component Dirac spinors into two-component Pauli spinors is often lengthy and cumbersome.

A more efficient method for computing short-distance coefficients is the covariant projector approach [67] [68] [69], which directly selects the heavy-quark pair state within the QCD amplitude. Using the fact that any QCD amplitude involving a final state heavy-quark pair can be expressed as a trace over spinor and colour indices $\mathcal{M} = \text{Tr}[(\dots)v\overline{u}]$, this method reduces the matching procedure to replacing the heavy pair spinor bilinear with an appropriate projection operator.

$$v(p_2, \lambda_2)\overline{u}(p_1, \lambda_1) \to \Lambda_C \otimes \Pi_S(p_1, p_2) \tag{2.27}$$

The Λ_C projectors are in charge to dictate the colour state of the system, separating the production of color-singlet heavy pairs from those in a color-octect state. For each of

these possibilities, the respective expression of the colour projector is

$$\Lambda_1 = \frac{\delta_{ab}}{\sqrt{N_c}} \qquad\qquad \Lambda_8^A = \frac{\mathrm{T}_{ab}^A}{\sqrt{T_F}} \tag{2.28}$$

where a and b are the quark's color indices, and $T_F = 1/2$ when $N_c = 3$. The second projector in (2.27) determines the spin of the heavy quark pair, which could be either singlet or triplet. In terms of the quark's spinors, its definition is given by

$$\Pi_S(p_1, p_2) = \sum_{\lambda_1 \lambda_2} v(p_2, \lambda_2)\overline{u}(p_1, \lambda_1) C_{S\, S_3}^{\lambda_1 \lambda_2} \tag{2.29}$$

where the Clebsch-Gordan coefficients

$$C_{S\, S_3}^{\lambda_1 \lambda_2} = \left\langle \frac{1}{2}, \lambda_1; \frac{1}{2}, \lambda_2 \;\middle|\; S, S_3 \right\rangle \tag{2.30}$$

indicate the spin-state composition of the heavy-quark pair.

To make practical use of the spin projector Π_S in calculations beyond leading order in v, we require a covariant and explicitly evaluable expression. That expression is not as simple as for the colour projector Λ_C. To understand it better, it is useful to derive it from scratch, so we will be able to see where each term comes from. To do so, we will to work on the Dirac base of gamma matrices, as it is specially useful to work on non-relativistic problems.

$$\gamma_0 = \begin{pmatrix} 1 & 0 \\ 0 & -1 \end{pmatrix} \qquad\qquad \gamma_j = \begin{pmatrix} 0 & \sigma_j \\ -\sigma_j & 0 \end{pmatrix} \tag{2.31}$$

Let us begin our derivation of the spin projector by defining the rest frame spinors as

$$u_0(s) = \begin{pmatrix} \xi(s) \\ 0 \end{pmatrix} \qquad\qquad v_0(s) = \begin{pmatrix} 0 \\ \eta(s) \end{pmatrix} \tag{2.32}$$

where $\xi(s)$ and $\eta(s)$ can be recognized as the 2-component Pauli Spinors. This is true because in the Dirac's definition of gamma matrices the generators of Lorentz transformations take the form

$$S^{0j} = \frac{i}{4}[\gamma_0, \gamma_j] = \frac{i}{2}\gamma_0\gamma_j = \frac{i}{2}\begin{pmatrix} 0 & \sigma_j \\ \sigma_j & 0 \end{pmatrix} \tag{2.33}$$

$$S^{jk} = \frac{i}{4}[\gamma_j, \gamma_k] = \frac{\epsilon_{jk\ell}}{2}\begin{pmatrix} \sigma_\ell & 0 \\ 0 & \sigma_\ell \end{pmatrix} \tag{2.34}$$

corresponding to boosts and rotations, respectively. From (2.34), we see that the 4-component spinor rotation generators are simply duplicated versions of those for 2-component spinors, acting on $\xi(s)$ and $\eta(s)$ by separate.

To apply these 2-component spinors in spin dependent calculations, we need to specify their definitions for different spin states. In particular, if the spinors defined in (2.32) are related to each other through the unitary charge-conjugation transformation $v = i\gamma_2 u^*$, then the Pauli spinors must be related as $\eta(s) = -i\sigma_2\xi^*(s)$. Choosing the spinor basis such that ψ is an eigenstate of σ_3, the Pauli spinors are defined as

$$\xi(+) = \sqrt{2m}\begin{pmatrix} 1 \\ 0 \end{pmatrix} \qquad\qquad \xi(-) = \sqrt{2m}\begin{pmatrix} 0 \\ 1 \end{pmatrix} \tag{2.35}$$

for fermion spinors, and

$$\eta(+) = \sqrt{2m}\begin{pmatrix}0\\1\end{pmatrix} \qquad \eta(-) = \sqrt{2m}\begin{pmatrix}-1\\0\end{pmatrix} \tag{2.36}$$

for anti-fermion spinors. The $\sqrt{2m}$ factor is included to maintain the relativistic normalization.

To address the kinematics of the heavy quark-antiquark pair as a two particle system, we need to move from the rest frame of each individual particle to the rest frame of the heavy pair (the center-of-mass frame). To achieve that we need the corresponding expression of the Lorentz Boost, which in the Dirac's representation is given by

$$\begin{aligned} D(\boldsymbol{p}) &= \exp\!\left(-iy_j S^{0j}\right) = \exp\!\left(\frac{1}{2}\begin{pmatrix}0 & \boldsymbol{y}\cdot\boldsymbol{\sigma}\\ \boldsymbol{y}\cdot\boldsymbol{\sigma} & 0\end{pmatrix}\right) \\ &= \cosh(y/2) + \sinh(y/2)\begin{pmatrix}0 & \hat{\boldsymbol{n}}\cdot\boldsymbol{\sigma}\\ \hat{\boldsymbol{n}}\cdot\boldsymbol{\sigma} & 0\end{pmatrix} \end{aligned} \tag{2.37}$$

where y is the rapidity. Since we are boosting from the rest frame of a massive particle to a frame where the particle carries a momentum $\boldsymbol{p}$, the transformation can be conveniently expressed as

$$D(\boldsymbol{p}) = \sqrt{\frac{E+m}{2m}}\begin{pmatrix}1 & \dfrac{\boldsymbol{p}\cdot\boldsymbol{\sigma}}{E+m}\\ \dfrac{\boldsymbol{p}\cdot\boldsymbol{\sigma}}{E+m} & 1\end{pmatrix} = \frac{m+\not{p}\gamma_0}{\sqrt{2m(E+m)}} \tag{2.38}$$

where we have used that $\cosh(y) = \gamma = E/m$.

Boosting the rest frame expressions (2.32) to the center-of-mass frame of the heavy pair, where the heavy quark and the heavy antiquark move in opposite directions with equal absolute spatial momentum q, we can express the Spin Projector definition (2.29) as

$$\Pi_S(p_1,p_2) = \frac{m_2+\not{p}_2\gamma_0}{\sqrt{E_2+m_2}}\left[\sum_{\lambda_1\lambda_2}\frac{v_0(\lambda_2)\overline{u}_0(\lambda_1)C_{S\,S_3}^{\lambda_1\lambda_2}}{\sqrt{2m_2}\sqrt{2m_1}}\right]\frac{m_1+\gamma_0\not{p}_1}{\sqrt{E_1+m_1}} \tag{2.39}$$

where p_1^μ and p_2^μ are respectively the center-of-mass momenta of the heavy quark and the heavy anti-quark. These momenta are related to the total momentum of the heavy quark pair P^μ as

$$p_1^\mu = (E_1,\boldsymbol{q}) = \frac{E_1}{M}P^\mu + q^\mu \qquad p_2^\mu = (E_2,-\boldsymbol{q}) = \frac{E_2}{M}P^\mu - q^\mu \tag{2.40}$$

$$P^\mu = (E_1+E_2,\boldsymbol{0}) = (M,\boldsymbol{0}) \qquad q^\mu = (0,\boldsymbol{q}) \tag{2.41}$$

where M is the invariant mass of the system.

When analysing eq. (2.39), the transformation properties of the bracketed term under Lorentz transformations are not immediately apparent, as its spinor structure does not take an obvious covariant form as a whole

$$v_0(\lambda_2)\overline{u}_0(\lambda_1) = \begin{pmatrix}0 & 0\\ \eta(\lambda_2)\xi^\dagger(\lambda_1) & 0\end{pmatrix} \tag{2.42}$$

To write the spin projector in a manifestly covariant form, it is useful to express it solely in terms of gamma matrices. For this purpose, we introduce the positive $\mathcal{P}_+$ and negative $\mathcal{P}_-$ covariant energy projectors, defined as

$$\mathcal{P}_+(p) = \frac{m + \not{p}}{2m} \qquad \mathcal{P}_-(p) = \frac{m - \not{p}}{2m} \tag{2.43}$$

These operators separate the spinors of positive $u(p)$ and negative $v(p)$ energy solutions of the Dirac equation, and their action on the four component spinors is just a restatement of the fact that they satisfy the two independent Dirac equations.

$$\mathcal{P}_+(p)u(p) = u(p), \qquad \mathcal{P}_-(p)v(p) = v(p) \tag{2.44}$$

$$\mathcal{P}_-(p)u(p) = 0, \qquad \mathcal{P}_+(p)v(p) = 0 \tag{2.45}$$

The reason we have introduced this energy projectors is because we can apply them on bracketed term using the properties shown in (2.44).

$$\sum_{\lambda_1\lambda_2} \frac{v_0(\lambda_2)\overline{u}_0(\lambda_1)C^{\lambda_1\lambda_2}_{SS_3}}{\sqrt{2m_2}\sqrt{2m_1}} = \mathcal{P}_-(0_2)\left[\sum_{\lambda_1\lambda_2} \frac{v_0(\lambda_2)\overline{u}_0(\lambda_1)C^{\lambda_1\lambda_2}_{SS_3}}{\sqrt{2m_2}\sqrt{2m_1}}\right]\mathcal{P}_+(0_1). \tag{2.46}$$

Having expressed the bracketed term in this form, the second set of properties of the energy projectors, given in (2.45), allows us to manipulate the expression more conveniently. In particular, these properties enable us to control the null components of the bracketed term, as the projectors ensure their vanishing. Consequently, as long as we retain the energy projectors, we are free to construct a fully covariant expression by the addition of a term in which the quark and antiquark exchange roles.

$$\sum_{\lambda_1\lambda_2} \frac{v_0(\lambda_2)\overline{u}_0(\lambda_1)}{\sqrt{2m_2}\sqrt{2m_1}}C^{\lambda_1\lambda_2}_{SS_3} \quad \Rightarrow \quad \Gamma_S = \sum_{\lambda_1\lambda_2} \frac{v_0(\lambda_2)\overline{u}_0(\lambda_1) + u_0(\lambda_2)\overline{v}_0(\lambda_1)}{\sqrt{2m_2}\sqrt{2m_1}}C^{\lambda_1\lambda_2}_{SS_3} \tag{2.47}$$

This additional term would naturally emerge if we were constructing the spin projector not for meson production, but for its decay. The result of this symmetrization is that the final expression for Γ_S evaluates to

$$\Gamma_{(S=0)} = \frac{\gamma_5}{\sqrt{2}}, \qquad \Gamma_{(S=1)} = \frac{\not{\varepsilon}^*}{\sqrt{2}}, \tag{2.48}$$

corresponding to the spin-singlet (pseudoscalar) and spin-triplet (vector) states, respectively. In the spin-triplet case, the spatial polarization vector is denoted by $\varepsilon^{\mu *}$.

Going back to eq. (2.39), we can now replace the bracketed term with its manifestly covariant counterpart, $\mathcal{P}_+(0_2)\Gamma_S\mathcal{P}_-(0_1)$. This yields the final covariant expression for the spin projector, which remains valid to all orders in the heavy quark's characteristic velocity v (or center-of-mass momentum q).

$$\Pi_S(p_1, p_2) = \frac{(\not{p}_2 - m_2)}{\sqrt{E_2 + m_2}}\,\Gamma_S\,\mathcal{P}_+(0)\,\frac{(\not{p}_1 + m_1)}{\sqrt{E_1 + m_1}}. \tag{2.49}$$

In this expression, the γ^0 factor appearing in the boost transformation in eq. (2.39) effectively reduces to a sign ($+1$ on the right and -1 on the left). This is simply because the structure of the energy projectors in the rest frame is

$$\mathcal{P}_-(0_1) = \frac{1 - \gamma^0}{2}, \qquad \mathcal{P}_+(0_1) = \frac{1 + \gamma^0}{2}, \tag{2.50}$$

which, when acting on γ^0, simply replace it by their respective eigenvalues ± 1. Moreover, the expression (2.49) contains only a single energy projector because the two rest-frame projectors can be commuted through Γ_S and combined into a single projector for the entire $Q\overline{Q}$ system. As a result, the expression (2.49) is often found in literature as

$$\Pi_S(p_1, p_2) = \frac{(\not{p}_2 - m_2)}{\sqrt{E_2 + m_2}} \Gamma_S \frac{M + \not{P}}{2M} \frac{(\not{p}_1 + m_1)}{\sqrt{E_1 + m_1}}, \tag{2.51}$$

where $M = E_1 + E_2$ is the invariant mass of the $Q\overline{Q}$ pair, and P^μ is the total four-momentum of the system.

Despite having expressed the spin projector in a manifestly covariant form, the matching with NRQCD still has to be performed in the rest frame. Therefore, the expression (2.51) is always calculated in the rest frame of the pair $Q\overline{Q}$. Only after expanding in terms of the heavy quark's momentum $\boldsymbol{q}$ to the desired order we can boost this expression to other frames. An exceptional simple case is when we neglect the contributions from all the powers of the heavy quark's rest frame momentum. This zeroth order approximation is equal to fix the value of the rest frame momenta $\boldsymbol{q}$ equal to zero, so the heavy quark and the heavy anti-quark will move in all frames with the same velocity. In this limit, the spin projector in the center-of-mass frame takes the particularly simple form

$$\Pi_S(0, 0) = \sqrt{2m_1}\sqrt{2m_2}\gamma^5 \frac{1 + \gamma^0}{2} \tag{2.52}$$

which can be easily boosted.

In the previous derivation, we worked assuming a space-time of $d = 4$ dimensions. Thus, the projector shown in (2.51) can be applied to compute only the short-distance coefficients of processes at tree-level. For loops calculations, the projection method has been generalized to arbitrary d dimensions in order to handle the UV and IR poles through dimensional regularization [70].

There is one final remark about the spin projector that is worth mentioning. If we need the expression for a decay process, or for the complex conjugate of the amplitude (as is required in cut diagrams), we can obtain it directly from the expression in (2.51) by applying the following transformation:

$$\Pi_S(p_1, p_2) \;\Rightarrow\; \overline{\Pi}_S(p_1, p_2) = \gamma_0 \Pi_S^\dagger(p_1, p_2) \gamma_0 \tag{2.53}$$

This relation is simply a reminder that our covariant expression for the spin projector is composed of spinor bilinears like $v\overline{u}$, and that these satisfy $v\overline{u} = \gamma_0 (u\overline{v})^\dagger \gamma_0$. In this way, we ensure that the covariant form of the spin projector remains valid and consistent when transitioning between production and decay processes.

2.5 NRQCD matrix elements

The cross sections expression (2.18) applies to any heavy meson H, with its specific state dependence entering only through the NRQCD matrix elements. While lattice QCD allows the computation of these matrix elements when they are related to the inclusive annihilation of heavy mesons, the same is not yet possible for their production. Despite this, these matrix elements are expected to be process-independent, meaning they do not

depend on the specific details of perturbative heavy-quark production. This universality enables their extraction from experimental data in one production process, allowing predictions for cross sections in other experiments.

It is also important to remember that the number of LDMEs increases with each order in v, leading to a large parameter space. Given our inability to compute all these values directly, reducing the number of independent parameters is crucial to prevent overfitting and simplify calculations. In this section, we address this problem by introducing several methods that help relate and simplify the matrix elements appearing in the inclusive production cross sections of heavy mesons.

Rotational Symmetry

The most straightforward method to reduce the number of relevant matrix elements is to restrict our analysis to the production of unpolarized heavy quark mesons. This choice is motivated by the fact that rotational symmetry is an exact symmetry in NRQCD, directly inherited from QCD. Namely, the consequence of this symmetry is that when matrix elements are summed over the polarizations of the heavy meson, the state projector becomes rotationally invariant. As a result, only those operators that are themselves invariant under rotations contribute to this sum.

Applying this observation to the production matrix elements of the spin-triplet S-wave state, we obtain

$$\sum_{S_3}\langle\chi^\dagger\sigma^i\psi\mathcal{P}_{H(S_3)}\psi^\dagger\sigma^j\chi\rangle = \frac{\delta_{ij}}{3}\langle\chi^\dagger\boldsymbol{\sigma}\psi\mathcal{P}_H\psi^\dagger\boldsymbol{\sigma}\chi\rangle = \frac{\delta_{ij}}{3}\langle\mathcal{O}^H(^3S_1^{[1]})\rangle, \tag{2.54}$$

$$\sum_{S_3}\langle\chi^\dagger\sigma^i T_a\psi\mathcal{P}_{H(S_3)}\psi^\dagger\sigma^j T_a\chi\rangle = \frac{\delta_{ij}}{3}\langle\chi^\dagger\boldsymbol{\sigma}T_a\psi\mathcal{P}_H\psi^\dagger\boldsymbol{\sigma}T_a\chi\rangle = \frac{\delta_{ij}}{3}\langle\mathcal{O}^H(^3S_1^{[8]})\rangle, \tag{2.55}$$

where $\mathcal{P}_H = \sum_{S_3}\mathcal{P}_{H(S_3)}$ is the polarization independent state projector.

Heavy Quark Spin Symmetry

While rotational symmetry is an exact symmetry of NRQCD, heavy-quark spin symmetry is only approximate within the NRQCD Lagrangian. Since this effective Lagrangian is derived from QCD through a matched expansion in the heavy quark's characteristic velocity v, we can always truncate at the leading order, resulting in predictions with a relative error of $\mathcal{O}(v^2)$. This minimal Lagrangian exhibits exact heavy-quark spin symmetry, as the dominant violations arise from spin-flip interactions

$$\psi^\dagger\boldsymbol{B}\cdot\boldsymbol{\sigma}\psi - \chi^\dagger\boldsymbol{B}\cdot\boldsymbol{\sigma}\chi, \tag{2.56}$$

whose effects are suppressed by a relative factor of v^2. Consequently, relations derived from heavy-quark spin symmetry hold up to corrections of relative order v^2. Despite this limitation, such relations significantly reduce the number of independent matrix elements contributing to the production of various spin states within a given radial and orbital excitation of a heavy quark bound state.

When applied to the production of S-wave states, heavy-quark spin symmetry allow us to relate the matrix elements associated with a spin-singlet state meson (A) and the

unpolarized spin-triplet state version (B). This follows from the fact that, in the absence of spin-flip interactions (2.56) in the NRQCD Lagrangian, the perturbatively produced heavy quark-antiquark pair can only transition into a heavy meson with the same spin configuration. As a result, the spin quantum numbers of the initial pair become irrelevant in the transition, leading to the relation

$$\langle \mathcal{O}^{\mathcal{B}}({}^3S_1^{[1]})\rangle = 3 \cdot \langle \mathcal{O}^{\mathcal{A}}({}^1S_0^{[1]})\rangle \Big(1 + O(v^2)\Big). \tag{2.57}$$

where the factor of 3 arises from the sum over the three possible polarization states of the spin-triplet configuration.

Vacuum-Saturation Approximation

The vacuum-saturation approximation assumes that the sum over fock state descomposition, present in the state projector $\mathcal{P}_H$, is dominated by the heavy meson state H plus the NRQCD vacuum, effectively "saturating" the sum with the lowest-energy contribution. For an operator $\mathcal{O}_{mn}$ applied to the production of a heavy meson H, the vacuum-saturation approximation allows its vacuum expectation values to be expressed in terms of vacuum-to-meson matrix elements.

$$\begin{aligned}
\langle \mathcal{O}^H_{nm}\rangle &= \langle 0|\chi^\dagger \mathcal{K}_n^\dagger \psi \mathcal{P}_H \psi^\dagger \mathcal{K}_m \chi|0\rangle \\
&= \langle 0|\chi^\dagger \mathcal{K}_n^\dagger \psi \left(\sum_X |H+X\rangle\langle H+X|\right) \psi^\dagger \mathcal{K}_m \chi|0\rangle \\
&\approx \langle 0|\chi^\dagger \mathcal{K}_n^\dagger \psi |H\rangle\langle H|\psi^\dagger \mathcal{K}_m \chi|0\rangle
\end{aligned} \tag{2.58}$$

As you can observe from this equation, only the heavy meson term $|H\rangle\langle H|$ is retained in the sum over states, neglecting higher Fock states such as $|H+g\rangle$ or $|H+gg\rangle$.

For a color-singlet operator, the approximation is controlled with a relative error of order v^4. This is because the matrix element describes a transition from a color-singlet $Q\overline{Q}$ state to a final state like $|H+S\rangle$, where S is a soft state. Since the meson H is a color singlet, the state S must also be a color singlet. Therefore, if S is not the NRQCD vacuum, it requires at least two gluon emissions to produce it. Each gluon emission brings a suppression by v^2, so the total contribution from this kind of interaction is suppressed by v^4 in the matrix element.

For colour-octet operators, however, this approximation is not valid. A transition from a colour-octet $Q\overline{Q}$ pair necessitates the presence of a colored soft part in the final state $|H+S\rangle$ to ensure colour conservation. Therefore, we can not force the soft part to be the NRQCD vacuum, and the vacuum-saturation approximation is inappropriate for colour-octet matrix elements.

Heavy Meson Wave Functions

While we cannot directly compute long-distance matrix elements using common techniques (such as Feynman diagrams), the special subset of LDME provided by the vacuum-saturation approximation, those corresponding to the trivial vacuum-to-quarkonium colour singlet transitions, exhibit a structure reminiscent of a wave function as defined in

[7]. For the sake of simplicity, let's consider a heavy quarkonium system. In a S-wave state, the wave functions are related to the matrix elements as follows

$$\Psi_S^1(\boldsymbol{r}) = \frac{1}{\sqrt{4\pi}} R_S(r) = \frac{1}{\sqrt{4MN_c}} \langle 0|\chi^\dagger\left(-\frac{\boldsymbol{r}}{2}\right)\psi\left(\frac{\boldsymbol{r}}{2}\right)\Big|^1 S_0(0)\Big\rangle \tag{2.59}$$

$$\Psi_S^3(\boldsymbol{r},\boldsymbol{\epsilon}) = \frac{\boldsymbol{\epsilon}}{\sqrt{4\pi}} R_S(r) = \frac{1}{\sqrt{4MN_c}} \langle 0|\chi^\dagger\left(-\frac{\boldsymbol{r}}{2}\right)\boldsymbol{\sigma}\psi\left(\frac{\boldsymbol{r}}{2}\right)\Big|^1 S_0(0)\Big\rangle \tag{2.60}$$

where the heavy quarkonium mass M, not present in the definition given in [7], has been included as a factor to maintain the relativistic normalization of the states.

Following the classic result provided by Van Royen and Weisskopf [71], in the early years of QCD, it has become a common practice to approximate quantities involving relativistic bound states in terms of the values of the radial wave function $R_H(0)$ or its derivatives $R'_H(0)$ at the origin in coordinate space. In the case of NRQCD, this is also the case, as the matrix elements from the vacuum-saturation approximation are only evaluated at the origin, thus giving the following result

$$\langle \mathcal{O}^H({}^1S_0^{[1]})\rangle \approx \Big|\langle 0|\chi^\dagger\psi|H\rangle\Big|^2 = \frac{N_c M}{\pi}|R_S(0)|^2 \tag{2.61}$$

$$\langle \mathcal{O}^H({}^3S_1^{[1]})\rangle \approx \Big|\langle 0|\chi^\dagger\boldsymbol{\sigma}\psi|H\rangle\Big|^2 = 3\cdot\frac{N_c M}{\pi}|R_S(0)|^2 \tag{2.62}$$

Notice that we make no distinction between the ${}^1S_0$ and ${}^3S_1$ wave functions, as they are approximately equal due to heavy-quark spin symmetry.

We can show that (2.59) and (2.60) provide a good definition of the quarkonium wave function when working within a model in which the quarkonium consists only of a $Q\overline{Q}$ pair. To do so, we recall that the heavy quarks inside a meson are not free particles with definite momenta. Instead, those states must be integrated with the corresponding wave function $\Psi(\boldsymbol{k})$, whose squared absolute value describes the probability of finding a quark with momentum $\boldsymbol{k}$ inside the meson. Therefore, the state of a heavy quarkonium is expressed as a superposition of quark-antiquark colour-singlet states, where the constituent quark and antiquark move with opposite momenta in the bound state's rest frame.

$$\Big|^{2S+1}J_{S_3}(\boldsymbol{0})\Big\rangle = \sum_c \int \frac{d^3k}{(2\pi)^3}\frac{\Psi_J(\boldsymbol{k})}{\sqrt{N_c}}\sqrt{\frac{2E_H}{2E_Q 2E_{\overline{Q}}}} C_{S\,S_3}^{\lambda_1\lambda_2}\Big|Q^c_{\lambda_1}(\boldsymbol{k})\overline{Q}^c_{\lambda_2}(-\boldsymbol{k})\Big\rangle \tag{2.63}$$

Here, $\tilde{\Psi}_J(\boldsymbol{k})$ represents the wave function of the quarkonium state with angular momentum J in momentum space, while $C_{S\,S_3}^{\lambda_1\lambda_2}$ are the Clebsch-Gordan coefficients encoding the spin configuration of the quark-antiquark pair. The factor $1/\sqrt{N_c}$ accounts for the normalization over the three possible color-singlet states in which the $Q\overline{Q}$ pair can exist. Lastly, the term $\sqrt{2E_H/(2E_Q 2E_{\overline{Q}})}$ ensures that the state normalization is consistent with the relativistic normalization convention used in this work.

It is important to mention that the definition (2.63) was intentionally given in the hadron's rest-frame, as a covariant expression is usually bit more complicated. [72] provides a light-cone definition of light and heavy hadron's state in terms of the wave function in such a way that the boost in the plus direction is really simple.

Having clarified our assumptions regarding the quarkonium state, we now proceed with the derivation of the matrix element expression for the wave functions. For simplicity,

let us consider only the spin-singlet case. Using the momentum-space expressions (2.2), the matrix element from (2.59) can be rewritten as

$$\begin{aligned}\langle 0|\chi^\dagger\Big(-\frac{\boldsymbol{r}}{2}\Big)\psi\Big(\frac{\boldsymbol{r}}{2}\Big)\Big|^1S_0(0)\Big\rangle =& \frac{\sqrt{2M}}{(2\pi)^9}\iint\frac{d^3q_1d^3q_2}{2E_12E_2}e^{\frac{i}{2}\boldsymbol{r}\cdot(\boldsymbol{q}_1-\boldsymbol{q}_2)}\int\frac{d^3k}{2E_k}\frac{\tilde\Psi_S(\boldsymbol{k})}{\sqrt{N_c}} \\ & \sum_c\eta^\dagger(\boldsymbol{q}_2)\xi(\boldsymbol{q}_1)C_{SS_3}^{\lambda_1\lambda_2}\langle 0|a(\boldsymbol{q}_1)b^\dagger(\boldsymbol{q}_2)\Big|Q^c_{\lambda_1}(\boldsymbol{k})\overline{Q}^c_{\lambda_2}(-\boldsymbol{k})\Big\rangle\end{aligned} \tag{2.64}$$

Since the equation is lengthy, we will analyse it piece by piece.

Directly from the normalization condition of the states, the product between the states gives the following expression

$$\langle 0|a(\boldsymbol{q}_1)b^\dagger(\boldsymbol{q}_2)\Big|Q^c_{\lambda_1}(\boldsymbol{k})\overline{Q}^c_{\lambda_2}(-\boldsymbol{k})\Big\rangle = (2E_k)^2(2\pi)^6\delta^3(\boldsymbol{q}_1-\boldsymbol{k})\delta^3(\boldsymbol{q}_2+\boldsymbol{k}), \tag{2.65}$$

which ensures that the momenta, colour, and spin of the quarks created perturbatively match those present in the meson. On the other hand, if we expand the sum over the possible quark polarization combinations,

$$C_{SS_3}^{\lambda_1\lambda_2}\Big|Q^c_{\lambda_1}\overline{Q}^c_{\lambda_2}\Big\rangle = \frac{1}{\sqrt{2}}\Big(\Big|Q^c_-\overline{Q}^c_+\Big\rangle - \Big|Q^c_+\overline{Q}^c_-\Big\rangle\Big), \tag{2.66}$$

we observe that there are only two relevant products between Pauli spinors.

$$\eta^\dagger(+,\boldsymbol{q}_2)\xi(-,\boldsymbol{q}_1) = -\eta^\dagger(-,\boldsymbol{q}_2)\xi(+,\boldsymbol{q}_1) = \sqrt{2E_1}\sqrt{2E_2}. \tag{2.67}$$

Here, we have used the same definitions for the Pauli spinors as in (2.35) and (2.36). The only difference is that these spinors are not in the rest frame, and thus their normalization is slightly different, but fundamentally remains the same.

For a $^1S_0$ state, the wave function is spherically symmetric and can therefore be expressed as

$$\tilde\Psi_S(\boldsymbol{k}) = Y_0^0(\theta,\phi)\tilde R_S(k) = \frac{1}{\sqrt{4\pi}}\tilde R_S(k), \tag{2.68}$$

where Y_0^0 is the corresponding spherical harmonic for an S-wave state.

Finally, applying these last results and summing over the three possible colour states, we can rewrite the expression (2.64) as

$$\begin{aligned}\langle 0|\chi^\dagger\Big(-\frac{\boldsymbol{r}}{2}\Big)\psi\Big(\frac{\boldsymbol{r}}{2}\Big)\Big|^1S_0(0)\Big\rangle &= \sqrt{\frac{MN_c}{\pi}}\int\frac{d^3k}{(2\pi)^3}\tilde R_S(k) \\ &\quad \iint\frac{d^3q_1\,d^3q_2}{2E_12E_2}e^{\frac{i}{2}\boldsymbol{r}\cdot(\boldsymbol{q}_1-\boldsymbol{q}_2)}(2E_k)^2\delta^3(\boldsymbol{q}_1-\boldsymbol{k})\delta^3(\boldsymbol{q}_2+\boldsymbol{k}) \\ &= \sqrt{\frac{MN_c}{\pi}}\int\frac{d^3k}{(2\pi)^3}\tilde R_S(k)e^{i\boldsymbol{r}\cdot\boldsymbol{k}} \\ &= \sqrt{\frac{MN_c}{\pi}}R_S(r) = \sqrt{4MN_c}\Psi_S(\boldsymbol{r}),\end{aligned} \tag{2.69}$$

proving equation (2.59).

3 B_c meson production at LHCb

The study of heavy mesons in high-energy hadronic collisions offers a powerful probe of Quantum Chromodynamics (QCD), allowing access to both perturbative and non-perturbative aspects of the theory. In this context, the B_c stands out as a particularly interesting system, being the only known meson composed of two different heavy flavours (bottom and charm). This asymmetric composition sets it apart from quarkonium systems like charmonium ($c\bar{c}$) and bottomonium ($b\bar{b}$), as well as from other B mesons that contain only a single heavy quark. As such, the B_c system offers a valuable testing ground for the theoretical tools discussed in previous chapters.

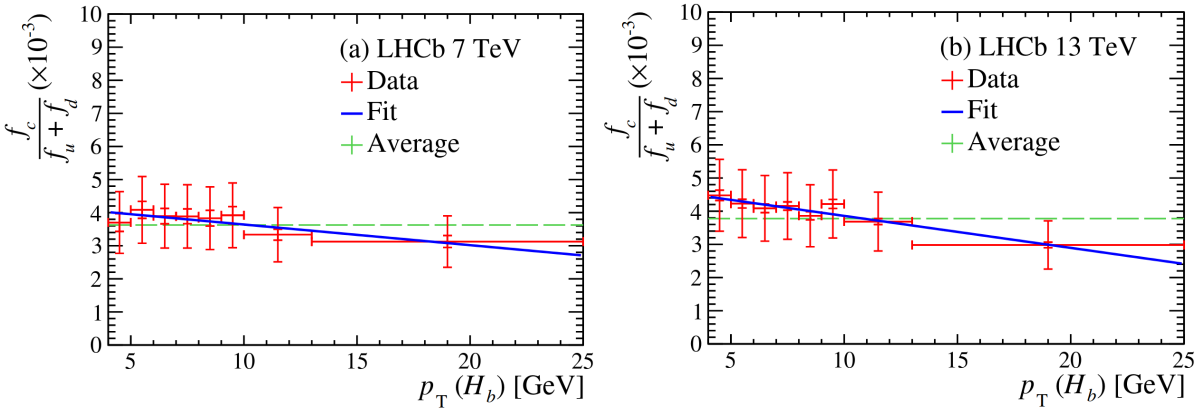

Figure 3.1: Ratio of production fractions [18]. The smaller error bars show the statistical uncertainties and the larger ones include the statistical and systematic uncertainties.

Currently, precise measurements of the B_c meson production cross section remain challenging due to the large uncertainties in many of its decay branching ratios, as well as the high energy required to produce them. This is reflected in the fact that earlier studies reported only ratios of total cross sections, such as $\sigma(B_c^+)/\sigma(B_+)$ in [12], without kinematic information. However, more recently, the LHCb collaboration [18] has provided, for the first time, the transverse momentum dependence of the fragmentation ratio

$$\frac{f_c}{f_u + f_d} \sim \frac{\sigma(B_c)}{\sigma(B_u) + \sigma(B_d)} \tag{3.1}$$

where f_c, f_u, and f_d represent the production fractions of the B_c, B_u, and B_d mesons, respectively (we consider the sum of the particle and the anti-particle). In fig. 3.1 this ratio, measured for $\sqrt{s} = 7$ TeV and $\sqrt{s} = 13$ TeV, is shown as a function of the hadron's transverse momentum $p_T(H_b)$, in the range $2.5 < \eta < 4.5$ of forward pseudorapidity. Although the dependence on η is reported to be small, the ratio decreases noticeably with increasing p_T, especially for $\sqrt{s} = 13$ TeV. This observed trend suggests that the underlying production dynamics may vary across the kinematic range.

Despite the importance of these measurements, so far few studies have provided estimates for the integrated ratio $f_c/(f_u + f_d)$ from a production approach, and none has offered a prediction for its p_T-dependence. Additionally, in the kinematic range explored by LHCb, it is possible that multiple production mechanisms contribute significantly to B_c meson production. For these reasons, the study of the p_T-dependence can be a valuable tool for testing the range of validity of different theoretical approaches and getting new

insights on what we need to improve. Therefore, the objective of this chapter will be to reproduce the LHCb measurements using theoretical tools based in QCD.

In the usual NRQCD method (which we will call the *Direct Approach*) the hadroproduction of B_c mesons mainly comes from partonic subprocesses like gluon-gluon fusion $gg \to B_c + b\bar{c}$ and flavour excitation $g\bar{c} \to B_c + \bar{b}$. At leading order in the strong coupling constant, this calculation involves more than 40 Feynman diagrams, which makes it quite complicated. For this reason, we will follow an alternative but complementary (and less laborious) method known as the *Fragmentation Approach*.

We begin this chapter by introducing the fragmentation approach and discussing its range of validity in comparison with the direct approach. We then present a calculation of the fragmentation functions of partons into weakly decaying B_c mesons. These functions are then used to compute the differential cross sections for B_c production in pp collisions at $\sqrt{s} = 7$ TeV and $\sqrt{s} = 13$ TeV. Finally, we compare our theoretical predictions with LHCb measurements for the transverse momentum (p_T) dependence of the production ratio $f_c/(f_u + f_d)$.

3.1 NRQCD Fragmentation Approach

In the previous chapters, we reviewed the fundamental aspects of two formalisms that are particularly useful for computing scattering cross sections involving the production of heavy mesons. Both frameworks rely on factorization techniques, in which the concept of a *hard scale* Q plays a central role. As we saw, this scale corresponds to the characteristic energy or momentum transfer at which the short-distance dynamics occur. When Q is much larger than the typical hadronic scale Λ_{QCD}, it becomes possible to approximately separate the perturbative part of the process from the non-perturbative contributions. In the context of hadroproduction, the hard scale is often identified with the transverse mass of the produced particle, defined as $m_T = \sqrt{m^2 + p_T^2}$, where m is the particle's mass and p_T its transverse momentum.

When a heavy meson is produced in processes where the characteristic hard energy scale Q is comparable to the heavy-quark mass, $Q \sim m_Q$, the NRQCD factorization framework provides a reliable and systematic approach to describe its production. In such cases, the perturbatively calculable part of the process is dominated by a single hard scale associated with the creation of the $Q\overline{Q}$ pair, while the lower energy scales, of order $m_Q v$ and $m_Q v^2$, govern the subsequent non-perturbative evolution of the pair into the bound heavy meson state H.

When the characteristic energy scale of a process greatly exceeds the heavy-quark mass, $Q \gg m_Q$, the perturvative part of the process becomes a two scale problem. In this high-energy regime, large logarithmic terms appear in the cross section at each order in perturbation theory. Although the emission of extra partons is suppressed by powers of α_s, the presence of these large logarithms can disrupt the convergence of the expansion. Consequently, the perturbative series is no longer solely controlled by the smallness of α_s, and higher-order contributions may become comparable to or even larger than the leading-order terms.

In collinear factorization, scenarios as those described in the previous paragraph are addressed by resumming the leading logarithmic contributions to all orders in perturbation theory. For the hadro-production process of a heavy meson H, the result is that the scattering cross-section at high transverse momentum is given by the following equation

$$d\sigma_{AB\to HX} \approx \sum_q d\hat{\sigma}_{AB\to qX}\left(\frac{P_T}{z}, \mu, \mu_f\right) \otimes D_{q\to H}(z, \mu_f) + \mathcal{O}\left(\frac{m_Q^2}{P_T^2}\right), \tag{3.2}$$

which represents the leading-power factorization formula in the limit $m_Q^2 \ll P_T^2$. This relation includes only the dominant contribution arising from the convolution of universal fragmentation functions $D_{q/H}(z, \mu_f)$ with a partonic production cross section $d\hat{\sigma}_{AB\to qX}$, containing all the information on the nature of the process. The scale dependence of these fragmentation functions is governed by the Dokshitzer-Gribov-Lipatov-Altarelli-Parisi (DGLAP) evolution equations. Specifically, the evolution of a fragmentation function describing the transition of a parton q into a hadron H follows

$$\frac{d}{d\ln\mu^2} D_{q\to H}(z, \mu_f) = \sum_j \int_z^1 \frac{d\xi}{\xi} P_{jq}(\xi)\, D_{j\to H}\left(\frac{z}{\xi}, \mu_f\right), \tag{3.3}$$

where $P_{jq}(\xi)$ are the time-like splitting functions.

Although the evolution equation is derived entirely within perturbative QCD, solving it requires an initial condition at a lower scale $\mu_0 \sim m_Q$. This initial fragmentation function, $D_{q/H}(z, \mu_0)$, captures the non-perturbative physics of hadronization and must be extracted from experimental data. This is a limitation of the formalism, as collinear factorization does not provide a first-principles method to compute this initial condition. Instead, one typically resorts to phenomenological models, which still require calibration using experimental input.

To address this limitation, one promising idea is to use NRQCD to describe the non-perturbative structure of the initial fragmentation function $D_{q/H}(z, \mu_0)$, as it only involves physics below the scale $\mu_0 \sim m_Q$. In this context, the fragmentation function at the initial scale μ_0 can be expanded in terms of a finite number of NRQCD long-distance matrix elements. Then, by applying the DGLAP evolution, this formulation allows NRQCD to be extended to high-energy processes where the hard scale is much larger than the heavy-quark mass. This framework, which we will refer to as the *Fragmentation Function Approach*, expresses the inclusive production cross section of a heavy meson H in the same factorized form as collinear factorization in eq. (3.2), but replaces the initial condition of the fragmentation function with an NRQCD v-expansion

$$D_{q\to H}(z, \mu_0) = \sum_n d_{q/Q\overline{Q}[n]}(z, \mu_0) \langle \mathcal{O}_H(n) \rangle \tag{3.4}$$

where the Wilson coefficient $d_{q/Q\overline{Q}[n]}(z, \mu_0)$, which can be extracted after a matching with a calculation using the Feynman rules introduced in Chapter 1 and the projectors defined in Chapter 2, describes the distribution of $Q\overline{Q}$ pairs in the state labeled by n within a jet initiated by a parton q. The term $\langle \mathcal{O}_H(n) \rangle$ is proportional to the probability that this pointlike $Q\overline{Q}$ pair in the state n evolves into the heavy meson H. The light-cone momentum fraction z carried by the heavy meson H with respect to the parent parton q is identified with that of the $Q\overline{Q}$ pair, making the z-dependence of the fragmentation function perturbatively calculable.

This approach has the advantage of simplifying the computation, as the fragmentation functions are easier to calculate than full fixed-order cross sections in α_s, and can also be extended in a straightforward way to include higher orbital angular momentum states like P-wave and D-wave mesons. Another benefit is that this approach only requires extracting a few universal NRQCD long-distance matrix elements from experimental data to fully determine the fragmentation function. However, its main limitation is that it remains valid only in the regime of high transverse momentum p_T.

Although a formal proof to all orders in perturbation theory is still lacking, there has been some progrues to it [73], [74], and this formalism has been extensively applied to heavy quarkonium production. Examples can be found in [75] [76] [77] [78] [79] [80].

3.2 DGLAP Initial Condition for B_c

Many fragmentation functions for B_c mesons have been computed in the literature. The first such calculation was performed in 1993 by Braaten, Cheung, and Yuan [75], where the fragmentation functions of b and c quarks into S-wave states (specifically the B_c and B_c^* mesons) were computed at order α_s^2. Subsequent works extended these results to excited states. The FFs for P-wave states were calculated in [81] [82], and the D-wave excitations were obtained in [83].These results were originally derived using a model-based definition of fragmentation functions. They were later confirmed using the formal light-cone definition within the framework of collinear factorization in [84] and [85]. More recently, for S-wave mesons, next-to-leading order (NLO) α_s corrections to b and c quark fragmentation were computed in [86], and the leading α_S contribution to gluon fragmentation (appearing at order α_s^3) was calculated in [87] [88].

To apply any of these results to reproduce the production rates observed at LHCb, it is important to note that B_c mesons are detected experimentally only through their weak decays. In contrast, the NRQCD formalism provides predictions for the production of the heavy mesons at the moment of their creation. Whether or not an excited state contributes to the observed weakly decaying B_c mesons depends on their decay channels. Since strong and electromagnetic transitions typically occur much faster than weak decays, they can significantly enhance the population of lower states. In the case of B_c mesons, since they are composed of two different quark flavors, their excited states are protected from annihilation into light hadrons or photons. Moreover, according to potential model calculations [8], the $1S$, $1P$, $1D$, $2S$, and possibly the full set of $2P$ states lie below the BD threshold (the mass at which the meson can decay into a pair of B and D mesons). As a result, many excited states decay quickly to the ground state via electromagnetic or pionic radiation, substantially enhancing the observed number of weakly decaying B_c mesons.

With this physical context in mind, we now turn to the derivation of the fragmentation functions weakly decaying B_c mesons at the initial scale μ_0. We aim to provide a rough estimate by working at the lowest nontrivial order in both α_s and the heavy quark's characteristic velocity v^2. In general, we will follow the work presented in [86] [85], whose derivation combines the frameworks of Collineal Factorization and NRQCD for computing fragmentation functions for B_c and B_c^* mesons.

Relevant Contributions at Leading Order

Before proceeding with the calculations, let us clarify what is meant by leading order in the context of B_c meson production. This case differs significantly from the more extensively studied quarkonium systems, and identifying which contributions are the most important at the level of precision we are using is essential. In the NRQCD factorization approach, the calculation involves two separate expansions. One expansion is in powers of α_s, which includes more complex short-distance interactions as we go to higher orders. The other expansion is in powers of v^2, in which higher order terms account for more complex non-perturbative transitions or the production of excited heavy meson states.

From a parton-level perspective, the simplest mechanism for producing a B_c meson involves a virtual b quark (escaping from the hard scattering) radiating a $c\bar{c}$ pair and subsequently binding with the charm antiquark to form the meson. A schematic illustration of this heavy-quark fragmentation process at leading order in the strong coupling (α_s^2) is shown in fig. 3.2. Gluon fragmentation, on the other hand, requires the production

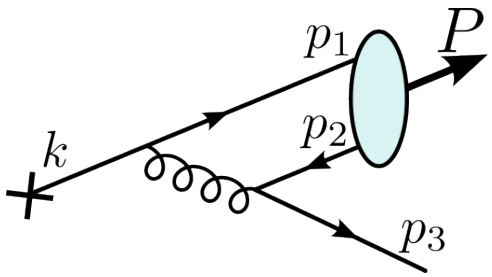

Figure 3.2: Schematic Feynman diagram of a heavy quark fragmenting into a B_c meson at leading order in α_s.

of both a $b\bar{b}$ and a $c\bar{c}$ pair. This is only possible starting at order α_s^3, which means it is perturbatively suppressed compared to quark fragmentation. Moreover, from a kinematic point of view, it is more difficult because the gluon needs to have a virtuality large enough to produce the combined masses of both heavy quark pairs.

According to NRQCD power counting, the leading contributions at small v^2 come from long distance matrix elements describing transitions where the $b\bar{c}$ pair evolves into an S-wave meson without changing its spin or colour configuration. This is partially because the lowest-order four-fermion operators in the v-expansion of the NRQCD Lagrangian correspond to S-wave, colour-singlet configurations. Besides, any change in quantum numbers (such as transitioning from a colour-octet to a colour-singlet state or flipping the spin) requires soft gluon emissions, each of which introduces an additional suppression by a factor of v^2 to the long-distance matrix elements (LDME). Therefore, the most probable production channels are those involving trivial transitions, where the initial $b\bar{c}$ pair and the final meson have identical quantum numbers. These include ${}^1S_0^{[1]} \to B_c(1^1S_0)$ and ${}^3S_1^{[1]} \to B_c^*(1^3S_1)$, which produce the ground state and the first spin-excited state of the $b\bar{c}$ system, respectively.

In summary, there are only two contributions at leading order to the initial fragmentation functions responsible for producing ($b\bar{c}$) bound states.

$$D_{b\to B_c}(z,\mu_0) = d_{{}^1S_0^{[1]}}(z,\mu_0)\langle\langle\mathcal{O}^{B_c}({}^1S_0^{[1]})\rangle + \mathcal{O}(v^2) \tag{3.5}$$

$$D_{b\to B_c^*}(z,\mu_0) = d_{{}^3S_1^{[1]}}(z,\mu_0)\langle\mathcal{O}^{B_c^*}({}^3S_1^{[1]})\rangle + \mathcal{O}(v^2) \tag{3.6}$$

Due to the current lack of experimental data, the values of these LDMEs remain unconstrained. Consequently, our only option is to use the vacuum saturation approximation, so these colour-singlet NRQCD matrix elements can be related to the radial wavefunction at the origin $R_S(0)$, which can be computed using phenomenological potential models. As shown in section 2.5, the corresponding expressions are

$$\langle \mathcal{O}^{B_c}({}^1S_0^{[1]})\rangle = M\frac{N_c}{\pi}|R_S(0)|^2 \tag{3.7}$$

$$\langle \mathcal{O}^{B_c^*}({}^3S_1^{[1]})\rangle = M\frac{3N_c}{\pi}|R_S(0)|^2 \tag{3.8}$$

where M denotes the mass of the corresponding meson.

Matching Procedure

To calculate the perturbative coefficients appearing in eqs. (3.5) and (3.6), we follow the standard matching procedure described in Chapter 2. This involves replacing the physical B_c or B_c^* state for a free quark pair $b\bar{c}$ carrying the appropriate quantum numbers and making sure that the cases of full QCD and NRQCD provide the same results. Specifically, we need to compute first the perturbative fragmentation functions

$$D_{b\to b\bar{c}[{}^1S_0^{[1]}]} \quad \text{and} \quad D_{b\to b\bar{c}[{}^3S_1^{[1]}]}$$

from which the short-distance coefficients can be extracted using the matching conditions

$$D_{b\to b\bar{c}[{}^1S_0^{[1]}]}(z,\mu_0) = d_{{}^1S_0^{[1]}}(z,\mu_0)\langle \mathcal{O}^{b\bar{c}[{}^1S_0^{[1]}]}({}^1S_0^{[1]})\rangle + O(v^2) \tag{3.9}$$

$$D_{b\to b\bar{c}[{}^3S_1^{[1]}]}(z,\mu_0) = d_{{}^3S_1^{[1]}}(z,\mu_0)\langle \mathcal{O}^{b\bar{c}[{}^3S_1^{[1]}]}({}^3S_1^{[1]})\rangle + O(v^2) \tag{3.10}$$

where the vacuum matrix elements are

$$\langle \mathcal{O}^{b\bar{c}[{}^1S_0^{[1]}]}({}^1S_0^{[1]})\rangle = \sum_X \left|\langle 0|\chi_c^\dagger\psi_b\Big|b\bar{c}({}^1S_0^{[1]})+X\Big\rangle\right|^2 = (2m_b)(2m_c)(2N_c) \tag{3.11}$$

$$\langle \mathcal{O}^{b\bar{c}[{}^1S_0^{[1]}]}({}^3S_1^{[1]})\rangle = \sum_X \left|\langle 0|\chi_c^\dagger\boldsymbol{\sigma}\psi_b\Big|b\bar{c}({}^3S_1^{[1]})+X\Big\rangle\right|^2 = 3(2m_b)(2m_c)(2N_c) \tag{3.12}$$

just a normalization of the states in NRQCD.

Using the Collins-Soper definition presented in Section 1.3, the fragmentation function is obtained by summing over all possible cut diagrams that produce the desired inclusive final state from a single virtual quark. As illustrated in Fig. 3.3 and discussed in detail in Section 1.3, each diagram involves a Wilson line that connects a quark-field operator on the left side of the cut to the conjugate operator on the right side. Single virtual fermion lines are attached to each operator, and they are connected through QCD interactions involving gluon and quark propagators. Additional gluon emissions may also attach to the Wilson line (unless we work in the light-cone gauge). The cut passes through the Wilson line, the line corresponding to the final-state particle into which the b-quark is fragmenting, and possibly through additional gluon or quark lines.

The computation of the fragmentation functions proceeds by applying their specific Feynman rules to the relevant cut diagrams shown in Fig. 3.3. These rules were introduced in Section 1.3; here, we provide a more detailed and guided description of how they

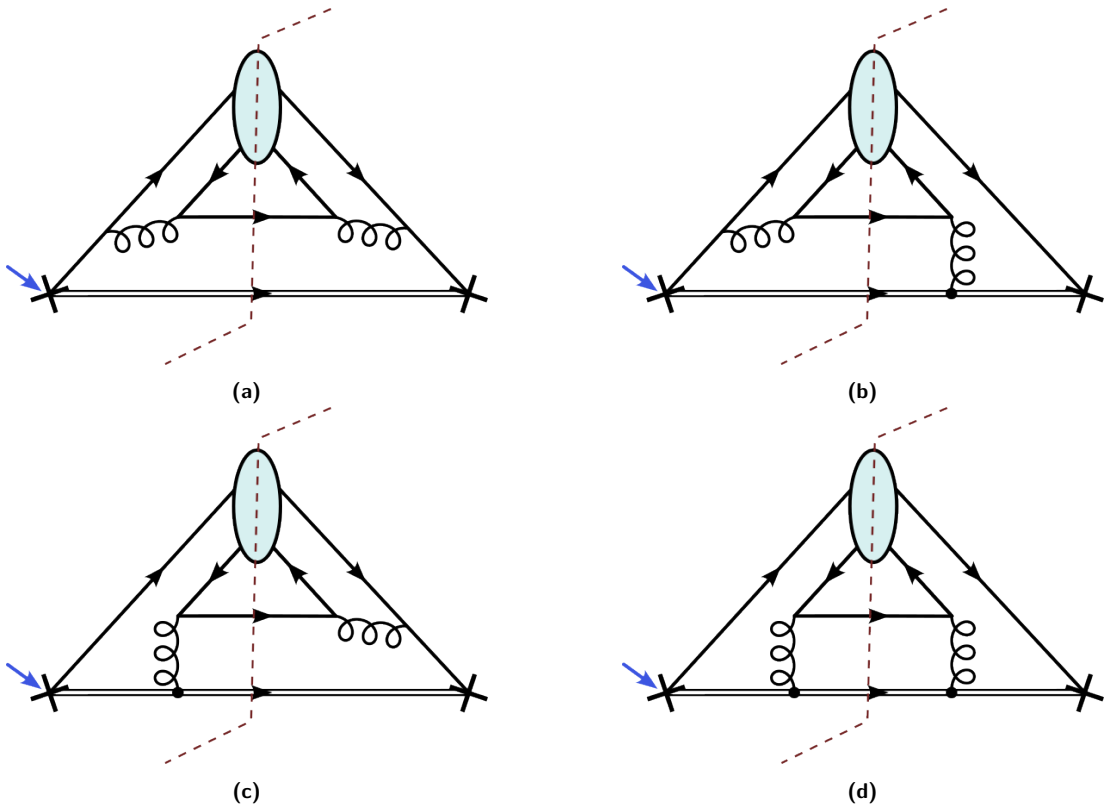

Figure 3.3: Cut diagrams relevant for the computation of the fragmentation functions at leading order in α_S. The crossed vertices indicate the action of the quark field operators from the FFs defintion, meanwhile the circle in the final state cut represents the action of the NRQCD state projectors.

are applied in practice, to make the construction of the corresponding amplitudes more transparent.

The first and most important point to emphasize is that, by definition, there are no on-shell initial particles. Instead, the four-momentum k of the fragmenting quark, as defined in Fig. 3.2, enters the diagram through the operator vertex on the left side of the Wilson line and exits through the operator on the right side. This is reflected in the calculation by the presence of an integral over d^4k, which accounts for the flux of external momentum:

$$D(z,\mu_0) = \frac{1}{4N_c}\int d\Pi_X \int \frac{d^4k}{(2\pi)^4}\,\delta(zk^+ - P^+)\,|\mathcal{M}|^2\,. \tag{3.13}$$

where $d\Pi_X$ is the final phase space.

The momentum k entering through the operator can be divided between the virtual fermion line and the Wilson line, allowing gluons to attach to the latter. When a gluon attaches to the Wilson line, the corresponding Feynman rules can be summarized as follows:

- A vertex where a gluon attaches to an eikonal line contributes a factor $ig_s\,n^\mu\,t^a_{ij}$, where μ and a are the Lorentz and color indices of the gluon, respectively, and n^μ is the direction vector of the Wilson line.
- An internal eikonal line carrying momentum q from the operator toward the cut side is associated with the propagator $i\,\delta_{ij}/(q\cdot n + i0)$.

The remaining Feynman rules are those of QCD.

Since fragmentation functions are defined in a Lorentz-invariant way, we can perform the calculation in any reference frame. For convenience, we choose the rest frame of the $b\bar{c}$ pair. In this frame, at leading order in the velocity expansion, the initial-state quark, the final-state bc pair, and the final-state charm quark, respectively, have the momenta

$$k^\mu = \Big(k^+, k^-, \boldsymbol{k}_T\Big), \qquad P^\mu = \frac{1}{\sqrt{2}}(M, M, 0), \qquad p_3^\mu = \left(p_3^+, k^- - \frac{M}{\sqrt{2}}, \boldsymbol{k}_T\right), \tag{3.14}$$

where $M = m_c + m_b$, and the momenta of the heavy quarks inside the pair are

$$p_1^\mu = r_b P^\mu \quad p_2^\mu = r_c P^\mu \tag{3.15}$$

where $r_b = m_b/M$ and $r_c = m_c/M$.

To project the $b\bar{c}$ pair onto the desired color and spin states, we employ the covariant projector technique. At zeroth order in the quark relative momentum, this corresponds to making the substitution

$$v\overline{u} \to \Pi_s \otimes \Lambda_C, \quad \Pi_s = \sqrt{2m_c}\sqrt{2m_b}\gamma_5 \frac{1+\gamma_0}{2}, \quad \Lambda_C = \frac{\mathbf{1}}{\sqrt{2N_c}}, \tag{3.16}$$

in accordance with the discussion we gave in Section 2.4.

Finally, putting all this things together, we can get the following cut amplitudes

$$|\mathcal{M}|^2_{(a)} = g_S^4 |\mathcal{M}|^2_{Col} \mathrm{Tr}\left[\frac{\not{n}(\not{P} + \not{p}_3 + m_b)\gamma_\mu \Pi_S \gamma^\mu (\not{p}_3 - m_c)\gamma^\nu \overline{\Pi}_S \gamma_\nu (\not{P} + \not{p}_3 + m_b)}{((P+p_3)^2 - m_b^2)^2 (p_1+p_3)^4}\right] \tag{3.17}$$

$$|\mathcal{M}|^2_{(b)} = g_S^4 |\mathcal{M}|^2_{Col} \mathrm{Tr}\left[\frac{\not{n}(\not{P} + \not{p}_3 + m_b)\gamma_\mu \Pi_S \gamma^\mu (\not{p}_3 - m_c)\not{n}\overline{\Pi}_S}{(p_1+p_3)\cdot n)((P+p_3)^2 - m_b^2)(p_1+p_3)^4}\right] \tag{3.18}$$

$$|\mathcal{M}|^2_{(c)} = g_S^4 |\mathcal{M}|^2_{Col} \mathrm{Tr}\left[\frac{\not{n}\Pi_S \not{n}(\not{p}_3 - m_c)\gamma^\nu \overline{\Pi}_S \gamma_\nu (\not{P} + \not{p}_3 + m_b)}{(p_1+p_3)\cdot n)((P+p_3)^2 - m_b^2)(p_1+p_3)^4}\right] \tag{3.19}$$

$$|\mathcal{M}|^2_{(d)} = g_S^4 |\mathcal{M}|^2_{Col} \mathrm{Tr}\left[\frac{\not{n}\Pi_S \not{n}(\not{p}_3 - m_c)\not{n}\overline{\Pi}_S}{((p_1+p_3)\cdot n)^2 (p_1+p_3)^4}\right] \tag{3.20}$$

where

$$|\mathcal{M}|^2_{Col} = \mathrm{Tr}\Big[T^a \Lambda_C T^a T^b \Lambda_C T^b\Big] \tag{3.21}$$

is a common colour factor.

The last step is to integrate over the diferential phase space of the final particles (besides the meson which has an specified momentum). In light cone coordinates, differential phase space for the LO FFs can be written as

$$d\Pi_{LO} = \frac{1}{S}\delta\Big(k^+ - P^+ - p_3^+\Big)\Theta(k^+)\frac{dp_3^+}{2p_3^+}\frac{d^2p_{3T}}{(2\pi)^2}\Theta(p_3^+) \tag{3.22}$$

In the equation above, the usual delta function encoding 4-momentum conservation is absent because it is used in to integrate out some of the momenta

Analytical Expressions for Fragmentation Functions

Now, we present the leading order expressions for the colour-singlet FFs. Although the authors from [86] published their results for the NLO FFs, they do not provide complete analytical expressions where we can set our own choice for the value of the heavy quark masses. Therefore, we use only the leading order expressions.

$$D^{LO}_{b\to B_c}(z) = \frac{2\alpha_s^2 z(1-z)^2|R_s(0)|^2}{81\pi r_c^2(1-r_b z)^6 M^3}[6-18(1-2r_c)z+(21-74r_c+68r_c^2)z^2 - 2r_b(6-19r_c+18r_c^2)z^3+3r_b^2(1-2r_c+2r_c^2)z^4] \tag{3.23}$$

$$D^{LO}_{b\to B_c^*}(z) = \frac{2\alpha_s^2 z(1-z)^2|R_s(0)|^2}{27\pi r_c^2(1-r_b z)^6 M^3}[2-2(3-2r_c)z+3(3-2r_c+4r_c^2)z^2 - 2r_b(4-r_c+2r_c^2)z^3+r_b^2(3-2r_c+2r_c^2)z^4] \tag{3.24}$$

Here, $R_s(0)$ denotes the radial wave function of the B_c meson at the origin, assumed identical for both contributions. The FFs for the charm quark are obtained by interchanging r_c and r_b in both equations.

3.3 Theoretical Framework of Meson Production

Before presenting our numerical results, we first outline the theoretical framework and computational tools used to obtain the partonic and hadronic cross sections relevant for heavy meson production in proton-proton collisions. Since our objective is to compare our NRQCD predictions for B_c production with experimental measurements, we aim to reproduce the production ratio reported by the LHCb collaboration between B_c mesons and the light-heavy mesons B_u and B_d. However, within the framework of NRQCD it is not possible to calculate the production of light-heavy mesons, as they contain only one heavy flavour. As a result, we rely on precise experimental measurements of their production cross sections in order to construct a meaningful comparison via the $B_c/(B_u + B_d)$ production ratio.

Fortunately, the LHCb collaboration has provided integrated and differential cross sections for B_u mesons at $\sqrt{s} = 7\,\text{TeV}$ and $\sqrt{s} = 13\,\text{TeV}$, within the kinematic ranges $0 < p_T < 40\,\text{GeV}$ and $2.0 < y < 4.5$, corresponding to the forward rapidity region [89]. These results include both B^+ and B^- mesons, quoted collectively as $B^\pm$. Furthermore, double-differential distributions in transverse momentum and rapidity are available, offering a comprehensive dataset.

By action of the approximate flavor symmetry in QCD, which is particularly effective for the u and d quarks, the production cross sections of B_u and B_d mesons can be considered approximately equal. As a result, we can safely use the experimental data reported by LHCb to construct the denominator of the $B_c/(B_u + B_d)$ production ratio.

However, while a direct comparison between the NRQCD predictions and the measured $B_u + B_d$ cross section is possible, any scheme dependent uncertainties present in the B_c calculation (such as as those associated with scale choices, parton densities, or higher-order corrections) would propagate to the ratio. To reduce these ambiguities and obtain a more stable prediction, we compute the production cross sections for both B_c and the mesons B_u and B_d within the same theoretical framework, with the exception that NRQCD is

not used for the light-heavy mesons. Instead, we describe $B^{\pm}$ meson production using a phenomenological fragmentation function fitted to experimental data. By evaluating both the numerator and denominator of the ratio consistently in the same theoretical framework, many common sources of uncertainty cancel out, leading to a more reliable and meaningful comparison with the experimental measurements of the $B_c/B_u + B_d$ production ratio at LHCb.

Parton Production Cross Section

In the framework of collinear factorization, the differential cross section for single-inclusive parton production in proton-proton collisions is given by

$$\frac{d\sigma_{pp\to jX}}{dydp_t}(y, p_t, \mu_f) = \sum_{a,b} \int dy_4 \, f_a(x_1, \mu_i) \, f_b(x_2, \mu_i) \, \frac{d\hat{\sigma}_{ab\to j+X}}{dydp_t}(x_1, x_2, y, p_t, \mu_i, \mu_f), \quad (3.25)$$

where the parton j is produced with rapidity y and transverse momentum p_t, and the integral runs over the rapidity y_4 of the second outgoing parton. The variables μ_i and μ_f denote the factorization and fragmentation scales, respectively, and we took $\mu_i = \mu_R$. The functions $f_a(x_1, \mu_i)$ and $f_b(x_2, \mu_i)$ are the parton distribution functions, evaluated at longitudinal momentum fractions x_1 and x_2 of the incoming partons. The quantity $d\hat{\sigma}_{ab\to jX}$ represents the partonic differential cross section for the hard subprocess $ab \to jX$.

Working with the General-Mass Variable Flavor Number scheme, we consider only the production of heavy mesons coming from the fragmentation of heavy quarks Q and gluons g. For this reason, we only include the single-inclusive production of these particles. For heavy quark production, we consider the following hard subprocesses

$$gg \to Q\overline{Q}, \quad Qg \to Qg, \quad Qq \to Qq, \quad Q\overline{q} \to Q\overline{q}, \quad (3.26)$$

where Q is a heavy quark (charm or bottom), and q is a light quark (up, down, or strange). For gluon production, we include the following channels

$$gg \to gg, \quad gq \to gq, \quad g\overline{q} \to g\overline{q}, \quad (3.27)$$

which describe gluon-gluon scattering and gluon interaction with light quarks. We do not include the production by quark-antiquark annihilation because the convolution of two small parton distribution functions results in a negligible effect on the cross section.

The parton hadro-production cross section (3.25) is computed at leading order in α_s using the Monte Carlo event generator SHERPA [90] [91], interfaced with LHAPDF [92] for the input from parton distribution functions, and employing COMIX [93] for matrix element generation. For consistency with leading-order calculations, we utilize two different LO PDF sets, CT14LO [94], and NNPDF23_LO_AS_0119_QED [95]. While both of these sets use the same value of the bottom quark mass $m_b = 4.75\,\text{GeV}$ they differ in their chosen values for the charm quark mass, with CT14LO adopting $m_c = 1.3\,\text{GeV}$, and NNPDF using $m_c = 1.41\,\text{GeV}$. Consistently, we will use the same values from the heavy quark masses in our calculations depending on which set we are using.

Hadronic Production Cross Section

While the left-hand side of eq. (3.25) is formally independent of the factorization scale μ_i at all orders, it retains a dependence on the fragmentation scale μ_f. This scale dependence

is eliminated once we convolute the partonic cross section with fragmentation functions to obtain the hadronic cross section:

$$\frac{d\sigma_{pp\to HX}}{dY dP_T^2}(Y, P_T) = \sum_j \int_0^1 \frac{dz}{z^2} D_{j\to H}(z, \mu_f) \frac{d\hat{\sigma}_{pp\to jX}}{dy dp_T^2}\left(y, \frac{P_T}{z}, \mu_f\right) \tag{3.28}$$

where H denotes a hadron produced in the fragmentation of the parton j, and (Y, P_T) are its rapidity and transverse momentum. The fragmentation variable z is defined as $\boldsymbol{P} = z\boldsymbol{p}$.

Besides rapidity, another commonly used kinematic variable in collider physics is the *pseudo-rapidity*, denoted by η. Unlike rapidity, which depends on both the energy and the longitudinal momentum of a particle, pseudo-rapidity has a purely geometric nature, being related to the angle of a particle's momentum relative to the beam axis. It is defined as

$$\eta = -\ln\left[\tan\left(\frac{\theta}{2}\right)\right], \tag{3.29}$$

where θ is the polar angle between the particle's three-momentum $\mathbf{p}$ and the positive direction of the beam axis.

In the limit where the particle's mass is negligible compared to its momentum, the pseudorapidity becomes approximately equal to rapidity. Specifically, one can make an expansion for $m/p_T \ll 1$ and see that

$$y = \frac{1}{2}\ln\left(\frac{E + p_z}{E - p_z}\right) = \ln\left(\frac{\sqrt{m^2 + p_T^2\cosh^2\eta} + p_T\sinh\eta}{\sqrt{m^2 + p_T^2}}\right) \approx \eta - \frac{\tanh\eta}{2}\left(\frac{m}{p_T}\right)^2 \tag{3.30}$$

Thus, at large P_T, pseudo-rapidity provides a good approximation to rapidity and is widely used to represent detector coverage and kinematic distributions in high-energy collider experiments. Moreover, since pseudo-rapidity is related to the deviation angle of scattered particles, the pseudo-rapidity of a fragmenting parton and the produced hadron are identical in collinear factorization. This allows us to simplify the convolution formula (3.28) as

$$\frac{d\sigma_{pp\to HX}}{d\eta dP_T}(\eta, P_T) = \sum_j \int_0^1 \frac{dz}{z} D_{j\to H}(z, \mu_f) \frac{d\hat{\sigma}_{pp\to jX}}{d\eta dp_T}\left(\eta, \frac{P_T}{z}, \mu_f\right) \tag{3.31}$$

where both cross sections are now differential in the same pseudorapidity variable.

Scale Choices and Uncertainties

In practice, the hadronic cross section retains an explicit dependence on the initial-state factorization scale μ_i and the final-state fragmentation scale μ_f, resulting in the usual theoretical scale uncertainties. Our choice for these scales is

$$\mu_i = \frac{m_{1T} + m_{2T}}{2} \qquad\qquad m_T = \sqrt{m^2 + p_T^2} \tag{3.32}$$

where m is the heavy quark mass, p_T is the transverse momentum of the parton. For the final-state fragmentation scale, we adopt

$$\mu_f = \sqrt{P_T^2 + M^2}, \tag{3.33}$$

where M and P_T are the mass and the transverse momentum of the produced hadron.

In estimating theoretical uncertainties due to scale variation, we note that next-to-leading-order predictions typically exhibit reduced sensitivity to scale choices. At LO, however, scale dependence remains more pronounced. To account for this and to remain conservative, we estimate uncertainties by varying both μ_i and μ_f together by a factor of $\sqrt{2}$ around their central values.

Fragmentation Functions and Time-like Evolution

As mentioned earlier, in our analysis we include only the contributions coming from fragmentation functions of heavy quarks $D_{Q\to H}$ and gluons $D_{g\to H}$, while neglecting the contributions from light flavors. The gluon FF would be considered as a product of the DGLAP evolution meanwhile the heavy quark FF will be the only one with a non-zero initial value and is assumed to freeze below the starting scale μ_0.

For the initial condition of the heavy quark FF associated with light-heavy B mesons, we adopt the Peterson parametrization (1.79):

$$D_{b\to B_u}(z,\mu_0) = f(b\to B_u)\,\frac{N(\epsilon_p)}{z\left(1-\frac{1}{z}-\frac{\epsilon_p}{1-z}\right)^2}\,, \tag{3.34}$$

where the $f(b\to B_u)$ normalization and the Peterson's parameter ϵ_p, are the only free parameters of this model. The latter we take it to be $\epsilon_p = 0.001$, following the value reported in [96]. The value of $f(b\to B_u)$ can be estimated as the fragmentation fraction f_u i.e. the fraction of b quarks fragmenting into light-heavy B mesons. This value can be obtanined from experimental results that show the relative production of B_u, B_d, B_s, and Λ_b^0 hadrons in the same p_T range. If we assume that the total production of b-hadrons is normalized to one, and we neglect the small contribution from charmed hadrons, we can use the condition

$$f_u + f_d + f_s + f_{\text{baryons}} = 1 \tag{3.35}$$

along with the flavour symmetry $f_u \approx f_d$, to extract the normalization of the FFs. Such an estimation can be found in the compilation [97], where the LEP data for b hadron production taken at the Z-pole is considered, and provides the following value

$$f_u = f_d = 0.407 \pm 0.007. \tag{3.36}$$

We also checked the LHCb measurements at $\sqrt{s} = 13\,\text{TeV}$, focusing on the high p_T region where fragmentation typically dominates [98]. Ignoring the contributions from baryons other than Λ_b^0, we find a similar result

$$f_u = f_d = 0.409 \pm 0.004 \tag{3.37}$$

Since both results agree well, we choose to use the central value from eq. (3.36) in our analysis.

For the initial fragmentation function of weakly decaying B_c mesons, we consider the sum of the two FFs, (3.23) and (3.24), calculated in NRQCD for B_c and B_c^* mesons. Given that the mass difference between these two states is around 50 MeV [8], the momentum shift of a B_c originating from a B_c^* decay is negligible within the kinematic range of LHCb.

Therefore, the total B_c production cross section can be approximated as the sum of the direct (excluding decays) production cross sections of B_c and B_c^* mesons.

$$D^{weak}_{b\to B_c}(z,\mu_0) = D_{b\to B_c}(z,\mu_0) + D_{b\to B_c^*}(z,\mu_0) \tag{3.38}$$

We replace the value of $|R_s(0)|^2$ used in [86] with $|R_s(0)|^2 = 6.21\,\text{GeV}^3$, as reported in [99]. This choice is motivated by Ref. [100], which notes that the smaller value employed in [86] leads to predictions for B_c production that are roughly a factor of four below experimental observations.

For both the light-heavy B mesons and the heavy B_c meson, we set the initial scale for time-like DGLAP evolution equal to the mass of the produced hadron $\mu_0 = M_H$. This corresponds to $M_{B_u} \simeq 5.28$ GeV for the light-heavy case [101], and $M_{B_c} \simeq 6.27$ GeV for the heavy case [102].

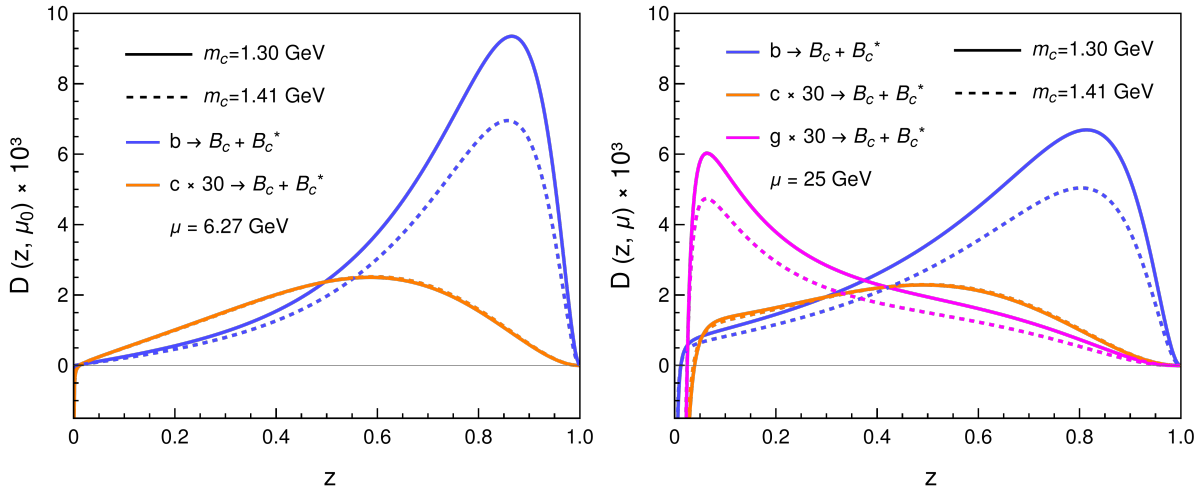

Figure 3.4: LO FFs for weakly decaying B_c mesons. The gluon and charm FFs have been scaled by a factor of 30 to facilitate comparison with the bottom FF.

To perform the DGLAP evolution of the fragmentation functions at next-to-leading order (two loops), we use QCDNUM [103], a software designed to numerically solve the evolution equations for parton distribution and fragmentation functions in perturbative QCD.

In Fig. 3.4, we present the gluon, charm, and bottom fragmentation functions at the starting scale $\mu = \mu_0$ (left panel) and after evolving to $\mu = 25$ GeV (right panel). In each plot, we illustrate how the FFs change when adopting the charm-quark mass used in the CT14 set, $m_c = 1.3$ GeV (solid lines), versus the one used in the NNPDF2.3 set, $m_c = 1.41$ GeV (dashed lines). These plots reveal that the initial bottom quark FF is notably sensitive to the value of the charm-quark mass. This sensitivity can be partially explained by the presence of the overall factor

$$D_{b\to B_c^{(*)}} \propto \frac{1}{r_c^2 M^3} = \frac{1}{m_c^2(m_c+m_b)}, \tag{3.39}$$

which results in a suppression of approximately 20% when increasing m_c from 1.3 to 1.41 GeV. Furthermore, since the initial charm quark FF is related to the bottom-quark FF by interchanging the roles of m_c and m_b, the same proportionality introduces a

suppression factor of roughly $(m_b/m_c)^2 \approx 10$ between the bottom and charm FFs, making the latter significantly smaller in general. Nevertheless, because charm quarks are produced more abundantly than bottom quarks in high-energy collisions, their contribution to B_c production cannot be neglected a priori.

For completeness, in Fig. 3.5 we present the gluon and bottom fragmentation functions for the production of light-heavy B_u mesons. As seen in the figure, the initial bottom-quark fragmentation function taken from [96] peaks at large values of z, indicating that at such low scales, the heavy quark retains most of its momentum during hadronization.

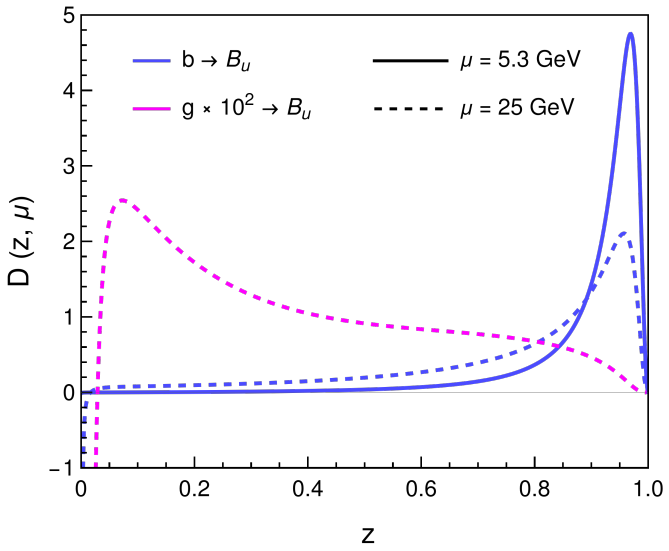

Figure 3.5: Peterson's FFs for B_u mesons. The gluon FF have been scaled by a factor of 100 to facilitate comparison with the bottom FF.

3.4 Results for B_c production and comparison with LHCb data

Production Cross Sections

We begin the discussion about our results by first testing the validity of the framework described in the previous section. To do this, in Fig. 3.6, we compared the theoretical prediction for the production cross section of B_u mesons with the corresponding measurements reported by LHCb. The calculation tends to overestimate the total cross section at low P_T, although it agrees reasonably well with the data at higher P_T values, where the gluon fragmentation contribution becomes more relevant. At lower P_T, however, the bottom-quark contribution alone appears sufficient to describe the data. This behavior is expected, since both $f_b(x, \mu_i = m_b) = 0$ and $D_{g\to B_u}(z, \mu_f = M_B) = 0$ vanish at their respective starting scales and increase rapidly with the scale through their logarithmic dependence on $\ln(\mu/m_b)$. Despite the discrepancy with the central values of our results, the experimental measurements below $P_T < 10$ GeV remain within the theoretical uncertainty band (indicated by the gray shaded region).

Additionally, we observe no significant difference between the results obtained using the CT14 and NNPDF2.3 PDF sets. This is also expected, as both sets adopt the same

value for the bottom-quark mass.

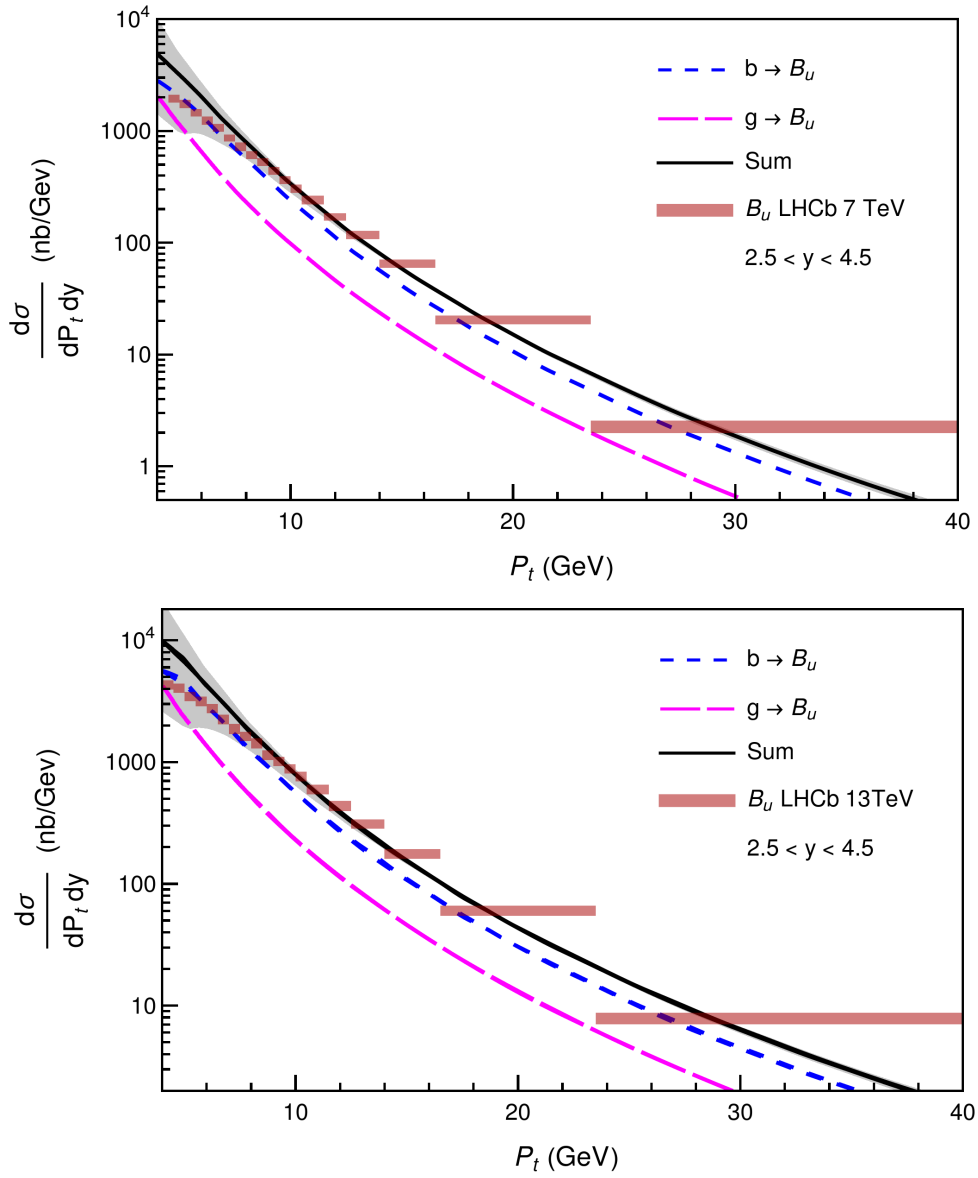

Figure 3.6: Theoretical results for the production cross section of B_u mesons (B^- and B^+) at 7 TeV (at the top) and 13 TeV (at the bottom) center-of-mass energies, compared with LHCb measurements in the rapidity range $2.5 < y < 4.5$ [89].

In Fig. 3.7, we show our results for the production cross section of weakly decaying B_c mesons at 7 TeV and 13 TeV center-of-mass energies, evaluated in the same kinematic range as the most recent LHCb measurements [18]. The curves are shown with a hatched width that represents their dependence on the PDF set used, which, even if the sets have other differences, mainly affects the results through the charm-quark mass chosen in each one. This uncertainty mainly originates from the previously discussed sensitivity of the bottom-quark fragmentation function to this parameter. Consequently, the upper edge of the band corresponds to the smaller charm mass, $m_c = 1.3$ GeV, while the lower edge reflects the larger value, $m_c = 1.41$ GeV.

Despite this mass dependence, we can observe from these plots that, similarly to the light-heavy B mesons, the gluon contribution remains smaller than the one from the

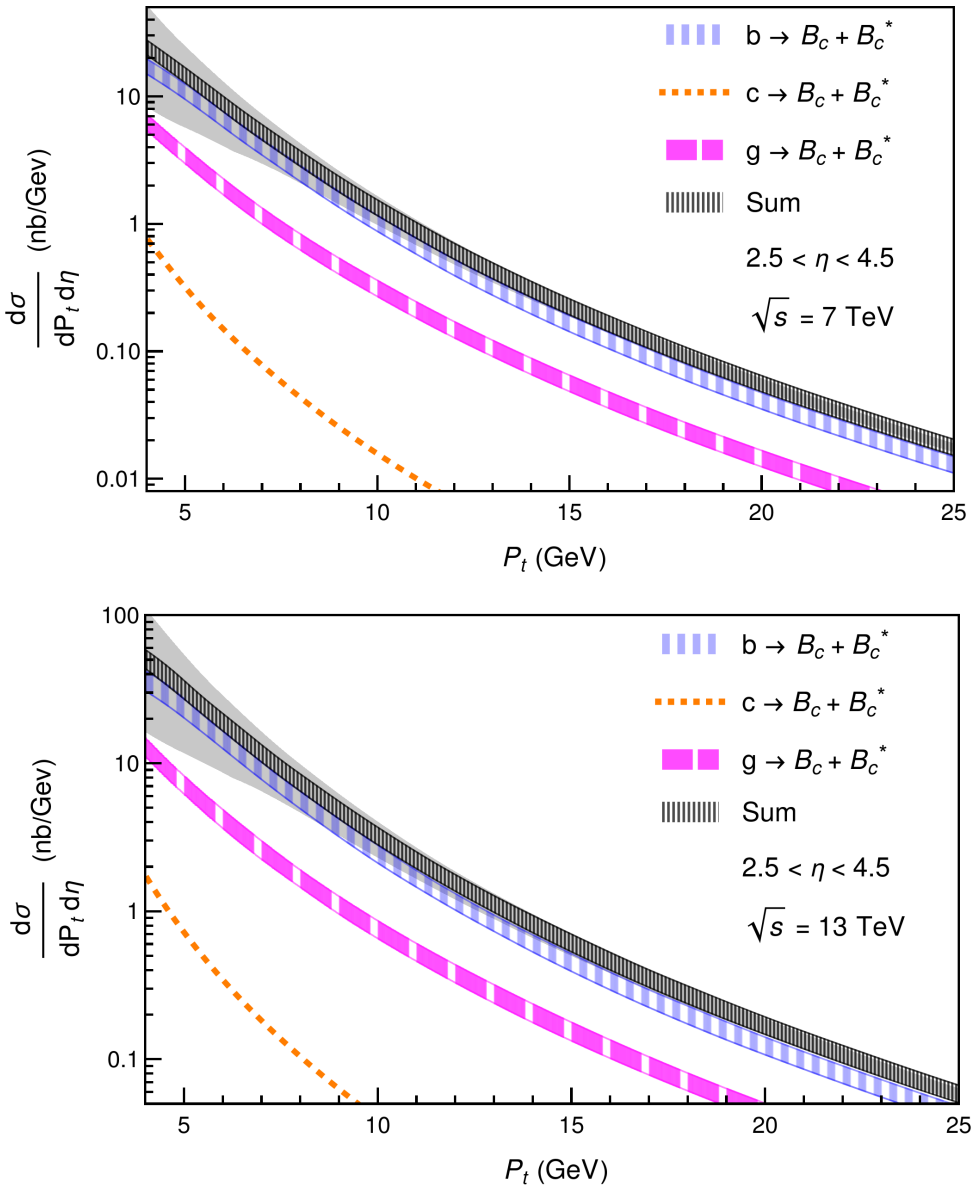

Figure 3.7: Calculated cross sections for the production of weakly decaying B_c mesons at 7 TeV (at the top) and 13 TeV (at the bottom) center-of-mass energies. The hatched bands reflect the variation due to different charm-quark mass values associated with the CT14 and NNPDF2.3 PDF sets. The flat gray band indicates the theoretical uncertainty associated with scale variation, as in the case of B_u mesons.

bottom quark. However, in this case, the gluon curve stays well below the bottom-quark one even at low P_T, without approaching it. This behavior is due to the higher initial scale involved in B_c production, which slows down the evolution of the fragmentation functions. As a result, for the same P_T values, the gluon FF is smaller in B_c production than in the case of light-heavy B_u mesons.

As a final remark, it is worth noting that the contribution from charm quark fragmentation is negligible in both plots, and its dependence on the charm-quark mass is not noticeable.

Fragmentation Ratio

To conclude our discussion, we present in Fig. 3.8 our theoretical predictions for the fragmentation ratio defined in eq. (3.1), compared with the LHCb measurements at $\sqrt{s} = 7$ TeV and 13 TeV. The results are shown as two separate bands, each corresponding to a different PDF set or, equivalently, to a different charm quark mass value. From these graphs, we observe that the prediction obtained using $m_c = 1.3$ GeV approaches the experimental uncertainty band in the highest-P_T bin, but underestimates the measurements at lower P_T. Furthermore, when using the slightly higher charm quark mass value of $m_c = 1.41$ GeV, the prediction remains entirely outside the experimental uncertainty bands.

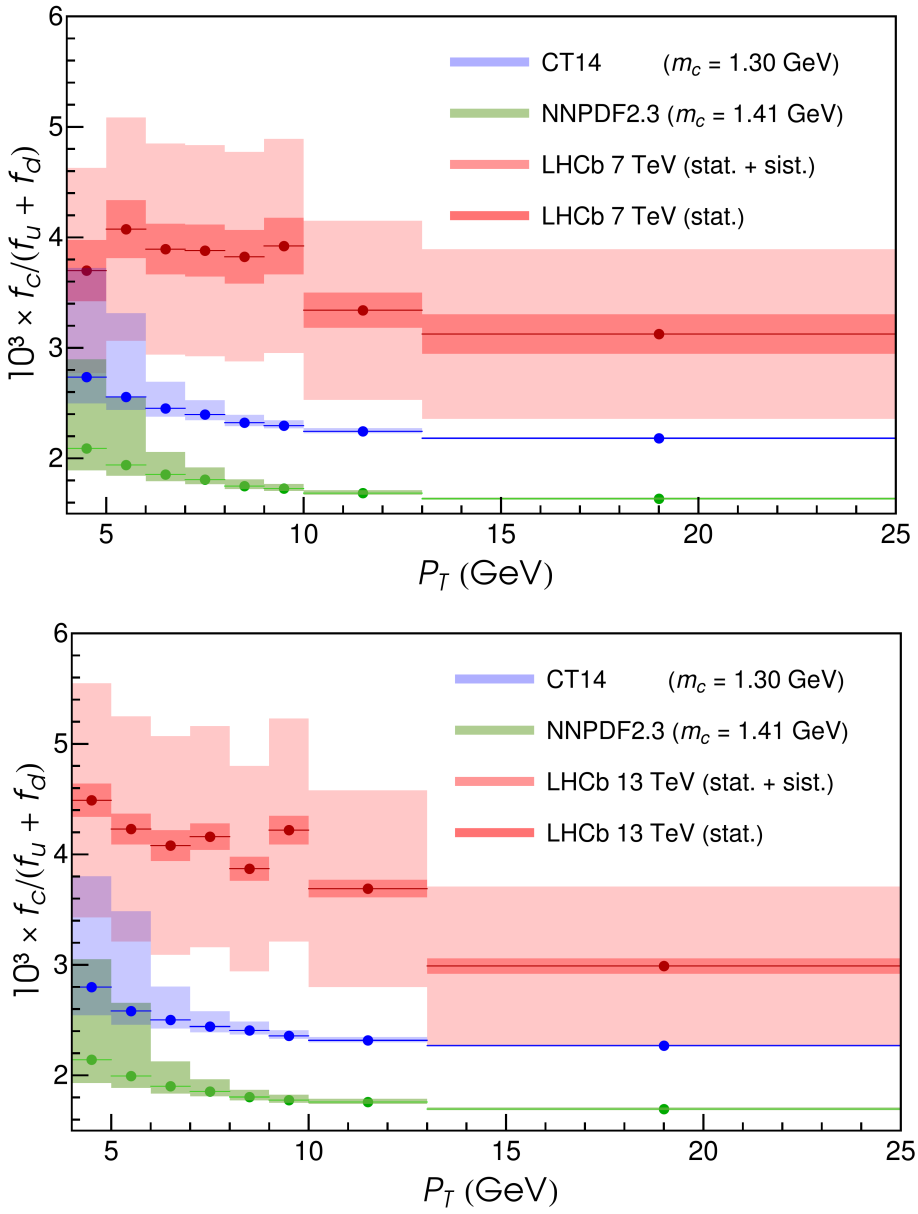

Figure 3.8: Fragmentation ratio as a function of P_T at $\sqrt{s} = 7$ TeV and 13 TeV in the pseudo-rapidity range $2.5 < \eta < 4.5$.

This difference can be partly explained by missing contributions in our fragmentation-based calculation. In particular, we did not include the color-octet mechanism, which

also contributes at leading order in α_s. However, the corresponding long-distance matrix elements (LDMEs) are usually small (typically suppressed by a factor of v^4 compared to the color-singlet ones) and they cannot be reliably determined because there is limited experimental data. For reference, we take the ratios between the phenomenological estimates [104] of the colour-singlet and colour-octet LDMEs for the J/ψ meson (which is much better studied than the B_c):

$$\frac{\langle \mathcal{O}^{J/\psi}(^1S_0^{[8]})\rangle}{\langle \mathcal{O}^{J/\psi}(^3S_1^{[1]})\rangle} \lesssim 2\cdot 10^{-2} \qquad \frac{\langle \mathcal{O}^{J/\psi}(^3S_1^{[8]})\rangle}{\langle \mathcal{O}^{J/\psi}(^3S_1^{[1]})\rangle} \lesssim 6\cdot 10^{-4} \qquad \frac{\langle \mathcal{O}^{J/\psi}(^3P_0^{[8]})\rangle}{\langle \mathcal{O}^{J/\psi}(^3S_1^{[1]})\rangle} \to 0 \tag{3.40}$$

These results show that the octet contributions are indeed small, and suggest that neglecting them in our calculation is a reasonable approximation.

Another possibility, discussed in the context of $p\overline{p}$ collisions at Tevatron energies ($\sqrt{s} = 1.96$ TeV), is that, according to Refs. [105] [106], the fragmentation contribution does not dominate the production of a heavy meson H in association with a heavy quark pair ($gg \to H + Q\overline{Q}$) unless the meson is produced at very large transverse momentum (a regime that was experimentally inaccessible at Tevatron and remains beyond the P_T range reported by LHCb for B_c production).

Although this may seem to be an extreme case, it suggests that a similar situation could occur in the LHCb measurements of single-inclusive B_c meson production. Since protons do not contain intrinsic charm or bottom quarks, both heavy quark pairs must be created in the collision, leading to the same problematic process we described. This implies that, at the currently accessible P_T values, there is no need to resum logarithms of P_T/m_b, as the fragmentation contribution alone is insufficient to describe the data accurately. Moreover, we can speculate that the direct production mechanism, where both heavy quark pairs are produced in the hard scattering process, should provide a sufficient description.

4 Conclusions

In this thesis, we have first reviewed the theoretical foundations that make perturbative calculations in Quantum Chromodynamics applicable to high–energy processes. We began examining the physical picture underlying the parton model and then introduced its rigorous realization in Quantum Field Theory, known as Collinear Factorization. We saw that in this framework, the hard scattering is the part that we can evaluate in perturbation theory, while the long-distance physics is separated and encoded inside the parton distribution functions, whose evolution is governed by the DGLAP equations. We outlined the key assumptions of this framework and highlighted the practical results that enable predictions for inclusive cross sections.

We then presented Non–Relativistic QCD (NRQCD), an effective theory created for the study of systems containing heavy quark–antiquark pairs. In NRQCD, we found a second factorization where short–distance coefficients encode the production of a nearly on–shell $Q\overline{Q}$ pairs, while universal long–distance matrix elements describe its non–perturbative evolution into a meson state. We showed the power–counting rules in the heavy–quark velocity v and the procedure to make calculations for the production of heavy mesons. We also explained that NRQCD can be combined with Collinear Factorization, to evaluate perturbatively the fragmentation functions related to heavy mesons.

Having established these two complementary factorization approaches, we applied them to the inclusive production of weakly decaying B_c mesons at the proton-proton collisions ocurring in LHC. To do so, we presented the computation of the leading–order color–singlet fragmentation functions using NRQCD, the Collinear Factorization definition, and evolving them with DGLAP. We then obtained predictions for the P_T dependent production cross sections of these mesons and compared our results to a similar calculation that used a phenomenological fragmentation function for the light-heavy mesons B_u (B^+ and B^-). This comparison allowed us to test the validity of our calculation against recent LHCb data for B_u production. Finally, we studied the transverse-momentum dependence of the ratio between these two calculations and compared it with one of the few available experimental observables related to B_c production, the experimental fragmentation ratio

$$\frac{f_c}{f_u + f_d} \sim \frac{\sigma(B_c)}{\sigma(B_u) + \sigma(B_d)} \sim \frac{\sigma(B_c)}{2\sigma_{B_u}}$$

This value was measured by LHCb at center of mass energies of 7 TeV and 13 TeV, within the range $2.5 < \eta < 4.5$ of pseudorapidity. We analyzed both cases separately.

Given that the fragmentation function is defined as the leading contibution when the hard scale $Q \sim P_T$ becomes suficiently large, we expected some discrepancies at the lowest P_T values, but an agreement with the data at P_T a few times bigger than the meson's mass M_{B_c}. However, our results show that the fragmentation approach underestimates the fragmentation ratio in the whole P_T range reported by LHCb, speacially in the lowest values where $P_T \sim M_{B_c}$.

This increasing underestimation at lower P_T can possibly be attributed to the fact that we have neglected corrections of relative order m_b^2/p_T^2 to the fragmentation function. In particular, direct production channels such as

$$gg \;\rightarrow\; B_c + b + \bar{c},$$

where both the $b\bar{b}$ and $c\bar{c}$ pairs are produced in the hard scattering, are expected to dominate at low p_T (a behavior that has been extensively studied in quarkonium production). Including these next-to-leading power contributions, as discussed in Refs. [107], [108], should significantly improve the agreement with experimental data.

In summary, we observed that the fragmentation function contribution is not enough to provide a good description of the B_c production in the current observable range of the LHCb, an we anticipate that a complete description of the P_T spectrum (especially in the region probed by LHCb) requires also including next-to-leading power corrections and color-octet mechanisms (whose long-distance matrix elements are small and poorly constrained). Future work should consider these contributions, hoping that such a comprehensive treatment will bring theoretical predictions into closer agreement with experimental measurements and deepen our understanding of B_c meson production in QCD.

References

Back-references to the pages where the publication was cited are given by •.

[1] Gerard 't Hooft and M. J. G. Veltman. Regularization and Renormalization of Gauge Fields. *Nucl. Phys. B*, **1972**.
DOI: 10.1016/0550-3213(72)90279-9 2

[2] D. J. Gross and Frank Wilczek. Asymptotically Free Gauge Theories - I. *Phys. Rev. D*, **1973**.
DOI: 10.1103/PhysRevD.8.3633 2

[3] H. David Politzer. Reliable Perturbative Results for Strong Interactions? *Phys. Rev. Lett.*, **1973**. ed. by J. C. Taylor.
DOI: 10.1103/PhysRevLett.30.1346 2

[4] Matthias Neubert. Heavy quark symmetry. *Phys. Rept.*, **1994**.
DOI: 10.1016/0370-1573(94)90091-4 ARXIV: hep-ph/9306320 3

[5] Matthias Neubert. Heavy quark effective theory. *Subnucl. Ser.*, **1997**. ed. by A. Zichichi.
ARXIV: hep-ph/9610266 3

[6] W. E. Caswell and G. P. Lepage. Effective Lagrangians for Bound State Problems in QED, QCD, and Other Field Theories. *Phys. Lett. B*, **1986**.
DOI: 10.1016/0370-2693(86)91297-9 3, 30

[7] Geoffrey T. Bodwin, Eric Braaten, and G. Peter Lepage. Rigorous QCD analysis of inclusive annihilation and production of heavy quarkonium. *Phys. Rev. D*, **1995**. [Erratum: Phys.Rev.D 55, 5853 (1997)].
DOI: 10.1103/PhysRevD.55.5853 ARXIV: hep-ph/9407339 3, 30, 31, 43

[8] Qi Li, Ming-Sheng Liu, Long-Sheng Lu, Qi-Fang Lü, Long-Cheng Gui, and Xian-Hui Zhong. Excited bottom-charmed mesons in a nonrelativistic quark model. *Phys. Rev. D*, **2019**.
DOI: 10.1103/PhysRevD.99.096020 ARXIV: 1903.11927 [hep-ph] 3, 48, 56

[9] R. Barate et al. Search for the B_c meson in hadronic Z decays. *Phys. Lett. B*, **1997**.
DOI: 10.1016/S0370-2693(97)00461-9 4

[10] P. Abreu et al. Search for the B(c) Meson. *Phys. Lett. B*, **1997**.
DOI: 10.1016/S0370-2693(97)00254-2 4

[11] K. Ackerstaff et al. Search for the B_c meson in hadronic Z^0 decays. *Phys. Lett. B*, **1998**.
DOI: 10.1016/S0370-2693(97)01569-4 ARXIV: hep-ex/9801026 4

[12] F. Abe et al. Observation of the B_c meson in $p\bar{p}$ collisions at $\sqrt{s} = 1.8$ TeV. *Phys. Rev. Lett.*, **1998**.
DOI: 10.1103/PhysRevLett.81.2432 ARXIV: hep-ex/9805034 4, 45

[13] F. Abe et al. Observation of B_c mesons in $p\bar{p}$ collisions at $\sqrt{s} = 1.8$ TeV. *Phys. Rev. D*, **1998**.
DOI: 10.1103/PhysRevD.58.112004 ARXIV: hep-ex/9804014 4

[14] V. M. Abazov et al. Observation of the B_c Meson in the Exclusive Decay $B_c \to J/\psi\pi$. *Phys. Rev. Lett.*, **2008**.
DOI: 10.1103/PhysRevLett.101.012001 ARXIV: 0802.4258 [hep-ex] 4

[15] Roel Aaij et al. Measurement of B_c^+ production in proton-proton collisions at $\sqrt{s} = 8$ TeV. *Phys. Rev. Lett.*, **2015**.
DOI: 10.1103/PhysRevLett.114.132001 ARXIV: 1411.2943 [hep-ex] 4

[16] Vardan Khachatryan et al. Measurement of the ratio of the production cross sections times branching fractions of $B_c^\pm \to J/\psi\pi^\pm$ and $B^\pm \to J/\psi K^\pm$ and $\mathcal{B}(B_c^\pm \to J/\psi\pi^\pm\pi^\pm\pi^\mp)/\mathcal{B}(B_c^\pm \to J/\psi\pi^\pm)$ in pp collisions at $\sqrt{s} = 7$ TeV. *JHEP*, **2015**.
DOI: 10.1007/JHEP01(2015)063 ARXIV: 1410.5729 [hep-ex] 4

[17] Albert M Sirunyan et al. Observation of Two Excited B_c^+ States and Measurement of the $B_c^+(2S)$ Mass in pp Collisions at $\sqrt{s} = 13$ TeV. *Phys. Rev. Lett.*, **2019**.
DOI: 10.1103/PhysRevLett.122.132001 ARXIV: 1902.00571 [hep-ex] 4

[18] Roel Aaij et al. Measurement of the B_c^- meson production fraction and asymmetry in 7 and 13 TeV pp collisions. *Phys. Rev. D*, **2019**.
DOI: 10.1103/PhysRevD.100.112006 ARXIV: 1910.13404 [hep-ex] 4, 45, 59

[19] Richard P. Feynman. Very high-energy collisions of hadrons. *Phys. Rev. Lett.*, **1969**. ed. by L. M. Brown.
DOI: 10.1103/PhysRevLett.23.1415 6

[20] J. D. Bjorken and Emmanuel A. Paschos. Inelastic Electron Proton and gamma Proton Scattering, and the Structure of the Nucleon. *Phys. Rev.*, **1969**.
DOI: 10.1103/PhysRev.185.1975 6

[21] Matthew D. Schwartz. Quantum Field Theory and the Standard Model. Cambridge University Press, **2014**. 7

[22] Michael E. Peskin and Daniel V. Schroeder. An Introduction to quantum field theory. Addison-Wesley, **1995**.
DOI: 10.1201/9780429503559 7, 9

[23] W. Greiner, S. Schramm, and E. Stein. Quantum chromodynamics. **2007**. 7

[24] Boris Lazarevich Ioffe, Victor Sergeevich Fadin, and Lev Nikolaevich Lipatov. Quantum chromodynamics: Perturbative and nonperturbative aspects. Cambridge Univ. Press, **2010**.
DOI: 10.1017/CBO9780511711817 7

[25] S. M. Berman, J. D. Bjorken, and John B. Kogut. Inclusive Processes at High Transverse Momentum. *Phys. Rev. D*, **1971**.
DOI: 10.1103/PhysRevD.4.3388 8

[26] R. P. Feynman. Photon-hadron interactions. W.A. Benjamin, Inc. Publishers, **1973**.

8

[27] Guido Altarelli and G. Parisi. Asymptotic Freedom in Parton Language. *Nucl. Phys. B*, **1977**.
DOI: 10.1016/0550-3213(77)90384-4 9, 17

[28] Yuri L. Dokshitzer. Calculation of the Structure Functions for Deep Inelastic Scattering and e+ e- Annihilation by Perturbation Theory in Quantum Chromodynamics. *Sov. Phys. JETP*, **1977**.
17

[29] V. N. Gribov and L. N. Lipatov. Deep inelastic e p scattering in perturbation theory. *Sov. J. Nucl. Phys.*, **1972**.
17

[30] W. Furmanski and R. Petronzio. Singlet parton densities beyond leading order. *Physics Letters B*, **1980**.
DOI: https://doi.org/10.1016/0370-2693(80)90636-X 17

[31] M. Stratmann and W. Vogelsang. Next-to-leading order evolution of polarized and unpolarized fragmentation functions. *Nucl. Phys. B*, **1997**.
DOI: 10.1016/S0550-3213(97)00182-X ARXIV: hep-ph/9612250 17

[32] A. Vogt, S. Moch, and J. A. M. Vermaseren. The Three-loop splitting functions in QCD: The Singlet case. *Nucl. Phys. B*, **2004**.
DOI: 10.1016/j.nuclphysb.2004.04.024 ARXIV: hep-ph/0404111 17

[33] Valerio Bertone, Stefano Carrazza, and Emanuele R. Nocera. Reference results for time-like evolution up to $\mathcal{O}(\alpha_s^3)$. *JHEP*, **2015**.
DOI: 10.1007/JHEP03(2015)046 ARXIV: 1501.00494 [hep-ph] 17

[34] John C. Collins and Davison E. Soper. Parton Distribution and Decay Functions. *Nucl. Phys. B*, **1982**.
DOI: 10.1016/0550-3213(82)90021-9 18

[35] John C. Collins, Davison E. Soper, and George F. Sterman. Factorization of Hard Processes in QCD. *Adv. Ser. Direct. High Energy Phys.*, **1989**.
DOI: 10.1142/9789814503266_0001 ARXIV: hep-ph/0409313 18

[36] John Collins. Foundations of Perturbative QCD. Cambridge University Press, **2011**.
DOI: 10.1017/9781009401845 18, 19

[37] Andreas Metz and Anselm Vossen. Parton Fragmentation Functions. *Prog. Part. Nucl. Phys.*, **2016**.
DOI: 10.1016/j.ppnp.2016.08.003 ARXIV: 1607.02521 [hep-ex] 23

[38] John C. Collins and Wu-Ki Tung. Calculating Heavy Quark Distributions. *Nucl. Phys. B*, **1986**. ed. by S. C. Loken.
DOI: 10.1016/0550-3213(86)90425-6 27

[39] John C. Collins. Hard scattering factorization with heavy quarks: A General treatment. *Phys. Rev. D*, **1998**.
DOI: 10.1103/PhysRevD.58.094002 ARXIV: hep-ph/9806259 27

[40] M. A. G. Aivazis, Frederick I. Olness, and Wu-Ki Tung. Leptoproduction of heavy

quarks. 1. General formalism and kinematics of charged current and neutral current production processes. *Phys. Rev. D*, **1994**.
DOI: 10.1103/PhysRevD.50.3085 arXiv: hep-ph/9312318 27

[41] M. A. G. Aivazis, John C. Collins, Fredrick I. Olness, and Wu-Ki Tung. Leptoproduction of heavy quarks. 2. A Unified QCD formulation of charged and neutral current processes from fixed target to collider energies. *Phys. Rev. D*, **1994**.
DOI: 10.1103/PhysRevD.50.3102 arXiv: hep-ph/9312319 27

[42] R. S. Thorne and W. K. Tung. PQCD Formulations with Heavy Quark Masses and Global Analysis. in: *HERA and the LHC: 4th Workshop on the Implications of HERA for LHC Physics*. **2008**.
arXiv: 0809.0714 [hep-ph] 28

[43] C. Peterson, D. Schlatter, I. Schmitt, and Peter M. Zerwas. Scaling Violations in Inclusive e+ e- Annihilation Spectra. *Phys. Rev. D*, **1983**.
DOI: 10.1103/PhysRevD.27.105 28

[44] P. D. B. Collins and T. P. Spiller. The Fragmentation of Heavy Quarks. *J. Phys. G*, **1985**.
DOI: 10.1088/0305-4616/11/12/006 28

[45] V. G. Kartvelishvili, A. K. Likhoded, and V. A. Petrov. On the Fragmentation Functions of Heavy Quarks Into Hadrons. *Phys. Lett. B*, **1978**.
DOI: 10.1016/0370-2693(78)90653-6 28

[46] D. Buskulic et al. Measurement of the effective b quark fragmentation function at the Z resonance. *Phys. Lett. B*, **1995**.
DOI: 10.1016/0370-2693(95)00988-W 28

[47] G. Abbiendi et al. Inclusive analysis of the b quark fragmentation function in Z decays at LEP. *Eur. Phys. J. C*, **2003**.
DOI: 10.1140/epjc/s2003-01229-x arXiv: hep-ex/0210031 28

[48] Kenji Abe et al. Precise measurement of the b quark fragmentation function in Z0 boson decays. *Phys. Rev. Lett.*, **2000**.
DOI: 10.1103/PhysRevLett.84.4300 arXiv: hep-ex/9912058 28

[49] J. Abdallah et al. A study of the b-quark fragmentation function with the DELPHI detector at LEP I and an averaged distribution obtained at the Z Pole. *Eur. Phys. J. C*, **2011**.
DOI: 10.1140/epjc/s10052-011-1557-x arXiv: 1102.4748 [hep-ex] 28

[50] Bernd A. Kniehl, Gustav Kramer, Ingo Schienbein, and Hubert Spiesberger. Finite-mass effects on inclusive B meson hadroproduction. *Phys. Rev. D*, **2008**.
DOI: 10.1103/PhysRevD.77.014011 arXiv: 0705.4392 [hep-ph] 28

[51] J. J. Aubert et al. Experimental Observation of a Heavy Particle J. *Phys. Rev. Lett.*, **1974**.
DOI: 10.1103/PhysRevLett.33.1404 29

[52] J. E. Augustin et al. Discovery of a Narrow Resonance in e^+e^- Annihilation. *Phys. Rev. Lett.*, **1974**.
DOI: 10.1103/PhysRevLett.33.1406 29

[53] S. W. Herb et al. Observation of a Dimuon Resonance at 9.5-GeV in 400-GeV Proton-Nucleus Collisions. *Phys. Rev. Lett.*, **1977**.
DOI: 10.1103/PhysRevLett.39.252 29

[54] Johann H. Kuhn, Jean Kaplan, and El Ghali Oudrhiri Safiani. Electromagnetic Annihilation of e+ e- Into Quarkonium States with Even Charge Conjugation. *Nucl. Phys. B*, **1979**.
DOI: 10.1016/0550-3213(79)90055-5 29

[55] B. Guberina, Johann H. Kuhn, R. D. Peccei, and R. Ruckl. Rare Decays of the Z0. *Nucl. Phys. B*, **1980**.
DOI: 10.1016/0550-3213(80)90287-4 29

[56] F. Abe et al. Inclusive J/ψ, $\psi(2S)$ and b quark production in $\bar{p}p$ collisions at $\sqrt{s} = 1.8$ TeV. *Phys. Rev. Lett.*, **1992**.
DOI: 10.1103/PhysRevLett.69.3704 30

[57] S. Abachi et al. J/ψ production in $p\bar{p}$ collisions at $\sqrt{s} = 1.8$-TeV. *Phys. Lett. B*, **1996**.
DOI: 10.1016/0370-2693(96)00067-6 30

[58] Mathias Butenschoen and Bernd A. Kniehl. World data of J/psi production consolidate NRQCD factorization at NLO. *Phys. Rev. D*, **2011**.
DOI: 10.1103/PhysRevD.84.051501 arXiv: 1105.0820 [hep-ph] 30

[59] Eric Braaten and Yu-Qi Chen. Helicity decomposition for inclusive J / psi production. *Phys. Rev. D*, **1996**.
DOI: 10.1103/PhysRevD.54.3216 arXiv: hep-ph/9604237 31, 34

[60] Eric Braaten, Sean Fleming, and Tzu Chiang Yuan. Production of heavy quarkonium in high-energy colliders. *Ann. Rev. Nucl. Part. Sci.*, **1996**.
DOI: 10.1146/annurev.nucl.46.1.197 arXiv: hep-ph/9602374 31

[61] Michael Krämer. Quarkonium production at high-energy colliders. *Prog. Part. Nucl. Phys.*, **2001**.
DOI: 10.1016/S0146-6410(01)00154-5 arXiv: hep-ph/0106120 31

[62] Martin Beneke. Nonrelativistic effective theory for quarkonium production in hadron collisions. in: *24th Annual SLAC Summer Institute on Particle Physics: The Strong Interaction, From Hadrons to Protons*. **1997**.
arXiv: hep-ph/9703429 31

[63] Benjamin Grinstein. A Modern introduction to quarkonium theory. *Int. J. Mod. Phys. A*, **2000**.
DOI: 10.1142/S0217751X00000227 arXiv: hep-ph/9811264 31

[64] G. Peter Lepage, Lorenzo Magnea, Charles Nakhleh, Ulrika Magnea, and Kent Hornbostel. Improved nonrelativistic QCD for heavy quark physics. *Phys. Rev. D*, **1992**.
DOI: 10.1103/PhysRevD.46.4052 arXiv: hep-lat/9205007 35

[65] Geoffrey T. Bodwin, Eric Braaten, and G. Peter Lepage. Rigorous QCD predictions for decays of p wave quarkonia. in: *7th Meeting of the APS Division of Particles Fields*. **1992**.

ARXIV: hep-ph/9211253 36

[66] Geoffrey T. Bodwin, Eric Braaten, and G. Peter Lepage. Rigorous QCD predictions for decays of P wave quarkonia. *Phys. Rev. D*, **1992**.
DOI: 10.1103/PhysRevD.46.R1914 ARXIV: hep-lat/9205006 36

[67] Geoffrey T. Bodwin and Andrea Petrelli. Order-v^4 corrections to S-wave quarkonium decay. *Phys. Rev. D*, **2002**. [Erratum: Phys.Rev.D 87, 039902 (2013)].
DOI: 10.1103/PhysRevD.66.094011 ARXIV: hep-ph/0205210 36

[68] Wei Wang and Rui-Lin Zhu. Radiative leptonic $B_c \to \gamma \ell \bar{\nu}$ decay in effective field theory beyond leading order. *Eur. Phys. J. C*, **2015**.
DOI: 10.1140/epjc/s10052-015-3583-6 ARXIV: 1501.04493 [hep-ph] 36

[69] Wei Wang, Ji Xu, Deshan Yang, and Shuai Zhao. Relativistic corrections to light-cone distribution amplitudes of S-wave B_c mesons and heavy quarkonia. *JHEP*, **2017**.
DOI: 10.1007/JHEP12(2017)012 ARXIV: 1706.06241 [hep-ph] 36

[70] Andrea Petrelli, Matteo Cacciari, Mario Greco, Fabio Maltoni, and Michelangelo L. Mangano. NLO production and decay of quarkonium. *Nucl. Phys. B*, **1998**.
DOI: 10.1016/S0550-3213(97)00801-8 ARXIV: hep-ph/9707223 40

[71] R. Van Royen and V. F. Weisskopf. Hadron Decay Processes and the Quark Model. *Nuovo Cim. A*, **1967**. [Erratum: Nuovo Cim.A 51, 583 (1967)].
DOI: 10.1007/BF02823542 43

[72] Chien-Wen Hwang. Charge radii of light and heavy mesons. *Eur. Phys. J. C*, **2002**.
DOI: 10.1007/s100520200904 ARXIV: hep-ph/0112237 43

[73] Gouranga C. Nayak, Jian-Wei Qiu, and George F. Sterman. Fragmentation, NRQCD and NNLO factorization analysis in heavy quarkonium production. *Phys. Rev. D*, **2005**.
DOI: 10.1103/PhysRevD.72.114012 ARXIV: hep-ph/0509021 48

[74] Gouranga C. Nayak, Jian-Wei Qiu, and George F. Sterman. Fragmentation, factorization and infrared poles in heavy quarkonium production. *Phys. Lett. B*, **2005**.
DOI: 10.1016/j.physletb.2005.03.031 ARXIV: hep-ph/0501235 48

[75] Eric Braaten, King-man Cheung, and Tzu Chiang Yuan. Perturbative QCD fragmentation functions for B_c and B_c * production. *Phys. Rev. D*, **1993**.
DOI: 10.1103/PhysRevD.48.R5049 ARXIV: hep-ph/9305206 48

[76] M. Beneke and I. Z. Rothstein. Psi-prime polarization as a test of color octet quarkonium production. *Phys. Lett. B*, **1996**. [Erratum: Phys.Lett.B 389, 769 (1996)].
DOI: 10.1016/0370-2693(96)00030-5 ARXIV: hep-ph/9509375 48

[77] Geoffrey T. Bodwin and Jungil Lee. Relativistic corrections to gluon fragmentation into spin triplet S wave quarkonium. *Phys. Rev. D*, **2004**.
DOI: 10.1103/PhysRevD.69.054003 ARXIV: hep-ph/0308016 48

[78] Geoffrey T. Bodwin, U-Rae Kim, and Jungil Lee. Higher-order relativistic corrections to gluon fragmentation into spin-triplet S-wave quarkonium. *JHEP*, **2012**. [Erratum: JHEP 07, 170 (2023)].
DOI: 10.1007/JHEP11(2012)020 ARXIV: 1208.5301 [hep-ph] 48

[79] Feng Feng, Saadi Ishaq, Yu Jia, and Jia-Yue Zhang. Fragmentation function of gluon into spin-singlet P-wave quarkonium. *Phys. Rev. D*, **2020**.
DOI: 10.1103/PhysRevD.102.014038 arXiv: 1712.09986 [hep-ph] 48

[80] Xu-Chang Zheng, Chao-Hsi Chang, and Xing-Gang Wu. NLO fragmentation functions of heavy quarks into heavy quarkonia. *Phys. Rev. D*, **2019**.
DOI: 10.1103/PhysRevD.100.014005 arXiv: 1905.09171 [hep-ph] 48

[81] Yu-Qi Chen. Perturbative QCD predictions for the fragmentation functions of the P wave mesons with two heavy quarks. *Phys. Rev. D*, **1993**.
DOI: 10.1103/PhysRevD.48.5181 48

[82] Tzu Chiang Yuan. Perturbative QCD fragmentation functions for production of P wave mesons with charm and beauty. *Phys. Rev. D*, **1994**.
DOI: 10.1103/PhysRevD.50.5664 arXiv: hep-ph/9405348 48

[83] King-man Cheung and Tzu Chiang Yuan. Heavy quark fragmentation functions for d wave quarkonium and charmed beauty mesons. *Phys. Rev. D*, **1996**.
DOI: 10.1103/PhysRevD.53.3591 arXiv: hep-ph/9510208 48

[84] J. P. Ma. Calculating fragmentation functions from definitions. *Phys. Lett. B*, **1994**.
DOI: 10.1016/0370-2693(94)91271-8 arXiv: hep-ph/9401249 48

[85] Deshan Yang and Wenjie Zhang. Relativistic corrections of the fragmentation functions for a heavy quark to B_c and B_c^*. *Chin. Phys. C*, **2019**.
DOI: 10.1088/1674-1137/43/8/083101 arXiv: 1905.02923 [hep-ph] 48

[86] Xu-Chang Zheng, Chao-Hsi Chang, Tai-Fu Feng, and Xing-Gang Wu. QCD NLO fragmentation functions for c or b^- quark to B_c or B_c^* meson and their application. *Phys. Rev. D*, **2019**.
DOI: 10.1103/physrevd.100.034004 48, 53, 57

[87] Xu-Chang Zheng, Chao-Hsi Chang, and Xing-Gang Wu. Fragmentation functions for gluon into B_c or B_c^* meson. *JHEP*, **2022**.
DOI: 10.1007/JHEP05(2022)036 arXiv: 2112.10520 [hep-ph] 48

[88] Feng Feng, Yu Jia, and Deshan Yang. Gluon fragmentation into Bc(*) in NRQCD factorization. *Phys. Rev. D*, **2022**.
DOI: 10.1103/PhysRevD.106.054030 arXiv: 2112.15569 [hep-ph] 48

[89] Roel Aaij et al. Measurement of the $B^{\pm}$ production cross-section in pp collisions at $\sqrt{s} = 7$ and 13 TeV. *JHEP*, **2017**.
DOI: 10.1007/JHEP12(2017)026 arXiv: 1710.04921 [hep-ex] 53, 59

[90] Enrico Bothmann, Marek Schönherr, and Steffen Schumann. Reweighting QCD matrix-element and parton-shower calculations. *Eur. Phys. J. C*, **2016**.
DOI: 10.1140/epjc/s10052-016-4430-0 arXiv: 1606.08753 [hep-ph] 54

[91] Enrico Bothmann et al. Event Generation with Sherpa 2.2. *SciPost Phys.*, **2019**.
DOI: 10.21468/SciPostPhys.7.3.034 arXiv: 1905.09127 [hep-ph] 54

[92] Andy Buckley, James Ferrando, Stephen Lloyd, Karl Nordström, Ben Page, Martin Rüfenacht, Marek Schönherr, and Graeme Watt. LHAPDF6: parton density access in the LHC precision era. *Eur. Phys. J. C*, **2015**.

DOI: 10.1140/epjc/s10052-015-3318-8 ARXIV: 1412.7420 [hep-ph] 54

[93] Tanju Gleisberg and Stefan Hoeche. Comix, a new matrix element generator. *JHEP*, **2008**.
DOI: 10.1088/1126-6708/2008/12/039 ARXIV: 0808.3674 [hep-ph] 54

[94] Sayipjamal Dulat, Tie-Jiun Hou, Jun Gao, Marco Guzzi, Joey Huston, Pavel Nadolsky, Jon Pumplin, Carl Schmidt, Daniel Stump, and C. P. Yuan. New parton distribution functions from a global analysis of quantum chromodynamics. *Phys. Rev. D*, **2016**.
DOI: 10.1103/PhysRevD.93.033006 ARXIV: 1506.07443 [hep-ph] 54

[95] Richard D. Ball et al. Parton distributions with LHC data. *Nucl. Phys. B*, **2013**.
DOI: 10.1016/j.nuclphysb.2012.10.003 ARXIV: 1207.1303 [hep-ph] 54

[96] F. E. Barattini, C. O. Dib, and B. Guiot. Heavy-hadron production based on k_t-factorization with scale-dependent fragmentation functions, **2025**.
ARXIV: 2501.17662 [hep-ph] 56, 58

[97] Y. Amhis et al. Averages of b-hadron, c-hadron, and τ-lepton properties as of summer 2016. *Eur. Phys. J. C*, **2017**.
DOI: 10.1140/epjc/s10052-017-5058-4 ARXIV: 1612.07233 [hep-ex] 56

[98] Roel Aaij et al. Measurement of b hadron fractions in 13 TeV pp collisions. *Phys. Rev. D*, **2019**.
DOI: 10.1103/PhysRevD.100.031102 ARXIV: 1902.06794 [hep-ex] 56

[99] Qi-Li Liao and Guo-Ya Xie. Heavy quarkonium wave functions at the origin and excited heavy quarkonium production via top quark decays at the LHC. *Phys. Rev. D*, **2014**.
DOI: 10.1103/PhysRevD.90.054007 ARXIV: 1408.5563 [hep-ph] 57

[100] S. P. Baranov and A. V. Lipatov. First estimates of the B_c wave function from the data on the B_c production cross section. *Phys. Lett. B*, **2018**.
DOI: 10.1016/j.physletb.2018.09.007 ARXIV: 1805.05390 [hep-ph] 57

[101] R. Aaij et al. Observation of a J/$\psi\Lambda$ Resonance Consistent with a Strange Pentaquark Candidate in B-$\to$J/$\psi\Lambda\bar{\text{p}}$ Decays. *Phys. Rev. Lett.*, **2023**.
DOI: 10.1103/PhysRevLett.131.031901 ARXIV: 2210.10346 [hep-ex] 57

[102] Roel Aaij et al. Precision measurement of the B_c^+ meson mass. *JHEP*, **2020**.
DOI: 10.1007/JHEP07(2020)123 ARXIV: 2004.08163 [hep-ex] 57

[103] M. Botje. QCDNUM: Fast QCD Evolution and Convolution. *Comput. Phys. Commun.*, **2011**.
DOI: 10.1016/j.cpc.2010.10.020 ARXIV: 1005.1481 [hep-ph] 57

[104] S. P. Baranov and A. V. Lipatov. Prompt charmonia production and polarization at LHC in the NRQCD with k_T-factorization. Part III: J/ψ meson. *Phys. Rev. D*, **2017**.
DOI: 10.1103/PhysRevD.96.034019 ARXIV: 1611.10141 [hep-ph] 62

[105] Chao-Hsi Chang, Yu-Qi Chen, and Robert J. Oakes. Comparative study of the hadronic production of B(c) mesons. *Phys. Rev. D*, **1996**.
DOI: 10.1103/PhysRevD.54.4344 ARXIV: hep-ph/9602411 62

[106] P. Artoisenet, J. P. Lansberg, and F. Maltoni. Hadroproduction of J/ψ and Υ in association with a heavy-quark pair. *Phys. Lett. B*, **2007**.
DOI: 10.1016/j.physletb.2007.04.031 ARXIV: hep-ph/0703129 62

[107] Zhong-Bo Kang, Yan-Qing Ma, Jian-Wei Qiu, and George Sterman. Heavy Quarkonium Production at Collider Energies: Factorization and Evolution. *Phys. Rev. D*, **2014**.
DOI: 10.1103/PhysRevD.90.034006 ARXIV: 1401.0923 [hep-ph] 64

[108] Kyle Lee, Jian-Wei Qiu, George Sterman, and Kazuhiro Watanabe. Subleading power corrections to heavy quarkonium production in QCD factorization approach. *EPJ Web Conf.*, **2022**.
DOI: 10.1051/epjconf/202227404005 ARXIV: 2211.12648 [hep-ph] 64